

Electronic Thesis and Dissertation Repository

12-8-2016 12:00 AM

Combined Analysis of Tide- and Wave-induced Water Table Fluctuations for Structural Characterization of a Coastal Aquifer

Victoria A. Trglavcnik, *The University of Western Ontario*

Supervisor: Dr. Clare Robinson, *The University of Western Ontario*

A thesis submitted in partial fulfillment of the requirements for the Master of Engineering Science degree in Civil and Environmental Engineering

© Victoria A. Trglavcnik 2016

Follow this and additional works at: <https://ir.lib.uwo.ca/etd>



Part of the [Environmental Engineering Commons](#)

Recommended Citation

Trglavcnik, Victoria A., "Combined Analysis of Tide- and Wave-induced Water Table Fluctuations for Structural Characterization of a Coastal Aquifer" (2016). *Electronic Thesis and Dissertation Repository*. 4299.

<https://ir.lib.uwo.ca/etd/4299>

This Dissertation/Thesis is brought to you for free and open access by Scholarship@Western. It has been accepted for inclusion in Electronic Thesis and Dissertation Repository by an authorized administrator of Scholarship@Western. For more information, please contact wlsadmin@uwo.ca.

Abstract

Understanding of coastal hydrogeology is essential for the assessment, management, and protection of coastal groundwater resources. Coastal groundwater is often an important source of drinking water for coastal communities but can be contaminated by saltwater or human-derived contaminants. The groundwater table in coastal aquifers fluctuates in response to various oceanic pressure forces acting at the shoreline, including tides, individual waves, and offshore storms. Measurements of water table fluctuations in response to tides and waves can be used to characterize coastal aquifers and provide important insight into the hydraulic properties and structure, including the connectivity between the aquifer and ocean. Most studies use simple laboratory, analytical, or numerical experiments to study the effects of ocean forces on coastal groundwater table fluctuations rather than collecting data in real field settings. This study presents an improved approach of understanding coastal aquifers by evaluating groundwater level fluctuations in response to pressure forces from tides and waves due to offshore storms (i.e. storm pulse). Long-term continuous groundwater level data collected on a sand barrier island (Sable Island, NS, Canada) suggest heterogeneous propagation of pressure forces from tides and storm-induced waves through the aquifer system. Groundwater levels in isolated inland areas were found to be highly fluctuating in response to tides and waves suggesting that the coastal aquifer is not homogeneous and isotropic as previously reported. It is hypothesized that observations are due to the presence of a layered aquifer system with localized leakage of pressure forces from an underlying confined aquifer that is connected to the ocean slightly offshore of the coastline. Two-dimensional numerical groundwater flow simulations were conducted in MODFLOW-2000 to test if the leaky confined-unconfined aquifer conceptualization is able to explain the tide-induced inland groundwater level fluctuations observed. The effects of key aquifer parameters (e.g. aquifer storage, depth of buried confining layer, width of leak) were investigated through model simulations and the presented model setup is consistent with observations. This study shows that analysis of both tidal and storm pulse propagation may be a valuable and affordable approach to investigate complex coastal aquifers. Comparison of field data with existing analytical solutions, however, suggests more work is required to describe the effects of tides and offshore storms on groundwater table fluctuations in complex aquifer settings. Improved methods for coastal

aquifer characterization will assist in the development of effective management strategies required for the many coastal aquifers worldwide that are impacted by human activities.

Keywords

Water table fluctuations, coastal aquifer, groundwater dynamics, tide propagation, offshore storms, groundwater pulse, shoreline setup, numerical modelling, field investigation

Co-Authorship Statement

This research was supplements work initiated by Environmental Sciences Group (ESG) from the Royal Military College of Canada (RMC) and commissioned by Parks Canada Agency (PCA). ESG and PCA provided logistical assistance before and during execution of the field program on Sable Island, NS, which was developed and carried out by ESG personnel, Dr. Clare Robinson, and the candidate. The candidate conducted data analysis and interpretation, numerical modelling, and drafts of all chapters of this thesis under the guidance of Dr. Clare Robinson. The co-authorship breakdown of Chapter 3 is as follows:

Chapter 3: Combined analysis of tide- and wave-induced water table fluctuations for structural characterization of a coastal aquifer.

Authors: Victoria Trglavcnik, Dean Morrow, Clare Robinson

Contributions:

Victoria Trglavcnik conducted collection and analysis of field data, numerical model development and simulation, and interpretation of results to prepare a draft of the chapter.

Dean Morrow, of ESG, assisted in developing and implementing the field monitoring program and with field data collection.

Clare Robinson initiated the topic of this research and field monitoring program with ESG, conducted field data collection, supervised data analysis and numerical simulations, and reviewed the draft chapter.

Acknowledgments

I would like to thank my advisor Dr. Clare Robinson for all the support and guidance she has offered me, firstly in my undergraduate years, and then while we completed this thesis. Her mentorship has largely contributed to my success at Western, and only through her suggestion did I even consider graduate school. Thank you Clare for your continuous encouragement, patience, and positivity throughout the duration of my Masters, and for providing me with the opportunity to study Sable Island and share our work.

I'd like to acknowledge Environmental Sciences Group (ESG) and Parks Canada Agency (PCA) who assisted in the development and implementation of the Sable Island project. I extend my immense gratitude to the field team, including Dean Morrow, Tom Partridge, Alaina Leslie, Jeremy Archer, and Capt. Shawn Burdett, and also Mike DeArruda who assisted with getting everyone (and all equipment) on and off site. Special thank-you to Dean for acting like an external advisor to me by providing his leadership and hard work ethic on site, while making field trips enjoyable. Valuable resources and experience was also provided by the ESG project management team, consisting of Dr. Kela Weber, Darren White, Viviane Paquin, and Dr. Daniela Loock. PCA commissioned the site assessment that inspired this research and facilitated transportation to the island, and Aaron Carpenter and Darryl Mooney (PCA) provided full access and support while the field team was on site.

Thank you to all my close friends (in and out of RESTORE) who supported me throughout my time at Western. I am grateful for all the encouragement you showed me, and for being a source of great stress relief – sharing copious amounts of coffee and nature walks on campus, spending time contemplating life and data trends in the Aquifer, and sharing in my work-life balance (i.e. music, movies, colouring, etc.).

Lastly, thank you to my entire family for their aggressive support and love that I've been lucky to receive my entire life. Honorable mention goes to my mother, Tina, my personal cheerleader and who suggested I study engineering in the first place; my father, Max, for his practical advice that helps me persevere through hardships; and to my older sister, Valentina, who can always cheer me up with her kindness and generosity.

Table of Contents

Abstract	ii
Co-Authorship Statement.....	iv
Acknowledgments.....	v
List of Tables	ix
List of Figures	x
List of Appendices	xiv
List of Symbols	xv
Chapter 1	1
1 Introduction	1
1.1 Background	1
1.2 Research Objectives.....	2
1.3 Thesis Outline	3
1.4 References.....	4
Chapter 2.....	5
2 Literature Review.....	5
2.1 Introduction.....	5
2.2 Influence of oceanic forcing on coastal aquifers	5
2.2.1 Tides.....	9
2.2.2 Waves.....	12
2.3 Aquifer characterization by analysis of tide and wave signal propagation	15
2.4 Numerical modelling of coastal aquifers	19
2.5 Sable Island: field site description	21
2.6 Summary.....	25
2.7 References.....	26

Chapter 3.....	32
3 Combined Analysis of Tide- and Wave-induced Water Table Fluctuations for Structural Characterization of a Coastal Aquifer.....	32
3.1 Introduction.....	32
3.2 Field Description and Methodology	37
3.2.1 Field Site	37
3.2.2 Data Collection	39
3.2.3 Analysis of Tidal Signal Propagation	41
3.2.4 Analysis of Storm Pulse Signal Propagation	44
3.2.5 Numerical Groundwater Flow Modelling.....	46
3.3 Results and Discussion	48
3.3.1 Time Series Analysis	48
3.3.2 Analysis of Tidal Signal Propagation	49
3.3.3 Analysis of Storm Pulse Signal Propagation	56
3.3.4 Numerical Groundwater Flow Model.....	60
3.4 Conclusions.....	63
3.5 References.....	65
Chapter 4.....	70
4 Summary and Conclusions.....	70
4.1 Summary.....	70
4.2 Recommendations.....	72
4.3 References.....	74
Appendices.....	76
Appendix A: Groundwater Monitoring Network.....	76
Appendix B: Calculation of Tidal Signal Attenuation Factors	80
Appendix C: Calculation of Storm Pulse Signal Attenuation Factors	89

Appendix D: Numerical Modelling Simulations	96
Appendix E: Governing Equations for MODFLOW-2000.....	103
Curriculum Vitae	106

List of Tables

Table 2-1 Historic precipitation climate normals (1971-2000) for Sable Island and Halifax, NS. Percent of annual total is indicated in parenthesis.....	24
Table 3-1 Aquifer parameters diffusivity (D) and slope factor (SF) estimated by amplitude-resolved (k_r) and phase-resolved (k_i) wave numbers calculated from tidal harmonics analysis.....	56
Table 3-2 Calculated and modelled amplitude attenuation factor (α_t) of an M2 semi-diurnal tide of 0.55 m amplitude.....	61
Table A-1 Continuous groundwater level monitoring well schedule.....	77
Table B-1 Tidal signal attenuation factors of amplitude attenuation (α_t) and phase lag ($\Delta\phi_t$) calculated at monitoring wells on Sable Island, by least-squares fitting of groundwater level and tide height time series data to the M2 semi-diurnal tidal harmonic oscillation ($\omega = 12.14$ rad/d).....	81
Table C-1 Non-dimensional storm pulse signal attenuation factors of amplitude attenuation (α_w) and phase lag ($\Delta\phi_w^*$), and distance to the shoreline (x^*), calculated at monitoring wells on Sable Island.....	91
Table D-1 Comparison of tidal signal attenuation factor (α_t) calculated from field data and from various saturated groundwater flow models simulated in MODFLOW-2000.....	97

List of Figures

Figure 2-1 Conceptual model adapted from Nielsen (2009) of a nearshore coastal aquifer exposed to fluctuations in instantaneous water surface [$\eta(x, t)$] due to tides and waves, and the resulting water table over height (η_w^+), shoreline setup (η_s), and wave setup (η^+) of the mean water surface (MWS) above still water level (SWL)..... 6

Figure 2-2 Comparison of signal propagation through a coastal aquifer, predicted by analytical solutions for tides (solid lines, according to Turner et al. (1997) non-dimensionalized by D and ω) and shoreline setup pulse (dashed line, according to Li et al. (2004) non-dimensionalized by D and storm duration parameter B)..... 19

Figure 2-3 Maps showing (a) location of Sable Island in the Atlantic Ocean relative to Nova Scotia, (b) Sable Island labelled with locations of the Main Station area. Imagery obtained by Google Earth. 22

Figure 3-1 Conceptual models to show the effects of tides and waves on a homogeneous unconfined aquifer system (top) versus a leaky confined-unconfined aquifer connected to the ocean offshore and with localized leakage landward of the shoreline (bottom)..... 36

Figure 3-2 Maps showing (a) location of Sable Island in the Atlantic Ocean relative to Nova Scotia, Canada, (b) locations of the Main Station area, Ocean Ltd. offshore wave buoy, Environment Canada weather station 8204703, and the Canadian Department of Fisheries and Oceans tide gauge station 550; and (c) the Main Station area with locations of continuous long-term monitoring wells indicated by white dots and select wells labelled with their respective I.D.s by red dots. 38

Figure 3-3 Geometry, boundary conditions, and parameters used to model an unconfined-leaky confined aquifer with a discontinuous impermeable confining layer that intersects the seabed 95 m offshore of the estimated mean shoreline position, i.e. the coordinate origin (0,0) (horizontally) which is at mean seal level (MSL) (vertically) as indicated by the dashed line. 47

Figure 3-4 Continuous data of (a) groundwater table elevation, measured in metres above sea level (masl); (b) significant wave height (masl), tide height (masl), and daily precipitation measured in millimeters (mm) from 20 June – 21 August, 2015. 49

Figure 3-5 Fast Fourier Transform (*FFT*) analysis results for (a) tide height data over the period of Aug 2014 - Dec 2015, and groundwater monitoring wells (b) Transect 1; (c) A2-14-MW-2; (d) A3-14-MW-2; (e) MW12-9. 50

Figure 3-6 Tidal signal propagation across Sable Island’s Main Station. Coloured contours represent (a) amplitude attenuation ratio (α_t) [-] and (b) phase lag ($\Delta\phi_t$) [hrs] of groundwater level fluctuation relative to the dominant M2 tidal signal ($\omega = 12.14$ rad/d). 52

Figure 3-7 Calculated amplitude attenuation α_t [-] versus phase lag ($\Delta\phi_t$) [hrs] for groundwater monitoring wells clustered in areas with high aquifer-ocean connectivity (a) adjacent to the north beach shoreline, (b) Area 1, and (c) Area 2. 54

Figure 3-8 Coloured contours of calculated (a) amplitude attenuation (α_t) [-] and (c) phase lag ($\Delta\phi_t$) [hrs] for Area 1, as an example of an area of enhanced tidal influence. 55

Figure 3-9 (a) Nearshore groundwater levels, in metres above sea level (masl), near the north (Transect 1) and south (Transect 6) shorelines, and shoreline setup (masl) calculated using data from an offshore wave buoy, from 14 Sept – 16 Nov, 2014. 57

Figure 3-10 Analysis of storm pulse propagation for two isolated wave events (a) $\ln(\alpha_w)$ [-] versus non-dimensionalized distance (x^*) inland [-], and (b) $\Delta\phi_w^*$ [-] versus x^* . Field data for all monitoring wells are shown with labels provided only for select monitoring wells. 58

Figure 3-11 Comparison of average calculated tide-induced groundwater level fluctuations (solid coloured lines) and numerical simulation results (black lines) for monitoring wells (a) Transect 1, (b) A2-14-MW-2, and (c) MW12-9. 62

Figure A-1 Sable Island Main Station labelled with monitoring wells used for continuous data collection for analysis of tidal and storm pulse signal propagation, and their respective I.D.s. Imagery provided by Esri Basemaps. 76

Figure B-2 Transect 1 harmonic least-squares fitting results for four subsets of time series data (a) 26 – 28 September, 2014, (b) 23 - 27 August, 2014 (c) 9 – 11 June, 2015 and (d) 15 – 22 August, 2015.	84
Figure B-3 A2-14-MW-2 harmonic least-squares fitting results for four subsets of time series data (a) 9 – 14 October, 2014, (b) 9 – 10 June, 2014 (c) 5 – 6 August, 2015 and (d) 16 - 20 August, 2015.	85
Figure B-4 MW12-9 harmonic least-squares fitting results for four subsets of time series data (a) 8 - 11 October, 2014, (b) 7 – 9 March, 2014 (c) 17 - 19 April, 2015 and (d) 8 – 12 June, 2015.	86
Figure B-5 LT-3 harmonic least-squares fitting results for four subsets of time series data (a) 23 – 26 November, 2014, (b) 26 – 28 December, 2014 (c) 7 – 10 March, 2015 and (d) 16 – 18 May, 2015.	87
Figure C-6 Gaussian least-squares fitting results for wave event 1 (15 – 21 September, 2014). All plots show Hamming filtered shoreline elevation in blue, and Hamming filtered groundwater levels for (a) Transect 1 (red), (b) A2-14-MW-2 (orange), (c) MW12-9 (green), and (d) A3-14-MW-2 (yellow).	93
Figure C-7 Gaussian least-squares fitting results for wave event 2 (1 – 8 October, 2014). All plots show Hamming filtered shoreline elevation in blue, and Hamming filtered groundwater levels for (a) Transect 1 (red), (b) A2-14-MW-2 (orange), (c) MW12-9 (green), and (d) A3-14-MW-2 (yellow).	94
Figure D-1 Simulation results for a heterogeneous leaky confined-unconfined aquifer with 10 m wide discontinuity (a – b, case 1 Table D-1), and with no discontinuity (c – d; case 2 in Table D-1).	99
Figure D-2 Simulation results for a homogeneous unconfined aquifer (a – b, case 3 Table D-1), and leaky confined-unconfined aquifer with shallow sloping confining layer (c – d; case 4 in Table D-1).	100

Figure D-3 Simulation results for a leaky confined-unconfined aquifer with uniform confining layer located at 3.5 m (a – b, case 7 in Table D-1), and 21.5 m (c – d; case 8 in Table D-1).
..... 101

Figure D-4 Simulated heads for varied leaky confined-unconfined aquifer domains (case 1 in Table D-1) varied with (a) $S_y = 0.36$ (case 5), (b) $S_y = 0.20$ (case 6), (c) $K_{confining\ layer} = 10^{-3}$ m/d (case 9), and (d) 5 m wide inland discontinuity (case 10). 102

List of Appendices

Appendix A: Groundwater Monitoring Network	76
Appendix B: Calculation of Tidal Signal Attenuation Factors	80
Appendix C: Calculation of Storm Pulse Signal Attenuation Factors	89
Appendix D: Numerical Modelling Simulations	96
Appendix E: Governing Equations for MODFLOW-2000	103

List of Symbols

Roman symbols

A_{GWL}	Amplitude of storm-induced groundwater level pulse, m.
A_{SL}	Amplitude of storm-induced shoreline elevation pulse, m.
B	Gaussian storm pulse time factor, $[T^{-2}]$.
C_u	Uniformity coefficient.
D	Aquifer diffusivity, or the ratio of T and S , m^2/s .
D_{amp}	Aquifer diffusivity calculated using tidal signal amplitude attenuation factor, m^2/s .
D_{pha}	Aquifer diffusivity calculated using tidal signal phase lag factor, m/s .
d	Aquifer depth, m.
d_{10}	Effective soil grain size, mm.
g	Gravitational constant, m/s^2 .
h	Groundwater level, or shoreline elevation, fluctuating in response to tides or storm-induced waves, m.
h_0	Mean groundwater level or shoreline elevation, m.
H_{0rms}	Offshore root mean square wave height, m.
H_s	Offshore significant wave height, m.
HWM	High water mark.
K	Hydraulic conductivity, m/s .
k_i	Wave number, or rate of tidal signal amplitude decay, m^{-1} .
k_r	Wave number, or rate of linear increase in tidal signal phase lag, $[T]/m$.
L_i	Specific leakage of groundwater from an unconfined aquifer, inland of the coast.
L_o	Specific leakage of seawater through a confining layer extending offshore.

L_0	Deep water wave length, m.
LWM	Low water mark.
MWS	Mean water surface.
S	Confined aquifer storage coefficient.
SF	Slope factor, ($= \sqrt{[D_{amp} \text{ and } D_{pha}]}$).
SWL	Still water level.
S_y	Unconfined aquifer specific yield.
T	Aquifer transmissivity, m^2/d .
t	time, [T].
t_0	Period of tidal fluctuations, [T].
T_p	Peak wave period, s.
$t_{p,GWL}$	Time of peak storm-induced groundwater level pulse.
$t_{p,SL}$	Time of peak storm-induced shoreline elevation.
x	Perpendicular distance to shoreline, or tidal line source, m.
x^*	Non-dimensional distance to the shoreline, or tidal line source.
z_{sl}	Elevation of shoreline position, metres above sea level (masl).
z_{tide}	Tide elevation, metres above sea level (masl).

Greek symbols

α_{GWL}	Amplitude of tide-induced groundwater level fluctuations, m.
α_t	Tidal signal amplitude attenuation factor ($= \alpha_{GWL}/\alpha_{tide}$).
α_{tide}	Amplitude of tidal fluctuations, m.
α_w	Storm pulse amplitude attenuation factor ($= A_{GWL}/A_{SL}$).
β	Slope, m/m.
$\Delta\phi_t$	Tidal signal phase lag factor ($= \phi_{GWL} - \phi_{tide}$).

ϕ_{GWL}	Phase of tide-induced groundwater level fluctuations, relative to a pure cosine wave, rads.
ϕ_{tide}	Phase of ocean level tidal fluctuations, relative to a pure cosine wave, rads.
$\Delta\phi_w$	Storm pulse phase lag factor ($=t_{p,GWL} - t_{p,SL}$).
$\Delta\phi_w^*$	Non-dimensional storm pulse phase lag factor.
η	Surface water elevation, metres above sea level.
η^+	Wave setup above the still water level, m.
η_s	Wave-induced shoreline setup above the still water level, m.
η_w^+	Water table over height above mean sea level, m.
τ	Non-dimensional storm pulse propagation parameter.
ω	Angular tidal frequency, rad/[T].

Chapter 1

1 Introduction

1.1 Background

Coastal groundwater dynamics are extremely complex due to various oceanic forcing (e.g. tides, waves) that impact groundwater levels and flows in coastal aquifers (Trefry and Bekele, 2004). There is a need for comprehensive understanding of coastal aquifer hydrogeology (i.e. aquifer structure and properties) to inform effective coastal water resource management decisions and programs aimed at the sustainable management of groundwater resources. For instance, coastal communities often rely on groundwater for drinking water supply, however, coastal aquifers are vulnerable to contamination by saltwater intrusion and anthropogenic contaminants. Groundwater contamination also poses a threat to important receptors, such as adjacent nearshore waters, with groundwater discharge now well recognized as a potentially important pathway for delivering contaminants to the ocean (e.g. Alcolea et al., 2007).

Tides and waves exert pressure forces on coastal aquifers at the aquifer-ocean interface and result in same-period fluctuations of groundwater levels. With increasing distance inland from the aquifer-ocean interface, the amplitude of water table fluctuations is damped and delayed relative to the forcing signal. The rate at which the forcing signal is attenuated landward of the aquifer-ocean interface depends on period of the forcing signal and aquifer storage properties (i.e. specific yield S_y for unconfined aquifers, or storage S for confined aquifers) (Turner et al., 1997). Extensive research has been conducted into propagation of tidal signals through coastal aquifers via analytical (e.g. Ferris, 1952) and numerical models (e.g. Alcolea et al., 2007) and has led to well-developed aquifer characterization methods using tides. Site investigations that use analysis of tide-induced groundwater level fluctuations can be beneficial over traditional field tests (e.g. pumping test) as this approach is more affordable and may provide information over greater spatial scales (Trefry and Bekele, 2004). However, tidal propagation methods are often implemented in simple aquifer settings (i.e. single layer permeable unconfined aquifer) with only a few studies

using analytical solutions derived for complex aquifer settings (e.g. Rotzoll et al., 2008; Sun et al., 2008). Also, analytical and numerical modelling studies often rely on a large number of assumptions (e.g. one dimension, vertical beach face) that may not be applicable in real-world settings. Generally, investigation of wave-induced groundwater dynamics has received little attention compared to tides with prior studies typically focusing on wave-induced groundwater flow patterns close to the shoreline (e.g. Robinson et al., 2014). Waves (which are characterized by enhanced wind speeds and wave heights) result in enhanced surface water elevations in the surf zone, termed wave setup, due to energy transfer as waves break offshore. Subsequently, wave setup leads to above-average elevation of shoreline position on the beach – this is called shoreline setup. Offshore storms (periods of intensified wave conditions) have been shown to enhance shoreline setup for multiple days (depending on the duration of the storm) such that setup oscillations can be represented by a Gaussian pulse force signal. Studies show that similar to tides, Gaussian storm pulse signals can propagate through coastal aquifers, and that due to a longer period, storm pulse signals can propagate farther inland relative to the tidal signal (Li et al., 2004). There is a large knowledge gap, however, since few studies have taken advantage of this difference to investigate inland propagation of storm pulse signals (e.g. Cartwright and Gibbes, 2011) or measured propagation rates of setup for the purpose of aquifer characterization (e.g. Rotzoll and El-Kadi, 2008). Analysis of both tidal and storm pulse signals may assist in evaluation of aquifer-ocean connectivity and considerably improve characterization of coastal aquifer systems to reveal the nature of complex aquifer structures (i.e. unconfined, confined, layered).

1.2 Research Objectives

The aim of this research is to provide insight into subsurface configuration of Sable Island, NS, Canada through combined analysis of tidal and storm pulse signal propagation through the coastal aquifer. Detailed analysis of groundwater level time series from an extensive groundwater monitoring network is used together with a groundwater flow model (MODFLOW-2000) to provide insight into the aquifer system's configuration on the elongated sand barrier island. This study is novel in that it is the first study with such a comprehensive groundwater level data set to analyze both tidal and storm pulse signal

propagation to provide understanding of the coastal hydrogeology. While data analysis presented in this thesis focuses on Sable Island, the approach used may be widely applicable to assist in characterization of complex coastal aquifers worldwide that are exposed to both tides and offshore storms (Cartwright and Gibbes, 2011).

1.3 Thesis Outline

This thesis is written in “Integrated Article Format.” A brief description of each chapter is presented below.

Chapter 1: Introduces the topic and states the research objectives.

Chapter 2: Describes the influence of tides and waves on coastal groundwater dynamics, and provides a review of relevant research previously conducted (e.g. analytical solutions developed for various coastal configurations and methods of aquifer characterization using tides and waves). A description of the island field site (Sable Island) is also provided.

Chapter 3: Details the field monitoring program, methods of analysis using groundwater level data, and numerical model development used in this study. Results are discussed and show the use of combined analysis of tides and offshore storms to evaluate coastal aquifer properties and provide insight into the configuration of the coastal aquifer system through numerical simulations.

Chapter 4: Summarizes findings and provides recommendations for future work.

Four appendices are included in this thesis to supplement data collection, methods, and results presented in Chapter 3.

Appendix A: Details the groundwater monitoring network used on Sable Island.

Appendix B: Describes the calculation of tidal signal attenuation factors and presents supplementary data for select groundwater monitoring wells.

Appendix C: Describes the calculation of storm pulse signal attenuation factors and presents supplementary data for select groundwater monitoring wells.

Appendix D: Provides governing equations for the numerical model used in this study (MODFLOW-2000).

1.4 References

Alcolea, A., E. Castro, M. Barbieri, J. Carrera and S. Bea (2007). "Inverse modeling of coastal aquifers using tidal response and hydraulic tests." Ground Water **45**(6): 711-722.

Cartwright, N. and B. Gibbes (2011). Oceanic Pulse Forcing of a Beach Groundwater System. 20th Australasian Coastal and Ocean Engineering Conference 2011, COASTS 2011 and the 13th Australasian Port and Harbour Conference 2011, PORTS 2011. Perth, West Australia, Curan Associates Inc: 197 - 202.

Ferris, J. G. (1952). Cyclic fluctuations of water level as a basis for determining aquifer transmissibility. Washington, D.C.

Li, L., N. Cartwright, P. Nielsen and D. Lockington (2004). "Response of coastal groundwater table to offshore storms." China Ocean Engineering **18**(3): 423-431.

Robinson, C., P. Xin, L. Li and D. A. Barry (2014). "Groundwater flow and salt transport in a subterranean estuary driven by intensified wave conditions." Water Resources Research **50**(1): 165-181.

Rotzoll, K. and A. I. El-Kadi (2008). "Estimating hydraulic properties of coastal aquifers using wave setup." Journal of Hydrology **353**(1-2): 201-213.

Rotzoll, K., A. I. El-Kadi and S. B. Gingerich (2008). "Analysis of an unconfined aquifer subject to asynchronous dual-tide propagation." Ground Water **46**(2): 239-250.

Sun, P., H. Li, M. C. Boufadel, X. Geng and S. Chen (2008). "An analytical solution and case study of groundwater head response to dual tide in an island leaky confined aquifer." Water Resources Research **44**(12): n/a-n/a.

Trefry, M. G. and E. Bekele (2004). "Structural characterization of an island aquifer via tidal methods." Water Resources Research **40**(1): W015051-W0150521.

Turner, I. L., B. P. Coates and R. I. Acworth (1997). "Tides, waves and the super-elevation of groundwater at the coast." Journal of Coastal Research **13**(1): 46-60.

Chapter 2

2 Literature Review

2.1 Introduction

This chapter reviews previous research focused on the response of coastal groundwater levels and flow patterns to oceanic forcing. Tides and waves produce pressure forcing signals at the shoreline. These forcing signals propagate through the aquifer matrix and induce same-period groundwater table fluctuations. However, the groundwater table fluctuations are damped and delayed relative to the forcing signal (i.e. tides or waves) with increasing inland distance from the coast due to aquifer storage. The rate at which oceanic forcing signals are attenuated with increasing inland distance can be calculated and used to estimate aquifer properties (e.g. specific yield [S_y] or storage [S], and transmissivity [T]) and provide insight into the subsurface structure (e.g. layered aquifer configuration). This chapter summarizes signal propagation methods currently used for coastal aquifer characterization, as well as numerical modelling studies that have investigated coastal water table response to tides and waves. This thesis is focused on analysis of data collected on Sable Island, NS, Canada, and therefore, a summary of site characteristics is also provided.

2.2 Influence of oceanic forcing on coastal aquifers

Groundwater levels and flow patterns in coastal aquifers are highly complex and dynamic due to oceanic forcing such as tides and waves (e.g. Nielsen, 1990; Hegge and Masselink, 1991; Hanslow and Nielsen, 1993; Turner et al., 1997). Oceanic forcing on coastal aquifers can impact the fate and transport of groundwater contaminants and can potentially threaten adjacent surface waters (i.e. the ocean), drinking water supplies, and overall integrity of coastal ecosystems (e.g. La Licata et al., 2011; Gonnee et al., 2013). For example, infiltration of seawater into the nearshore aquifer due to tides and waves, and consequent mixing with terrestrially-derived fresh groundwater, impacts groundwater flows and geochemical conditions in aquifers near the shore and subsequent discharge of groundwater contaminants to the ocean (e.g. Robinson et al., 2014). Groundwater table fluctuations

induced by tides and waves in the nearshore aquifer, particularly close to the aquifer-ocean interface, can also affect sediment transport and beach profile change (e.g. Duncan, 1964; Turner, 1995; Masselink et al., 2009). A simplified conceptual model of a coastal aquifer exposed to oceanic forcing is shown in Figure 2-1 to illustrate key features with respect to the way in which oceanic forcing influences nearshore groundwater dynamics. Important features of the nearshore environment include the surf zone, swash zone, and sloping aquifer-ocean interface separating the coastal aquifer from the adjacent coastal water body (i.e. the ocean). The offshore extent of the surf zone is where the largest waves start to break (location depends on tide height, wave parameters, and depth of the water column)

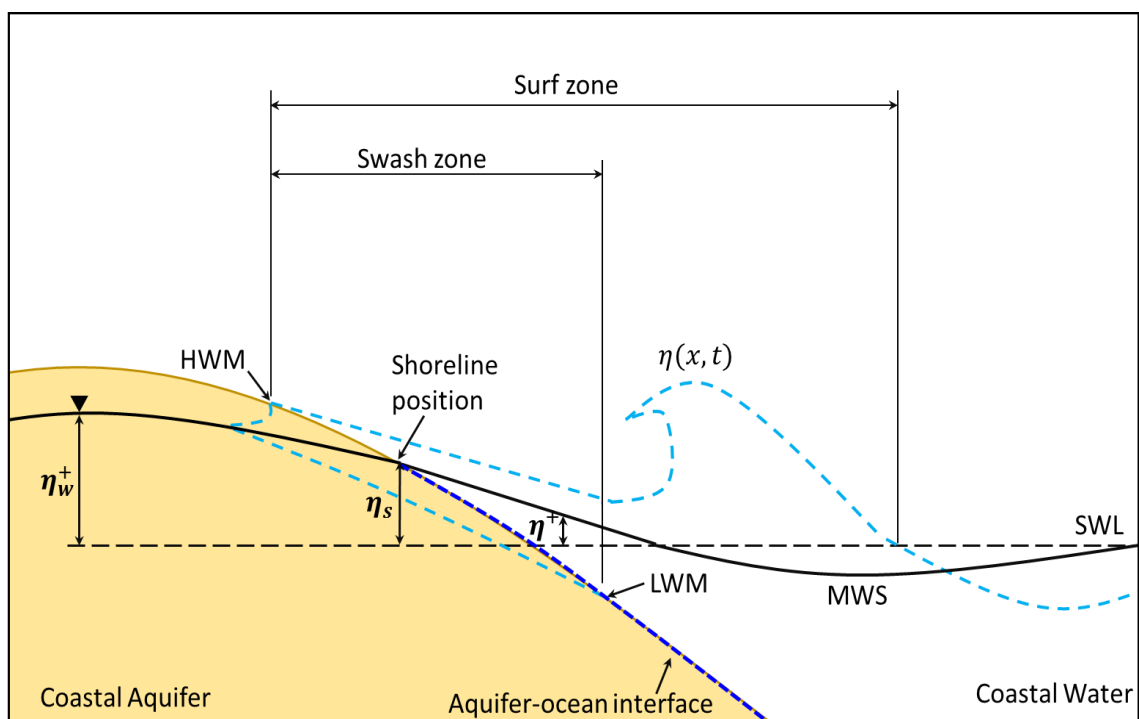


Figure 2-1 Conceptual model adapted from Nielsen (2009) of a nearshore coastal aquifer exposed to fluctuations in instantaneous water surface [$\eta(x, t)$] due to tides and waves, and the resulting water table over height (η_w^+), shoreline setup (η_s), and wave setup (η^+) of the mean water surface (MWS) above still water level (SWL). The nearshore environment is characterized by the swash zone (bounded by the high water mark [HWM] and low water mark [LWM]), and the surf zone (bounded by the HWM and offshore location of waves breaking). The aquifer-ocean interface is indicated by the blue dashed line.

and it extends to the farthest inland location reached by waves rushing the beach (i.e. the high water mark, HWM) (Nielsen, 2009). The swash zone is defined by the maximum and minimum wave run-up elevations (i.e. HWM and low water mark, LWM) (Nielsen, 2009). The still water level (SWL) is the mean surface water level (in the absence of waves) that fluctuates with the tides, while wave action results in changes in instantaneous surface water elevation [$\eta(x,t)$] (Nielsen, 2009). Oceanic forcing (i.e. tides and waves) cause inland groundwater levels to become elevated above the SWL. This is termed super elevation (or water table over height, η_w^+) (Turner et al., 1997), and has been shown to impact groundwater discharge rates and delivery of associated pollutants (e.g. nutrients, pesticides, heavy metals, hydrocarbons) to coastal waters (e.g. Li and Jiao, 2003; Robinson et al., 2009; Moore, 2010; Geng and Boufadel, 2015). However, studies often assume that the groundwater table elevation far inland of the shoreline is equivalent to mean sea level (i.e. SWL) (e.g. Jiao and Tang, 1999). In coastal environments individual waves (or longer period surface water oscillations) approach the beach, and cause instantaneous movement of the shoreline position up and down the beach face. This is termed wave run-up and is a function of beach slope, slope roughness, sand permeability (and sediment grain size), local wave climate (i.e. wave steepness), and nearshore bathymetry. Infiltration of seawater into the nearshore aquifer due to run-up (and also tides) results in η_w^+ (Turner et al., 1997). As waves break inside the surf zone, the transfer of wave energy causes a sloping increase of the phase averaged mean water surface (MWS) above the SWL, which is termed wave setup (η^+) (Nielsen, 2009). In contrast to wave setup, shoreline setup η_s is the time-averaged increase in the elevation of the shoreline above SWL. Shoreline setup is discussed in more detail in Section 2.2.2.

While studies show that understanding the influence of oceanic forcing on coastal aquifers is important for nearshore groundwater flow dynamics and contaminant transport, evaluating groundwater fluctuations in response to oceanic forcing can also provide substantial insight into coastal aquifer heterogeneity. Oceanic forcing acting at the aquifer-ocean interface (Figure 2-1) propagate inland through the aquifer and result in groundwater levels that fluctuate in direct response to the magnitude and frequency of the forcing signal, as well as aquifer storage properties (e.g. S_y , S , and T). Thus, analyzing the inland propagation of oceanic forcing signals can shed light on aquifer properties and the structure

of a coastal aquifer system. Most prior coastal groundwater studies evaluating the effects of oceanic forcing focus on analysis of groundwater levels, flow patterns and contaminant transport very close to the shore (e.g. Boufadel et al., 2007; Robinson et al., 2007; Anwar et al., 2014; Robinson et al., 2014), and the development of analytical solutions to evaluate and predict tide-induced water table fluctuations (Song et al., 2007). Few studies (e.g. Trefry and Bekele, 2004; Rotzoll et al., 2008; Sun et al., 2008; Xun et al., 2015) provide detailed analysis of field data compared to analytical or numerical solutions describing tide-induced propagation to improve coastal aquifer characterization, and significantly less studies analyze wave signal propagation through real coastal aquifers (Cartwright and Gibbes, 2011).

The beach sediment matrix has a filtering capacity such that only pressure fluctuations with larger amplitude and/or longer periods are able to propagate through the aquifer (Hegge and Masselink, 1991). Well-defined methods of tidal signal propagation analysis are available to characterize coastal aquifers using analytical solutions (e.g. Ferris, 1952; Erskine, 1991) or numerical modelling and parameter estimation tools (e.g. Alcolea et al., 2007; Rotzoll et al., 2008). These methods, however, are often based on numerous simplifying assumptions (e.g. homogeneous and isotropic one-layer aquifer) that are not always representative of real aquifer systems. Also, wave forcing is typically neglected and few studies consider propagation of wave forcing to estimate aquifer properties (Li et al., 2004). There is a need to improve techniques of characterizing complex coastal aquifers via analysis of oceanic forcing signals as this represents a low-resource intensive approach that enables larger scale evaluation rather than drilling multiple boreholes. Reliable estimates of aquifer structure and properties (e.g. aquifer depth [d], hydraulic conductivity [K]) are critical to inform the development of effective coastal water resource management tools (e.g. numerical models) including investigations of groundwater availability, source water protection for drinking water, and protection of coastal ecosystems from degradation due to groundwater contamination (i.e., saltwater intrusion, mobility of anthropogenic contaminants).

2.2.1 Tides

The influence of tides on coastal aquifers, in particular the propagation of the tidal signals through aquifers, has been extensively studied (e.g. Ferris, 1952; Carr and Van Der Kamp, 1969; Nielsen, 1990; Turner et al., 1997; Kim et al., 2005; Shih et al., 2008; Hsieh et al., 2015). Early studies by Jacob (1950) and Ferris (1952) developed simple analytical solutions for tide-induced groundwater table fluctuations through a horizontal, homogeneous and isotropic confined aquifer extending infinitely landward from a vertical beach face. Assuming a one-dimensional system exposed to a monochromatic sinusoidal tidal signal the fluctuating groundwater level h can be described by:

$$h(x, t) = \alpha_{tide} \exp\left(-x \sqrt{\pi S / t_0 T}\right) \sin\left(\frac{2\pi}{t_0} t - x \sqrt{\pi S / t_0 T}\right) \quad (2-1)$$

where x is perpendicular inland distance from the shoreline, α_{tide} and t_0 are amplitude and period of the tidal fluctuations, respectively, and S and T are the storage and transmissivity of the aquifer, respectively (Turner et al., 1997). When α_{tide} is relatively small compared to aquifer depth (d), vertical flows can be neglected and Eq. (2-1) can be applied in an unconfined aquifer setting (Ferris, 1952). The solution indicates that as the tidal signal propagates through an aquifer, the resulting water table fluctuations become increasingly damped (attenuated) and delayed (phase-shift) with increasing distance x from the coast. From Eq. (2-1) it can be seen that the rate of attenuation (i.e. amplitude damping, and phase lag, versus x) depends on t_0 and aquifer properties (i.e. S and T). In unconfined permeable coastal aquifers, complete attenuation may occur within a few hundred metres of the shoreline; however, decreased storage (S) in confined aquifers results in more rapid and less damped propagation of tidal fluctuations, and in some cases, fluctuations may reach thousands of metres inland (Jha et al., 2008). Analytical solutions (e.g Eq. (2-1), Jacob (1950)-Ferris (1952)) are often derived from the one-dimensional (1D) Boussinesq equation with many simplifying assumptions adopted (e.g. homogeneity, vertical beach face, non-linear effects such as capillarity and infiltration of wave run-up) to analyze fluctuations in simple aquifer settings (i.e. via laboratory experiments, 1D numerical studies). As such, findings derived from these solutions may not be applicable for complex settings.

More advanced analytical solutions have been developed for single layer aquifer characterizations that consider non-linear effects such as a sloping beach face (e.g. Nielsen, 1990; Li et al., 2000; Teo et al., 2003), seepage face formation (i.e. decoupling of the ocean surface and groundwater table on the beach) (e.g. Nielsen, 1990), and vertical capillary flow (e.g. Li et al., 2000; Jeng et al., 2005; Kong et al., 2013). Most solutions consider monochromatic diurnal (tidal fluctuations with one daily high and one daily low elevation) or semi-diurnal tidal forcing (tidal stage with two daily highs of similar stage and two daily lows of similar tidal stage), however, bichromatic (i.e. dual-frequency) spring-neap tides have also been studied (e.g. Raubenheimer et al., 1999; Li et al., 2000; Robinson et al., 2007; Heiss and Michael, 2014). Spring-neap tidal cycles are associated with a longer period relative to monochromatic tidal cycles (Li et al., 2000) which results in lower frequency water table fluctuations and ultimately greater inland propagation of the tidal signal through the coastal aquifer relative to diurnal or semi-diurnal tide-induced fluctuations (Jeng et al., 2005). Analytical solutions for dual-tidal forcing environments (as can occur on islands, atolls, peninsulas) where tidal signals propagate from opposite shorelines have also been developed (e.g. Townley, 1995; Rotzoll et al., 2008; Sun et al., 2008; Huang et al., 2012; Wang et al., 2013). Field studies show that interference of the tidal signal can occur at inland locations (i.e. mid-island) for narrow sand barrier islands (Trefry and Bekele, 2004).

While most analytical solutions have been developed for single-layer aquifer systems, complex layered aquifer systems are in reality more common (Li and Jiao, 2003). For example, a coastal aquifer system may consist of an unconfined aquifer overlying a confined aquifer with the aquifer units separated by a confining layer of relatively lower permeability (layering of multiple confining layers and aquifer units can also exist). Jiao and Tang (1999) developed an analytical solution for water table fluctuations in a layered aquifer system exposed to tides (and with a vertical beach face) where a thin semi-permeable confining layer (of negligible storage) separates an unconfined aquifer from a lower confined aquifer. They assumed that, due to relatively high S_y , tidal fluctuations are rapidly damped in the unconfined aquifer resulting in a constant water table equal to mean sea level; however, tides can propagate farther through the confined aquifer due to decreased confined storage (S). This leads to a head difference between the upper and lower

aquifer units that induces leakage, and results in significant damping of groundwater level fluctuations in the confined aquifer (Jiao and Tang, 1999). Other studies focused on two-layer unconfined-confined systems (e.g. Li et al., 2001; Jeng et al., 2002; Li et al., 2002) found that neglecting unconfined water table fluctuations may result in over prediction of the damping and under prediction of phase lags of fluctuations in the confined aquifer, and that the interaction between aquifer units depends on the amount of leakage as well as the ratios between aquifer transmissivity and storage values (e.g. transmissivity ratio $T_{ratio} = T_{unconfined}/T_{confined}$, storage ratio $S_{ratio} = S_u/S_c$). An important finding from Jeng et al. (2002) is that unconfined water table fluctuations increase in amplitude (and decrease in phase lag) with increased upwards leakage, and with decreased S_{ratio} or increased T_{ratio} . Leakage-induced water table fluctuations were also examined in the analytical study conducted by Li et al. (2002) for a leaky confined-unconfined aquifer system with a low- K barrier at the unconfined aquifer-ocean boundary. These are the only studies to describe the potential for enhanced water table fluctuations in the unconfined aquifer layer due to leakage from an underlying confined aquifer.

Many analytical studies (e.g. Jiao and Tang, 1999) assume all aquifer units terminate at the shoreline. This is often not reality and a confining layer may extend offshore for some distance creating an offshore roof. Analytical solutions for tide-induced groundwater fluctuations in submarine confined-unconfined aquifers have been developed (e.g. van der Kamp, 1972; Li and Chen, 1991; Guo et al., 2007). Li and Jiao (2001) combined the solutions of Li and Chen (1991) and Jiao and Tang (1999) to evaluate tide-induced groundwater level fluctuations in a layered leaky confined-unconfined coastal aquifer system with a finite offshore roof, and identified two distinct areas of leakage into the confined aquifer – seawater leakage through the roof (L_o), and inland groundwater leakage (L_i) from the unconfined aquifer. The offshore length of the roof, magnitude of leakage, and ratio of L_o and L_i , were found to be influencing factors on propagation of the tidal fluctuations through the confined aquifer. Chuang and Yeh (2007) and Chuang and Yeh (2008) more recently considered the effects of water table fluctuations in the overlying unconfined aquifer, which were found to enhance leakage and cause increased tide-induced groundwater fluctuations in the confined aquifer.

The importance of leakage on groundwater level fluctuations has also been shown in other aquifer settings (e.g. Guo et al., 2007; Xia et al., 2007; Chuang et al., 2010; Asadi-Aghbolaghi et al., 2014) which further indicate that leakage can transmit or inhibit tidal signal propagation through coastal aquifers. Additional studies by Li and Jiao (2001) and Chuang et al. (2012) found that storage and thickness of the semi-permeable confining layer and super elevation of groundwater levels in the unconfined nearshore aquifer (η_w^+) may also influence confined aquifer fluctuations under certain conditions. A large number of analytical solutions have been developed that explore tide-induced groundwater fluctuations for simple and complex aquifer settings; however, detailed analysis and interpretation of field data collected in complex aquifers is limited. There is a need to evaluate the applicability of these analytical solutions and their findings with real field data.

2.2.2 Waves

Deep surface water waves offshore propagate towards the shoreline until at some shallow water depth they become hydrodynamically unstable and break. Once a wave approaches the shoreline, it modifies the mean surface water level (MWS) at the beach, and in turn, groundwater levels near the aquifer-ocean interface (Figure 2-1) (Nielsen, 2009). Coastal groundwater table fluctuations and resulting groundwater flow patterns are impacted by wave processes (i.e. wave setup, shoreline setup, and wave run-up, as shown in Figure 2-1) that result in pressure forces (i.e. radiation stress) acting on the aquifer-ocean interface, and infiltration of seawater into the nearshore aquifer (Hegge and Masselink, 1991).

Wave setup is a time-averaged wave effect caused by deep water waves approaching a sloping beach face (Longuet-Higgins and Stewart, 1964). Wave setup is the upward tilt of the ocean water surface near the shoreline to balance dissipating wave energy from breaking waves and leads to an increase in elevation of the shoreline position (i.e. where the groundwater table and surface water intersect at the beach face) above the SWL. The enhanced elevation in the shoreline position is termed shoreline setup (η_s). Hanslow and Nielsen (1993) conducted a field study on four sandy beaches in New South Wales, Australia, and determined a relationship between η_s with offshore root mean square wave height (H_{0rms}) and deep water wave length (L_o):

$$\eta_s = 0.048\sqrt{H_{0rms}L_0} \quad (2-2)$$

H_{0rms} is a function of significant wave height (H_s), defined as the mean wave height of the highest third of waves. H_s is calculated as:

$$H_{0rms} = H_s / \sqrt{2} \quad (2-3)$$

L_0 is a function of the wave period and is calculated as:

$$L_0 = gT_p^2 / 2\pi \quad (2-4)$$

Hanslow and Nielsen (1993) also determined that setup on relatively flat beaches (i.e. with slope $\tan\beta < 0.06$) is independent of beach slope; however, better estimates of η_s were obtained for steep beaches when slope was considered. Shoreline setup also depends on beach permeability, and ultimately, the rate at which water drains from a beach (Hanslow and Nielsen, 1993). For example, steep, high permeability beaches are able to drain more efficiently and experience greater setup elevations compared to flat low permeability beaches (Hanslow and Nielsen, 1993). Infiltration of seawater across the beach face (aquifer-ocean interface) is enhanced by shoreline setup and wave run-up, and this increases super-elevation of groundwater levels (η_w^+) that are then super-positioned on elevation of the groundwater levels caused by tidal effects (Hanslow and Nielsen, 1993; Turner et al., 1997).

Tides and wave-induced shoreline setup cause fluctuations in the elevation of the shoreline position (z_{SL}) on a beach according to Cartwright and Gibbes (2011):

$$z_{SL} = z_{tide} + \eta_s \quad (2-5)$$

where z_{tide} is tide elevation (in metres above sea level). Propagation of wave forcing signals (i.e. wave-induced fluctuations of z_{SL}) through coastal aquifers have been observed to generate same-period fluctuations in nearshore groundwater levels (e.g. Turner et al., 1996; Rotzoll and El-Kadi, 2008; Cartwright and Gibbes, 2011). The filtering capacity of the beach sediment results in relatively high-frequency wave forcing (e.g. shoreline setup

fluctuations) to be rapidly damped and only detectable close to the shoreline (e.g. Hegge and Masselink, 1991; Li et al., 2004; Rotzoll and El-Kadi, 2008). Similar to tidal forcing, aquifer storage properties act to attenuate and lag wave-induced groundwater level fluctuations, with the degree of attenuation and time lag increasing with inland distance from the coast. For example, Turner et al. (1996) found strong statistical correlation between fluctuations in wave height and measured beach groundwater table elevations from a monitoring well transect, and observed increased lags at inland locations (e.g. a lag of 41.5 hours observed at a monitoring well installed 30 m inland of shoreline). However, offshore storms (characterized by enhanced wind speeds, above-average wave heights, and precipitation) can enhance shoreline setup, and consequently shoreline elevations, for extended periods (e.g. multiple days) (Cartwright et al., 2004) resulting in longer-period forcing on the coastal aquifer that can propagate relatively farther inland of the coast.

The rise and fall of shoreline elevation due to isolated offshore storms can be represented as a Gaussian pulse force acting on the aquifer at the beach face (in contrast to sinusoidal behavior of tidal forcing) (Li et al., 2004):

$$h(t) = h_0 + A \exp \left[-B(t - t_p)^2 \right] \quad (2-6)$$

where h is water level (groundwater or shoreline elevation z_{SL}) fluctuating about h_0 (mean groundwater level or shoreline elevation), A is the amplitude of the pulse, B is a time factor (where B^{-2} represents duration of the wave event or groundwater level response), and t_p is the time when the peak h occurs. A limitation of this approximation is that a Gaussian pulse does not capture the temporal asymmetry in fluctuations of groundwater levels and z_{SL} caused by faster filling of the nearshore aquifer (beach) relative to draining. The field study by Cartwright and Gibbes (2011), however, showed that Eq. (2-6) was able to adequately capture the rising limb of the storm pulse forcing (i.e. shoreline setup) on the aquifer. Li et al. (2004) derived a general analytical solution describing groundwater level response to storm pulse forcing (Eq. [2-6]) and compared propagation of the storm pulse (i.e. amplitude attenuation and phase lag) to that of the tidal signal. Their solution is derived from the 1D Boussinesq equation for horizontal groundwater flow through a homogeneous isotropic unconfined aquifer of uniform depth and a vertical beach face. The solution is given as:

$$h(x, t) = -2AB \int_{-\infty}^t (\tau - t_p) \exp[-B(\tau - t_p)^2] \operatorname{erfc}\left[\frac{x}{2\sqrt{D(t - \tau)}}\right] d\tau \quad (2-7)$$

where x is perpendicular inland distance from mean shoreline position, t_p is time of peak shoreline elevation, and D is aquifer diffusivity (which is the ratio of T and S_y). Eq. (2-7) is the only solution available to describe storm-induced pulse signal propagation through a coastal aquifer; however, Eq. (2-7) has not previously been tested to field data from a complex coastal aquifer and therefore the applicability of this solution to real field conditions is unclear.

2.3 Aquifer characterization by analysis of tide and wave signal propagation

Well-developed methods exist to estimate aquifer properties (e.g. D) by analyzing monochromatic tide-induced groundwater fluctuations inland of the coast, and using inverse modelling of analytical solutions or numerical model calibration. Comprehensive understanding of coastal hydrogeology is critical for coastal water resource management including investigations of groundwater availability and coastal aquifer contamination (i.e., saltwater intrusion, mobility of anthropogenic contaminants). In contrast to tidal methods, little attention has been given to the use of propagation of storm pulse (i.e. shoreline setup) signals to determine aquifer structure (such as identifying layered aquifer systems). However, as discussed above, storm-induced wave conditions can elevate the water level at the shoreline for relatively longer periods (compared to tides) enabling this signal to potentially propagate farther inland from the coast. It may be advantageous to evaluate both tide and storm signals since the forcing signals act at different periods and therefore will propagate differently through the aquifer. Tidal signals will propagate through any aquifer connected to the ocean whether the connection is at the shoreline or offshore. Pulse-like groundwater level fluctuations will occur in unconfined aquifers connected at the shoreline due to shoreline setup, however, it is unknown whether wave setup will impact confined aquifers connected to the ocean offshore and what happens if the confined aquifer-ocean connectivity occurs within the surf zone.

Aquifer characterization techniques have been developed (e.g. Ferris, 1952; Carr and Van Der Kamp, 1969) to estimate coastal aquifer properties based on analysis of the groundwater table response to various environmental forcing (e.g. barometric fluctuations, tides). Methods using tidal signal attenuation (i.e. tidal methods) have been widely implemented (e.g. Erskine, 1991; Trefry and Bekele, 2004; Jha et al., 2008; Rotzoll et al., 2008; Slooten et al., 2010; Wang et al., 2013) as they are often less-resource intensive relative to other field investigation methods (e.g. boring, pumping, tests) and can provide information over larger length scales. The amplitude and phase of tide-induced (sinusoidal) groundwater level fluctuations can be quantified, for example, by peak matching (e.g. Ferris, 1952), spectral analysis using Fast-Fourier transform (e.g. Trefry and Bekele, 2004), or least-squares fitting of data to dominant tidal component frequencies (e.g. Merritt, 2004; Rotzoll et al., 2008). These methods compare the amplitude and phase of the tidal signal (α_{tide} , ϕ_{tide}) to that of groundwater table fluctuations (α_{GWL} , ϕ_{GWL}), with propagation of the signal described by the attenuation factor α_t (equal to $\alpha_{GWL} / \alpha_{tide}$), and phase lag $\Delta\phi_t$ (equal to $\phi_{GWL} - \phi_{tide}$). Water table wave numbers k_r and k_i describe the rate of amplitude damping and phase lag, respectively, to indicate the rate of tidal signal propagation through the aquifer. When data is collected from a shore-perpendicular transect of monitoring wells located distances x from the shoreline, linear regression of $\ln(\alpha_t)-x$ and $\Delta\phi_t-x$ are used to calculate k_r and k_i , respectively. Considering signal propagation through a 1D sandy and homogeneous aquifer (described by Jacob [1950]) k_r and k_i should be equal (Nielsen, 1990):

$$k_r = k_i = \sqrt{\frac{S_y \omega}{2Kd}} \quad (2-8)$$

If reliable estimates of S_y and K are available, Eq. (2-6) can be used to estimate aquifer depth (d) and transmissivity T (which is equal to Kd). Tidal methods use calculated k_r and k_i to estimate amplitude-resolved and phase-resolved values of aquifer D (e.g. Rotzoll et al., 2008):

$$D_{amp,m} = \frac{\omega}{2k_r^2} \quad (2-9)$$

$$D_{pha,m} = \frac{\omega}{2k_i^2} \quad (2-10)$$

Like k_r and k_i , D_{amp} and D_{pha} should also be equal for 1D homogeneous aquifers; however, discrepancies, termed propagation bias (Trefry and Bekele, 2004), are often observed (e.g. Ferris, 1952; Carr and Van Der Kamp, 1969; Erskine, 1991). For example, propagation bias was observed in a laboratory study by Cartwright et al. (2004) who found that a truncated capillary fringe may have contributed to more rapid signal attenuation k_r relative to the speed of inland propagation k_i (i.e. they observed smaller lags than what was predicted by amplitude damping, resulting in $D_{pha} > D_{amp}$). The analytical study by Sun et al. (2008) demonstrated propagation bias may occur in a dual-tide leaky-confined aquifer, and in testing their solution to field data presented by Trefry and Bekele (2004), they confirmed that propagation bias observed in the field data could be due to heterogeneity in aquifer properties. These studies indicate that tidal methods developed from simplified analytical solutions may not be applicable for adequate characterization of complex aquifer settings.

Inverse modelling of aquifer properties (e.g. D , T , S , K , d) can also be conducted by evaluating groundwater level response to wave setup (Rotzoll and El-Kadi, 2008), however, no studies have used storm-induced groundwater level fluctuations for coastal aquifer characterization. The only known field study to investigate storm pulse propagation was conducted by Cartwright and Gibbes (2011). They applied Gaussian least-squares fitting of Eq. (2-6) to groundwater level data and estimated shoreline setup (Eq. [2-2]), to evaluate propagation of a storm pulse through a sandy and unconfined coastal aquifer located in Gold Coast, Australia. Using Eq. (2-6), and a shoreline-perpendicular transect of monitoring wells located distances x from the shoreline, they calculated amplitude and time of peak groundwater levels (A_{GWL} and $t_{p,GWL}$) and shoreline elevation (A_{SL} and $t_{p,SL}$). Storm pulse propagation values α_w (equal to A_{GWL}/A_{SL}) and phase lag $\Delta\phi_w$ (equal to $t_{p,GWL} - t_{p,SL}$) were calculated and compared to a non-dimensional form of Eq. (2-7) (Li et al., 2004). They found that Eq. (2-7) could model the observed lag of groundwater level fluctuations ($\Delta\phi_w$), however, data showed a poor match between observed and predicted

amplitude attenuation (α_w). They attributed these findings to simplifying assumptions used in developing the analytical solution, such as neglecting infiltration of seawater due to wave run-up. Aquifer values were determined by in-situ methods and were not assessed by inverse modelling of Eq. (2-7) to calculated α_w and $\Delta\phi_w$ values.

Only one study has presented data comparing both tidal and wave setup signal propagation for the purpose of coastal aquifer characterization. Investigations were conducted in a volcanic coastal aquifer located in Central Maui, Hawaii, to calculate aquifer properties by single-well aquifer tests and geostatistical estimation (Rotzoll et al., 2007), dual-tide signal propagation (Rotzoll et al., 2008), and analysis of propagation of the shoreline setup signals (Rotzoll and El-Kadi, 2008). A comparison of all estimated values was presented in Rotzoll and El-Kadi (2008); however, in contrast to the storm pulse forcing discussed above, their analysis assumed the shoreline setup time series was a complex sinusoidal forcing such that *FFT* and conventional tidal methods (i.e. Eq. [2-9] and [2-10]) could be used to estimate hydraulic parameters (D , K). Their use of tidal methods is inappropriate for observations of storm pulse signal propagation.

Apparent differences between tidal and storm pulse signal propagation through coastal aquifers is seen when plotting inland signal propagation predicted by Eq. (2-1) for sinusoidal tides and Eq. (2-7) for storm pulses (Figure 2-2). For direct comparison, the analytical solutions must be non-dimensionalized by D and ω for Eq. (2-1) and D and B for Eq. (2-7). Relative to tides, storm pulse signals are predicted to propagate farther and faster inland due to the smaller frequency of shoreline setup fluctuations (Li et al., 2004); a feature for which past research has not exploited for coastal aquifer characterization. More importantly, a combined method of aquifer response to both tides and storm-induced waves has not been used previously to study aquifer-ocean connectivity and to provide insight into the structure of complex coastal aquifer systems (i.e. layered or leaky confined-unconfined aquifers).

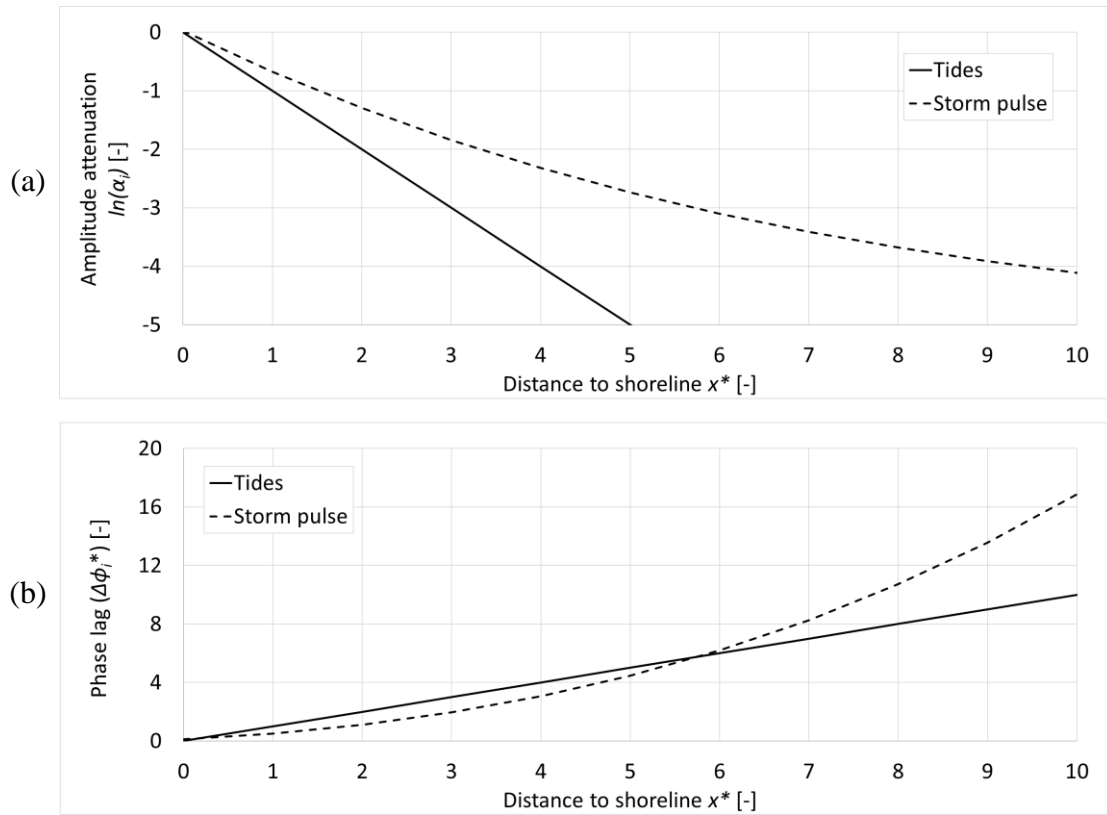


Figure 2-2 Comparison of signal propagation through a coastal aquifer, predicted by analytical solutions for tides (solid lines, according to Turner et al. (1997) non-dimensionalized by D and ω) and shoreline setup pulse (dashed line, according to Li et al. (2004) non-dimensionalized by D and storm duration parameter B). Relationships for non-dimensionalized signal amplitude attenuation $[\ln(\alpha_i)]$, and phase lag $(\Delta\phi_i^*)$, versus non-dimensionalized distance to the shoreline (x^*) are shown separately in (a) and (b), respectively.

2.4 Numerical modelling of coastal aquifers

Numerical modeling studies of coastal aquifers typically focus on simulating nearshore groundwater flow and transport dynamics, or the movement and location of the fresh groundwater-saltwater interface (e.g. Ataie-Ashtiani et al., 2001; Li et al., 2007; Robinson et al., 2014; Zhou et al., 2014; Geng and Boufadel, 2015). Numerical models are seldom used to investigate tide-induced groundwater table fluctuations inland of the shoreline (e.g.

Merritt, 2004; Pauw et al., 2014; Liu et al., 2016) for the purpose of understanding aquifer configuration and parameter values (e.g. D , K , d) estimated by analytical solutions.

A 1D numerical groundwater flow model was developed by Rotzoll et al. (2008) to simulate a cross-section of an unconfined, homogeneous isotropic volcanic island aquifer with a low- K sediment cover and dual-tide forcing acting on vertical aquifer-ocean boundaries. They obtained values for D and K using an automated parameter estimation routine. The model was then modified by Rotzoll and El-Kadi (2008) to implement one-sided shoreline setup fluctuations and D and K were determined by inverse modelling (i.e. Eq. [2-9] and [2-10]). Aquifer tests were also conducted on site (Rotzoll et al., 2007) to estimate aquifer values, and results between tide- and setup-derived estimates for D and K compared well to in-situ estimates. Simplifying assumptions such as a 1D aquifer were found to be adequate for the study area of Rotzoll and El-Kadi (2008); however, this may not be the case for more complex settings.

A combined field and modelling study of an island aquifer was conducted by Trefry and Bekele (2004) and shows how detailed analysis and numerical modelling can improve understanding of aquifer structure when observations do not follow what is predicted by simple 1D tidal signal propagation. They reported discrepancies between D_{amp} and D_{pha} values calculated from observed tide-induced groundwater table fluctuations. Numerical simulations revealed that the observed propagation bias ($D_{amp} \neq D_{pha}$) was likely due to large-scale structural heterogeneities (i.e. horizontal layering of aquifer units with variable K). Results generally suggested that moderate layering of aquifer properties (i.e. $K_{upper}/K_{lower} \ll 1$), or a combination of phreatic/capillary, density driven, or geometric effects (e.g. beach slope, variation in aquifer d due to sloping aquifer units) could result in propagation bias measured in other coastal settings.

Numerical studies on the influence of storm signal propagation through a coastal aquifer are limited and mostly focus on effects of storms on groundwater flows and salt transport close to the shoreline (Li and Barry, 2000; Cartwright et al., 2004; Geng et al., 2014; Robinson et al., 2014). Cartwright and Gibbes (2011) simulated groundwater flow conditions in a sandy unconfined coastal aquifer with a sloping beach face and subjected

to a storm pulse (i.e. storm-induced changes in shoreline elevation) using a finite element groundwater flow model (implemented in COMSOL). A good match was obtained between observed and simulated phase lag of groundwater levels in response to the storm pulse, as well as to the lag predicted by the analytical solution by Li et al. (2004). The observed pulse attenuation, however, was under-predicted by both the numerical model and analytical solution, suggesting that non-linear effects (e.g. capillary, infiltration of seawater due to wave run-up) may be important processes for storm pulse signal propagation (Cartwright and Gibbes, 2011). Overall, studies show discrepancies between field data, analytical, and numerical models, indicating that more work is needed to understand the effects of storm signals and tides on water table fluctuations in coastal aquifers with complex hydrogeology and where non-linear effects (such as capillary effects and sloping beach face) may impact pressure signal propagation.

2.5 Sable Island: field site description

Sable Island is an elongated sand barrier island located in the Atlantic Ocean on the Sable Island Bank of the Scotian Shelf (Figure 2-3). Situated 175 km southeast of the eastern coast of mainland Canada, Sable Island has a surface area of approximately 34 km² and is approximately 42 km long (Hennigar, 1976). It is 1.3 km across at its widest point resulting in a groundwater system that is highly connected to the ocean. Various users have occupied Sable Island since the 1700s, and the island has been extensively studied to understand island geology, meteorology and climate, botany, zoology, and history (Hennigar, 1976). General understanding of the hydrogeology of the island has been gained through historical site investigations (dating back to the 1700s) and more recent environmental and risk assessments (1990s – 2000s) conducted by various Canadian government and industry groups (ESG, 2015).

Various users have occupied the island since the 1700s with historical activities leading to legacy groundwater contamination across the island (ESG, 2015). The island is currently managed by Parks Canada Agency (PCA) with the minimal development on the island focused around a central area (herein called the Main Station, and labelled on Figure 2-3). This study focused on the Main Station and adjacent shoreline areas. The Main Station is defined by two well-developed sand dune ridges that run parallel to the north and south

beaches, while the inland area of the island is low lying relative to the steep dunes (Hennigar, 1976). Water supply on the island is provided by a groundwater pumping station located approximately 350 m from the Main Station area.

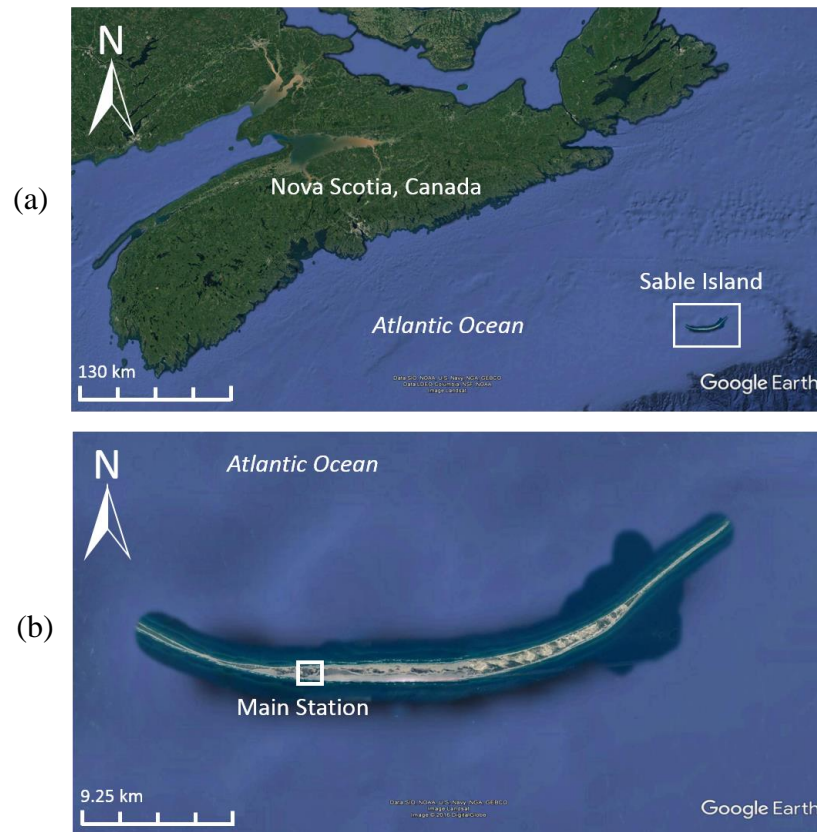


Figure 2-3 Maps showing (a) location of Sable Island in the Atlantic Ocean relative to Nova Scotia, (b) Sable Island labelled with locations of the Main Station area.

Imagery obtained by Google Earth.

Prior investigations indicate that Sable Island developed from glacial outwash sediments of the Scotian Shelf over the past several thousand years due to sea level rise and local ocean currents (Hennigar, 1976). The island topography is complex and dynamic with Gulf Stream currents resulting in northeast drift of sand along the south shoreline into the ocean, and Belle Isle currents shifting north shore sands to the southwest. Historical aerial photos suggest an overall easterly movement of the island, and indicate extensive dune erosion and blowouts of dune ridges along the north and south shoreline dues to intense winter

storms (Hennigar, 1976). Across the island, inland flooding is common and is either due to ocean inundation during storm events, or by groundwater levels reaching the ground surface during periods of high precipitation. Relative to the north shoreline, the south shoreline is flatter and experiences significant flooding of seawater during storms, and inland areas are flat with some areas of undulating topography (ESG, 2015). Small seasonal and perennial surface water ponds form in low relief areas with most surface water features being shallow (up to 2-3 m in depth), of variable quality (brackish and fresh water), and with water levels that vary seasonally (approximately 1 m). Ponds are often lined with low permeability organic materials (e.g. peat, mud), with larger permanent ponds underlain by significantly thicker layers of this material (Hennigar, 1976).

Historic drilling records collected from a borehole located outside of the Main Station indicate that Sable Island is underlain by approximately 300 m of Quaternary unconsolidated sands, 900 m of Tertiary sediments and 3,400 m of Cretaceous sediments (Hennigar, 1976). Surficial geology is reported as fine poorly sorted homogeneous sand ($d_{10} = 0.2$ mm, $C_u = 1.5$), and due to the island's glacial outwash formation experiences decreasing sand size and increased sorting in the southeasterly direction. Two pumping tests conducted by Hennigar (1976) suggest an average transmissivity (T) value of 462 m²/d and specific yield (S_y) of 0.36; however, tests were performed at wells located outside of the Main Station and so may not be indicative of conditions in the study area. In-situ infiltration tests estimate hydraulic conductivity (K) to be 46 m/d (Hennigar, 1976).

No bedrock outcropping or clay deposits have been reported on the island, however, horizons of dark organic material have been observed at various depths within the upper unconfined aquifer (up to 18 m deep) and along erosional faces of sand dunes suggesting that, over time, relic perennial ponds or vegetated areas have been buried by the infilling of blown sand into low lying depression areas (Hennigar, 1976). Vegetated cover is limited across the island and consists of several terrestrial and aquatic plant species, including sandwort community, various marram grasses, shrub-heath community, beach grass, juniper, centaury shrubs, and moss (Catling et al., 1984). Select wildlife are present on the island, including various species of birds, seals, and feral horses (ESG, 2015).

The climate on Sable Island is largely influenced by marine conditions that serve to moderate local temperatures relative to conditions on mainland Nova Scotia (Hennigar, 1976). Mean daily temperatures are equivalent between the island and main land (7.6°C and 6.6°C respectively), while the range of annual daily temperatures are 5.5°C for the island and 9.4°C for the main land. Seasonal variability of total precipitation on the island is comparable to the mainland and is evenly distributed throughout the year (Table 2-1). However, average historic climate normals (1971-2000) indicate slightly greater annual precipitation on Sable Island (1460 mm) relative to Halifax (1400 mm) (Environment Canada’s National Climate Archives, climate.weather.gc.ca).

Table 2-1 Historic precipitation climate normals (1971-2000) for Sable Island and Halifax, NS. Percent of annual total is indicated in parenthesis. Data obtained by Environment Canada’s National Climate Archives (climate.weather.gc.ca) for Sable Island weather station (STN 8204703) and Halifax Stanfield International Airport weather station (STN 8202250).

	Sable Island (%)	Halifax (%)
Winter	403 (28)	380 (27)
Spring	331 (23)	347 (25)
Summer	319 (22)	285 (20)
Fall	406 (28)	381 (27)
Annual total	1460	1400

Complex groundwater levels and flow patterns exist on the island with oceanic forcing acting on both shorelines, including a semi-diurnal tidal signal (with a range from 0.3 – 1.7 m, and 1.1 m on average) and intense offshore storms (Fisheries and Oceans Canada, tides.gc.ca). Local topography, surface water features, and seasonal and event-based precipitation also affect the groundwater dynamics (ESG, 2015). Geophysical surveys,

drilled boreholes, and water samples collected on the island in the 1970s, indicate that the freshwater lens across the island is located between 0.3 – 36 m below ground surface, and is overlying a deep saltwater wedge (Hennigar, 1976). Data show a symmetrical lens on the east half of the island (due to a greater island width and protective dune structures in this area); however, within the Main Station the lens is asymmetrical and becomes steadily deeper from the south shoreline to the north shoreline. It was proposed by Hennigar (1976) that this asymmetry is due to land development within the Main Station, as well as ocean flooding of topographically low lying areas adjacent to the south shoreline (especially during intense storms).

2.6 Summary

This chapter has described the effects of oceanic forcing on coastal groundwater, including the way in which tide and storm signals propagate (i.e. become attenuated and lagged) through coastal aquifers. There is generally good understanding of the impact of tides on coastal groundwater table fluctuations due to the extensive number of analytical, laboratory, and numerical studies conducted for tides. In contrast, few studies have examined the impacts of storm-induced waves on coastal groundwater table dynamics. There is a need to better understand the use of storm (i.e. periods of enhanced wave heights) signal propagation for coastal aquifer characterization, and in doing so, will shed light on the influence of storms on coastal groundwater dynamics. This is important given that storms are predicted to increase in frequency and intensity as the climate changes. Given the inherent differences between tide and storm signal forcing, combined analysis of both signals may provide greater insight into coastal aquifer properties and structure compared to analysis of only the tidal signal propagation. This may be especially true in more complex aquifer systems where existing tidal methods, that are derived from 1D groundwater flow equations, may be inappropriate. Chapter 3 of this thesis presents findings from a field and numerical modelling study to test the approach of using both tidal signal and storm pulse signal propagation analysis for characterization of Sable Island's aquifer system.

2.7 References

Alcolea, A., E. Castro, M. Barbieri, J. Carrera and S. Bea (2007). "Inverse modeling of coastal aquifers using tidal response and hydraulic tests." Ground Water **45**(6): 711-722.

Anwar, N., C. Robinson and D. A. Barry (2014). "Influence of tides and waves on the fate of nutrients in a nearshore aquifer: Numerical simulations." Advances in Water Resources **73**: 203-213.

Asadi-Aghbolaghi, M., M.-H. Chuang and H.-D. Yeh (2014). "Groundwater Response to Tidal Fluctuation in an Inhomogeneous Coastal Aquifer-Aquitard System." Water Resources Management **28**(11): 3591-3617.

Ataie-Ashtiani, B., R. E. Volker and D. A. Lockington (2001). "Tidal effects on groundwater dynamics in unconfined aquifers." Hydrological Processes **15**(4): 655-669.

Boufadel, M. C., H. Li, M. T. Suidan and A. D. Venosa (2007). "Tracer studies in a laboratory beach subjected to waves." Journal of Environmental Engineering **133**(7): 722-732.

Carr, P. A. and G. S. Van Der Kamp (1969). "Determining aquifer characteristics by the tidal method." Water Resources Research **5**(5): 1023-1031.

Cartwright, N. and B. Gibbes (2011). Oceanic Pulse Forcing of a Beach Groundwater System. 20th Australasian Coastal and Ocean Engineering Conference 2011, COASTS 2011 and the 13th Australasian Port and Harbour Conference 2011, PORTS 2011. Perth, West Australia, Curan Associates Inc: 197 - 202.

Cartwright, N., L. Li and P. Nielsen (2004). "Response of the salt-freshwater interface in a coastal aquifer to a wave-induced groundwater pulse: Field observations and modelling." Advances in Water Resources **27**(3): 297-303.

Cartwright, N., P. Nielsen and L. Li (2004). "Experimental observations of watertable waves in an unconfined aquifer with a sloping boundary." Advances in Water Resources **27**(10): 991-1004.

Catling, P. M., B. Freedman and Z. Lucas (1984). The vegetation and phytogeography of Sable Island, Nova Scotia. Proceedings of the Nova Scotia Institute of Science.

Chuang, M.-H. and H.-D. Yeh (2008). "Analytical Solution for Tidal Propagation in a Leaky Aquifer Extending Finite Distance under the Sea." Journal of Hydraulic Engineering **134**(4): 447-454.

Chuang, M. H., C. S. Huang, G. H. Li and H. D. Yeh (2010). "Groundwater fluctuations in heterogeneous coastal leaky aquifer systems." Hydrology and Earth System Sciences **14**(10): 1819-1826.

Chuang, M. H., A. A. Mahdi and H. D. Yeh (2012). "A perturbation solution for head fluctuations in a coastal leaky aquifer system considering water table over-height." Hydrological Sciences Journal **57**(1): 162-172.

Chuang, M. H. and H. D. Yeh (2007). "An analytical solution for the head distribution in a tidal leaky confined aquifer extending an infinite distance under the sea." Advances in Water Resources **30**(3): 439-445.

Duncan, J. R. (1964). "The effects of water table and tide cycle on swash-backwash sediment distribution and beach profile development." Marine Geology **2**(3): 186-197.

Environmental Sciences Group (ESG) (2015). 2015 Supplementary Phase III Environmental Site Assessment and Groundwater Dynamics Program Sable Island National Park Reserve Sable Island, Nova Scotia. Kingston, ON Canada, Royal Military College of Canada: 905.

Erskine, A. D. (1991). "Effect of tidal fluctuation on a coastal aquifer in the UK." Ground Water **29**(4): 556-562.

Ferris, J. G. (1952). Cyclic fluctuations of water level as a basis for determining aquifer transmissibility. Washington, D.C.

Geng, X. and M. C. Boufadel (2015). "Numerical study of solute transport in shallow beach aquifers subjected to waves and tides." Journal of Geophysical Research: Oceans **120**(2): 1409-1428.

Geng, X., et al. (2014). "Numerical study of wave effects on groundwater flow and solute transport in a laboratory beach." Journal of Contaminant Hydrology **165**: 37-52.

Gonnecta, M. E., A. E. Mulligan and M. A. Charette (2013). "Climate-driven sea level anomalies modulate coastal groundwater dynamics and discharge." Geophysical Research Letters **40**(11): 2701-2706.

Guo, Q., H. Li, M. C. Boufadel, Y. Xia and G. Li (2007). "Tide-induced groundwater head fluctuation in coastal multi-layered aquifer systems with a submarine outlet-capping." Advances in Water Resources **30**(8): 1746-1755.

Hanslow, D. and P. Nielsen (1993). "Shoreline Set-Up on Natural Beaches." Journal of Coastal Research(15): 1-10.

Hegge, B. J. and G. Masselink (1991). "Groundwater-Table Responses to Wave Run-up: An Experimental Study from Western Australia." Journal of Coastal Research **7**(3): 623-634.

Heiss, J. W. and H. A. Michael (2014). "Saltwater-freshwater mixing dynamics in a sandy beach aquifer over tidal, spring-neap, and seasonal cycles." Water Resources Research **50**(8): 6747-6766.

Hennigar, T. W. (1976). *Water Resources and Environmental Geology of Sable Island, Nova Scotia*, Nova Scotia Department of Environment: 56.

Hsieh, P. C., H. T. Hsu, C. B. Liao and P. T. Chiueh (2015). "Groundwater response to tidal fluctuation and rainfall in a coastal aquifer." *Journal of Hydrology* **521**: 132-140.

Huang, C.-S., H.-D. Yeh and C.-H. Chang (2012). "A general analytical solution for groundwater fluctuations due to dual tide in long but narrow islands." *Water Resources Research* **48**(5): n/a-n/a.

Jacob, C. E. (1950). *Flow of groundwater*. New York.

Jeng, D. S., L. Li and D. A. Barry (2002). "Analytical solution for tidal propagation in a coupled semi-confined/phreatic coastal aquifer." *Advances in Water Resources* **25**(5): 577-584.

Jeng, D. S., B. R. Seymour, D. A. Barry, L. Li and J. Y. Parlange (2005). "New approximation for free surface flow of groundwater: Capillarity correction." *Advances in Water Resources* **28**(10 SPEC. ISS.): 1032-1039.

Jha, M. K., D. Namgial, Y. Kamii and S. Peiffer (2008). "Hydraulic Parameters of Coastal Aquifer Systems by Direct Methods and an Extended Tide–Aquifer Interaction Technique." *Water Resources Management* **22**(12): 1899-1923.

Jiao, J. J. and Z. Tang (1999). "An analytical solution of groundwater response to tidal fluctuation in a leaky confined aquifer." *Water Resources Research* **35**(3): 747-751.

Kim, J. H., et al. (2005). "Use of time series analysis for the identification of tidal effect on groundwater in the coastal area of Kimje, Korea." *Journal of Hydrology* **300**(1-4): 188-198.

Kong, J., et al. (2013). "Capillary effect on water table fluctuations in unconfined aquifers." *Water Resources Research* **49**(5): 3064-3069.

La Licata, I., C. D. Langevin, A. M. Dausman and L. Alberti (2011). "Effect of tidal fluctuations on transient dispersion of simulated contaminant concentrations in coastal aquifers." *Hydrogeology Journal* **19**(7): 1313-1322.

Li, G. and C. Chen (1991). "Determining the length of confined aquifer roof extending under the sea by the tidal method." *Journal of Hydrology* **123**(1): 97-104.

Li, L. and D. A. Barry (2000). "Wave-induced beach groundwater flow." *Advances in Water Resources* **23**(4): 325-337.

Li, H. and J. J. Jiao (2001). "Analytical studies of groundwater-head fluctuation in a coastal confined aquifer overlain by a semi-permeable layer with storage." *Advances in Water Resources* **24**(5): 565-573.

- Li, H. and J. J. Jiao (2001). "Tide-induced groundwater fluctuation in a coastal leaky confined aquifer system extending under the sea." Water Resources Research **37**(5): 1165-1171.
- Li, H. and J. J. Jiao (2003). "Review of analytical studies of tidal groundwater flow in coastal aquifer systems. In Proceedings of the International Symposium on Water Resources and the Urban Environment. Wuhan, PR China." Nov: 9-10.
- Li, H., L. Li, D. Lockington, M. C. Boufadel and G. Li (2007). "Modelling tidal signals enhanced by a submarine spring in a coastal confined aquifer extending under the sea." Advances in Water Resources **30**(4): 1046-1052.
- Li, L., D. A. Barry and D. S. Jeng (2001). "Tidal fluctuations in a leaky confined aquifer: Dynamic effects of an overlying phreatic aquifer." Water Resources Research **37**(4): 1095-1098.
- Li, L., D. A. Barry, F. Stagnitti and J. Y. Parlange (2000). "Groundwater waves in a coastal aquifer: A new governing equation including vertical effects and capillarity." Water Resources Research **36**(2): 411-420.
- Li, L., D. A. Barry, F. Stagnitti, J. Y. Parlange and D. S. Jeng (2000). "Beach water table fluctuations due to spring-neap tides: Moving boundary effects." Advances in Water Resources **23**(8): 817-824.
- Li, L., N. Cartwright, P. Nielsen and D. Lockington (2004). "Response of coastal groundwater table to offshore storms." China Ocean Engineering **18**(3): 423-431.
- Li, L., D. S. Jeng and D. A. Barry (2002). "Tidal fluctuations in a leaky confined aquifer: localised effects of an overlying phreatic aquifer." Journal of Hydrology **265**(1-4): 283-287.
- Liu, Y., J. J. Jiao and X. Luo (2016). "Effects of inland water level oscillation on groundwater dynamics and land-sourced solute transport in a coastal aquifer." Coastal Engineering **114**: 347-360.
- Longuet-Higgins, M. S. and R. Stewart (1964). "Radiation stresses in water waves; a physical discussion, with applications." Deep Sea Research and Oceanographic Abstracts **11**(4): 529-562.
- Masselink, G., P. Russell, I. Turner and C. Blenkinsopp (2009). "Net sediment transport and morphological change in the swash zone of a high-energy sandy beach from swash event to tidal cycle time scales." Marine Geology **267**(1-2): 18-35.
- Merritt, M. L. (2004). Estimating Hydraulic Properties of the Floridan Aquifer System by Analysis of Earth-Tide, Ocean-Tide, and Barometric Effects, Collier and Hendry Counties, Florida. Tallahassee, Florida, United States Geological Survey: 76.

Moore, W. S. (2010). "The Effect of Submarine Groundwater Discharge on the Ocean." Annual Review of Marine Science **2**(1): 59-88.

Nielsen, P. (1990). "Tidal dynamics of the water table in beaches." Water Resources Research **26**(9): 2127-2134.

Nielsen, P. (2009). Coastal and Estuarine Processes. Singapore, World Scientific Publishing Co. Pt2. Ltd.

Pauw, P. S., et al. (2014). "Regional scale impact of tidal forcing on groundwater flow in unconfined coastal aquifers." Journal of Hydrology **517**: 269-283.

Raubenheimer, B., R. T. Guza and S. Elgar (1999). "Tidal water table fluctuations in a sandy ocean beach." Water Resources Research **35**(8): 2313-2320.

Robinson, C., A. Brovelli, D. A. Barry and L. Li (2009). "Tidal influence on BTEX biodegradation in sandy coastal aquifers." Advances in Water Resources **32**(1): 16-28.

Robinson, C., B. Gibbes, H. Carey and L. Li (2007). "Salt-freshwater dynamics in a subterranean estuary over a spring-neap tidal cycle." Journal of Geophysical Research: Oceans **112**(C9): C09007.

Robinson, C., P. Xin, L. Li and D. A. Barry (2014). "Groundwater flow and salt transport in a subterranean estuary driven by intensified wave conditions." Water Resources Research **50**(1): 165-181.

Rotzoll, K. and A. I. El-Kadi (2008). "Estimating hydraulic properties of coastal aquifers using wave setup." Journal of Hydrology **353**(1-2): 201-213.

Rotzoll, K., A. I. El-Kadi and S. B. Gingerich (2008). "Analysis of an unconfined aquifer subject to asynchronous dual-tide propagation." Ground Water **46**(2): 239-250.

Rotzoll, K., A. I. El-Kadi and S. B. Gingerich (2007). "Estimating Hydraulic Properties of Volcanic Aquifers Using Constant-Rate and Variable-Rate Aquifer Tests." JAWRA Journal of the American Water Resources Association **43**(2): 334-345.

Shih, D. C. F., G. F. Lin, Y. P. Jia, Y. G. Chen and Y. M. Wu (2008). "Spectral decomposition of periodic ground water fluctuation in a coastal aquifer." Hydrological Processes **22**(12): 1755-1765.

Slooten, L. J., J. Carrera, E. Castro and D. Fernandez-Garcia (2010). "A sensitivity analysis of tide-induced head fluctuations in coastal aquifers." Journal of Hydrology **393**(3-4): 370-380.

Song, Z., L. Li, J. Kong and H. Zhang (2007). "A new analytical solution of tidal water table fluctuations in a coastal unconfined aquifer." Journal of Hydrology **340**(3): 256-260.

Sun, P., H. Li, M. C. Boufadel, X. Geng and S. Chen (2008). "An analytical solution and case study of groundwater head response to dual tide in an island leaky confined aquifer." Water Resources Research **44**(12): n/a-n/a.

Teo, H. T., D. S. Jeng, B. R. Seymour, D. A. Barry and L. Li (2003). "A new analytical solution for water table fluctuations in coastal aquifers with sloping beaches." Advances in Water Resources **26**(12): 1239-1247.

Townley, L. R. (1995). "The response of aquifers to periodic forcing." Advances in Water Resources **18**(3): 125-146.

Trefry, M. G. and E. Bekele (2004). "Structural characterization of an island aquifer via tidal methods." Water Resources Research **40**(1): W015051-W0150521.

Turner, I. L. (1995). "Simulating the influence of groundwater seepage on sediment transported by the sweep of the swash zone across macro-tidal beaches." Marine Geology **125**(1): 153-174.

Turner, I. L., B. P. Coates and R. I. Acworth (1996). "The effects of tides and waves on water-table elevations in coastal zones." Hydrogeology Journal **4**(2): 51-69.

Turner, I. L., B. P. Coates and R. I. Acworth (1997). "Tides, waves and the super-elevation of groundwater at the coast." Journal of Coastal Research **13**(1): 46-60.

van der Kamp, G. (1972). "Tidal fluctuations in a confined aquifer extending under the sea." Proc. Int. Geol. Congr., 24th **24**(11): 101-106.

Wang, Q., H. Zhan and Z. Tang (2013). "Groundwater response to dual tidal fluctuations in a peninsula or an elongated island." International Journal for Numerical and Analytical Methods in Geomechanics **37**(15): 2456-2470.

Xia, Y., H. Li, M. C. Boufadel, Q. Guo and G. Li (2007). "Tidal wave propagation in a coastal aquifer: Effects of leakages through its submarine outlet-capping and offshore roof." Journal of Hydrology **337**(3-4): 249-257.

Zhou, P., G. Li, Y. Lu and M. Li (2014). "Numerical modeling of the effects of beach slope on water-table fluctuation in the unconfined aquifer of Donghai Island, China." Hydrogeology Journal **22**(2): 383-396.

Chapter 3

3 Combined Analysis of Tide- and Wave-induced Water Table Fluctuations for Structural Characterization of a Coastal Aquifer

3.1 Introduction

Coastal groundwater tables fluctuate in response to various oceanic forcing including tides (semi-diurnal, diurnal, spring-neap), individual waves and offshore storm events (e.g. Raubenheimer et al., 1999; Robinson et al., 2007; Cartwright and Gibbes, 2011). Groundwater table fluctuations impact groundwater flows and the transport of contaminants in coastal aquifers, as well as groundwater discharge rates and associated chemical fluxes to the ocean (e.g. Li et al., 1999; Robinson et al., 2007; Moore, 2010; Geng et al., 2014). Water table fluctuations near the groundwater aquifer-ocean interface may also affect sediment transport and beach profile change (e.g. Duncan, 1964; Turner, 1995; Masselink et al., 2009). The way in which oceanic forcing signals propagate through a coastal aquifer, and cause water table fluctuations, depends on the nature of the forcing signal (i.e. amplitude and period) and connectivity between the aquifer and ocean, as well as the structure and hydraulic properties of the coastal aquifer.

Propagation of tidal signals through coastal aquifers has been extensively studied (e.g. Jacob, 1950; Ferris, 1952; Carr and Van Der Kamp, 1969; Nielsen, 1990; Turner et al., 1997; Kim et al., 2005; Shih et al., 2008; Guo et al., 2010; Hsieh et al., 2015). The tidal signal propagates through an aquifer from the ocean with water table fluctuations becoming increasingly damped (attenuated) and delayed (phase-shift) with increasing distance from the coast. It is well established that the rate of attenuation (i.e. amplitude damping and phase lag versus distance inland) depends on the period of the tidal oscillation, as well as aquifer properties (i.e. storage S or specific yield S_y , hydraulic conductivity K) and structural configuration (i.e. single/multi-layered aquifer system, aquifer depth d). In permeable unconfined coastal aquifers, complete attenuation may occur within a few hundred metres of the shoreline (defined by Hegge and Masselink (1991) as the line of intersection between the mean surface water level and the beach face). Decreased storage

in confined aquifers, however, results in more rapid and less damped propagation of tidal pressure fluctuations. In some cases, fluctuations may reach thousands of metres inland in confined aquifers (Jha et al., 2008).

Many analytical solutions exist for homogeneous, single layer aquifer systems (e.g. Jacob, 1950; Nielsen, 1990; Song et al., 2007). Solutions for more complex coastal aquifer configurations have also been developed and include solutions for submarine confined aquifers (e.g. Van Der Kamp and Gale, 1983; Li and Chen, 1991; Guo et al., 2007), and submarine leaky confined aquifers with an overlying unconfined aquifer (e.g. Jiao and Tang, 1999; Li and Jiao, 2001; Jeng et al., 2002; Xia et al., 2007; Chuang and Yeh, 2008; Chuang et al., 2010; Asadi-Aghbolaghi et al., 2014). While most studies evaluate the propagation of the diurnal or semi-diurnal tidal signals; bichromatic longer period spring-neap tides have also been studied (e.g. Li et al., 2000; Robinson et al., 2007; Heiss and Michael, 2014; Dong et al., 2016). The spring-neap tidal signal propagates farther through the coastal aquifer (relative to primary tidal signals) due to the longer period of the oscillation (Jeng et al., 2005). Many analytical solutions are derived from the one-dimensional Boussinesq equation and assume a homogeneous, isotropic unconfined aquifer exposed to a single, sinusoidal tidal signal applied at a vertical beach boundary. There are, however, solutions that incorporate non-linear effects such as a sloping beach face (e.g. Nielsen, 1990; Li et al., 2000; Teo et al., 2003) and vertical capillary flow (e.g. Li et al., 2000; Jeng et al., 2005; Kong et al., 2015). Coastal aquifer hydrogeology is often extremely complex, and while analytical solutions provide important insight into the controls governing tidal signal propagation, compared to the various analytical solutions available, there are surprisingly limited field investigations that provide detailed evaluation of fluctuations in complex coastal settings.

Comprehensive understanding of coastal hydrogeology is critical for coastal water resource management including investigations of groundwater availability and coastal aquifer contamination (i.e., saltwater intrusion, mobility of anthropogenic contaminants). Aquifer characterization techniques have been developed (Ferris, 1952; Carr and Van Der Kamp, 1969) to estimate aquifer properties (e.g. diffusivity D , which is the ratio of T and S) based on analysis of the groundwater table response to environmental forces (e.g. barometric

fluctuations, tides). These methods have been widely implemented (e.g. Trefry and Bekele, 2004; Alcolea et al., 2007; Rotzoll et al., 2008; Slooten et al., 2010; Wang et al., 2013) as they are often less-resource intensive relative to other investigative methods (e.g. boring, pumping tests) and can provide information over larger length scales. Independent estimates of D can be made using tidal attenuation and phase lag data to calculate amplitude-resolved (D_{amp}) and phase-resolved (D_{pha}) diffusivity values. Considering one-dimensional tidal signal propagation through a homogeneous aquifer as described by Jacob (1950), D_{amp} and D_{pha} should be equal; however, discrepancies are often observed. Trefry and Bekele (2004) evaluated time series data from eight groundwater wells and tide height on Garden Island, Australia. Through numerical experiments they determined that the propagation bias ($D_{amp} \neq D_{pha}$) was due to large-scale structural heterogeneities, in particular, horizontal layering of highly conductive aquifer units below low- K units. Similar bias was observed by Cartwright et al. (2004) who showed via sand flume experiments that a truncated capillary fringe may have contributed to observed lags being less than the observed amplitude attenuation (i.e. $D_{pha} > D_{amp}$). Coastal aquifers are complex and analysis of the tidal signal propagation alone may not be sufficient to adequately characterize coastal hydrogeology. In this study, we propose that analysis of the propagation of multiple oceanic forcing through a coastal aquifer, in particular tides and storms, may provide significant insight into aquifer structure, rather than analysis of only tidal signal propagation.

The response of the coastal water table to waves has been examined previously with most studies focused on water table fluctuations close to the shoreline (i.e. beach water table fluctuations) (e.g. Hegge and Masselink, 1991; Turner et al., 1997; Li and Barry, 2000; Cartwright et al., 2004; Xin et al., 2010; Geng et al., 2014; Robinson et al., 2014). Due to the high frequency of individual wave run up (e.g. time scale of seconds), the resulting water table fluctuations are rapidly damped inland, and therefore, only detectable close to the shoreline (Hegge and Masselink, 1991; Li et al., 2004). Waves are also associated with wave setup which is an increase in the elevation of the mean water level within the surf zone caused by the momentum transfer associated with breaking waves. According to Hanslow and Nielsen (1993), wave setup elevates the mean water level at the shoreline to the order of $0.4H_{0rms}$ (root-mean-square deep water wave height). The elevation of the

shoreline position on the beach above the mean shoreline is termed shoreline setup. Shoreline setup can occur for multiple days depending on the duration of an offshore storm (i.e. period of intensified wave conditions). Oscillations of shoreline setup in response to offshore storms can be represented by a Gaussian pulse (herein called a storm pulse), and similar to sinusoidal tidal forcing, result in groundwater table fluctuations that are damped and delayed with increasing landward distance, relative to the driving storm pulse signal (Li et al., 2004). Due to the longer time period of a storm pulse signal compared to a tidal signal, the storm pulse may propagate farther and more rapidly into an aquifer, and therefore, can provide information over greater distances inland; this was illustrated by Li et al. (2004), who presented an analytical solution for a homogeneous, isotropic uniform-depth aquifer exposed to a pulse signal at a vertical beach boundary. Cartwright and Gibbes (2011) compared the analytical solution to field observations in a sandy unconfined aquifer and showed reasonable comparison between the solution and observed attenuation rates. This analytical solution however has not been applied in more complex coastal environments. To our knowledge, Rotzoll and El-Kadi (2008) is the only study to estimate coastal aquifer properties based on analysis of the propagation of wave setup through an aquifer. In their analysis, however, Rotzoll and El-Kadi (2008) assumed wave setup as a continuous sinusoidal forcing signal rather than a Gaussian pulse signal which is known to better represent offshore storm events.

The objective of this study was to take advantage of key differences between tidal and storm pulse forcing and conduct combined analysis of propagation of both signals to provide insight into complex coastal hydrogeological conditions. Tidal signals will propagate through any aquifer connected to the ocean regardless of whether the connection occurs at the shoreline or offshore (Figure 3-1). While pulse signals (i.e. shoreline setup) associated with storms are known to propagate through unconfined aquifers, here we propose that confined aquifers extending offshore (but connected to the ocean within the surf zone) may be exposed to an attenuated pulse forcing signal that is able to propagate far inland. Localized upwards leakage from the confined aquifer may transmit both the tidal and storm pulse signals to the unconfined aquifer and induce water table fluctuations far inland from the shore (Figure 3-1). To our knowledge, combined analysis of these signals has not been done previously, with propagation of storm pulses having received

little attention. Storm-induced groundwater level fluctuations occurring significantly inland of the coast have not been previously reported. Further, there is currently a gap in

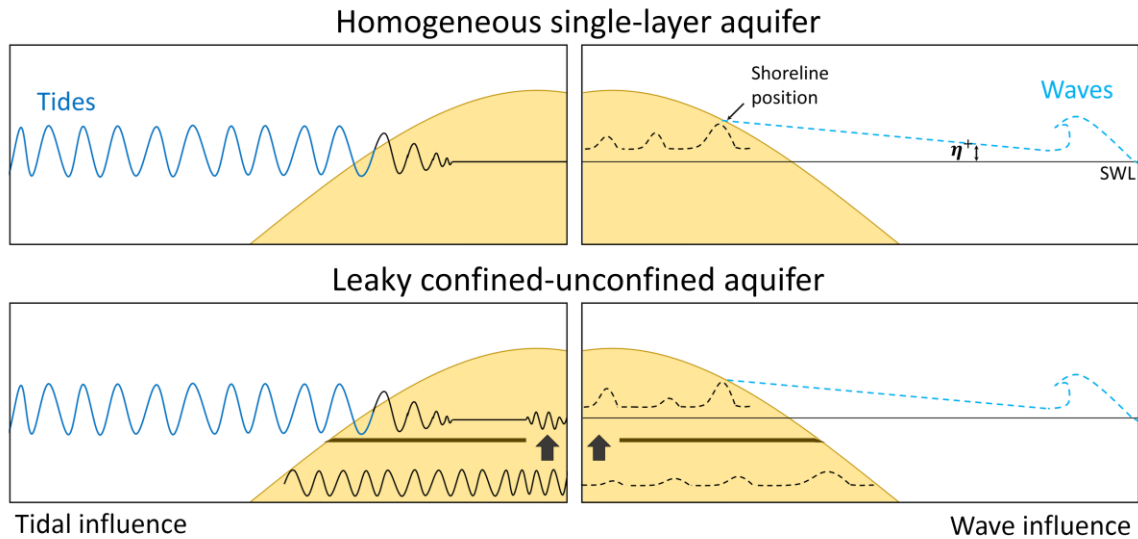


Figure 3-1 Conceptual models to show the effects of tides and waves on a homogeneous unconfined aquifer system (top) versus a leaky confined-unconfined aquifer connected to the ocean offshore and with localized leakage landward of the shoreline (bottom). Tidal influence on the system is shown separately on the left, and wave influence shown separately on the right where breaking waves cause an upward tilt of the mean surface water level towards the beach above the standing water level (SWL) which is termed wave setup (η^+).

the implementation of aquifer characterization methods and analysis of observed water fluctuations for complex coastal aquifer settings. While a large number of analytical solutions for complex aquifer systems exist, they are rarely tested with real data, and field studies typically only analyze propagation of primary tidal signals in simple sandy aquifer settings. This study also aims to advance understanding of the propagation of pulse forcing through coastal aquifers; this will address the increasing need to understand the impact of offshore storms on coastal groundwater resources given predicted climate change impacts such as the increasing intensity and frequency of storm events (Danard et al., 2003; Gonneea et al., 2013).

Data collected from an extensive groundwater monitoring network installed on a sand barrier island (Sable Island, NS, Canada) was first analyzed using harmonic and Gaussian signal processing to evaluate the propagation of the tidal and storm pulse signals (i.e. increased shoreline elevation), respectively, through the aquifer to provide insight into the configuration of the coastal aquifer system. Combined analysis of the tidal and storm pulse signals indicates a leaky confined-unconfined aquifer system, and a two-dimensional numerical groundwater model was used to test this aquifer conceptualization. Findings from this work indicate that evaluating the influence of both tides and storm pulse forcing together leads to greater understanding and characterization of complex coastal aquifers. With most coastlines exposed to both tides and offshore storms, this approach may be widely applicable to assist in characterization of complex coastal aquifer settings worldwide.

3.2 Field Description and Methodology

3.2.1 Field Site

Sable Island is a sand barrier island located in the Atlantic Ocean on the Sable Island Bank of the Scotian Shelf. Situated 175 km southeast of the eastern coast of mainland Canada (Figure 3-2a), Sable Island has a surface area of approximately 34 km² and is approximately 42 km long. It is 1.3 km across at its widest point resulting in a groundwater system that is highly connected to the ocean. Various users have occupied Sable Island since the 1700s and historical activities have led to legacy groundwater contamination. The island is now managed by Parks Canada with the minimal development on the island focused around a central location that is herein called the Main Station. This study focused on the Main Station and adjacent shoreline areas as shown in Figure 3-2. The Main Station area is defined by two well-developed sand dune ridges that run parallel to the north and south beaches. Inland areas between these dune ridges are low lying with gentle undulating topography.

Sable Island developed from glacial outwash sediments of the Scotian Shelf over the past several thousand years due to sea level rise and local ocean currents (Hennigar, 1976). The island topography is dynamic with Gulf Stream currents causing a northeast drift of sand

along the south shoreline into the ocean and Belle Isle currents shifting north shore sands to the southwest. Historical aerial photos suggest an overall easterly movement of the island. Small seasonal and perennial surface water ponds form in some low relief areas with most surface water features being shallow (up to 2-3 m in depth) with seasonally variable water levels (approximately 1 m) and variable quality (brackish and fresh water). Ponds are often lined with low permeability organic materials (e.g. peat, mud), with larger permanent ponds underlain by significantly thicker layers of this material (Hennigar, 1976).

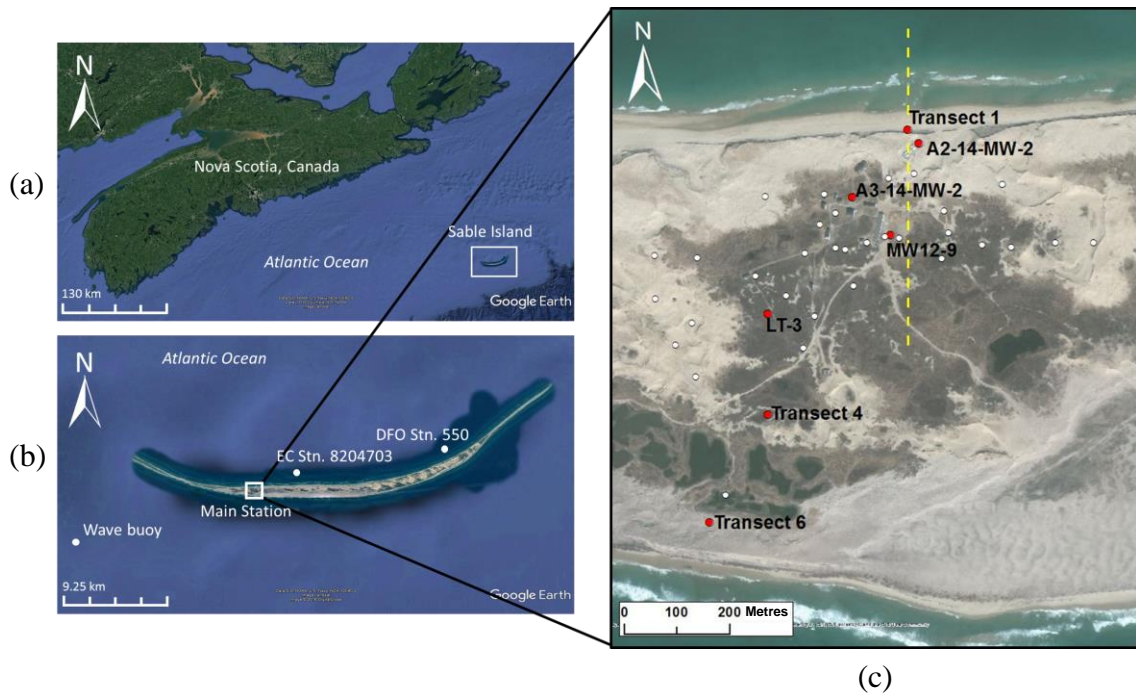


Figure 3-2 Maps showing (a) location of Sable Island in the Atlantic Ocean relative to Nova Scotia, Canada, (b) locations of the Main Station area, Ocean Ltd. offshore wave buoy, Environment Canada weather station 8204703, and the Canadian Department of Fisheries and Oceans tide gauge station 550; and (c) the Main Station area with locations of continuous long-term monitoring wells indicated by white dots and select wells labelled with their respective I.D.s by red dots. The yellow dash line in (c) indicates the cross-shore transect used in the numerical model. Imagery provided by Google Earth in (a) and (b) and Esri Basemaps in (c).

Drilling records collected from a borehole located outside of the Main Station area indicate that Sable Island is underlain by approximately 300 m of Quaternary unconsolidated sands, 900 m of Tertiary sediments and 3,400 m of Cretaceous sediments (Hennigar, 1976). Surficial geology is reported to be fine poorly graded homogeneous sand ($d_{10} = 0.2$ mm, $C_u = 1.5$). While no bedrock outcropping or clay deposits have been reported, horizons of sandy peat material have been observed at various depths below surface (up to 18 m deep) and along erosional faces of sand dunes. This suggests that blown sand may, over time, have deposited and buried low lying surface water features or previously vegetated areas (Hennigar, 1976).

Typical for island environments, the groundwater table is dynamic and fluctuates in response to oceanic forcing including tides and offshore storms. Sable Island is exposed to semi-diurnal tides with the tidal range varying between 0.3–1.7 m (approximately 1.1 m on average) (Hennigar, 1976). Local topography, surface water features, and seasonal and event-based precipitation also impact the groundwater table dynamics on the island. Prior site investigation found that the freshwater lens within the Main Station is asymmetrical atop a saltwater wedge, and that the lens near the south shoreline is thinner relative to the north shoreline (Hennigar, 1976). Hydraulic conductivity (K) values have been estimated by various methods (e.g. field pumping and infiltration method; Hazen (1982); Shepherd (1989)) and give a range of values of 1.54 – 95 m/d, which spans the range of expected K values for uniform sand (Freeze and Cherry, 1979). Average transmissivity (T) has been estimated to be 462 m²/d, and specific yield (S_y) is estimated to be 0.36 from pumping tests conducted at two wells located outside of the Main Station area (Hennigar, 1976).

3.2.2 Data Collection

A network of 95 monitoring wells around the Main Station were used to obtain groundwater level data. Groundwater wells were installed along cross-island transects to dissect the Main Station area from north-to-south (shoreline to shoreline) and east-to-west, with additional wells installed in the central Main Station area. Approximately 50 of the groundwater wells were installed in 2014-2015 using a hand-held soil core auger, and due to sloughing, were only installed to approximately 1 m below the standing water table. All

other monitoring wells were installed during previous site investigations and these wells, also shallow, provided supplementary groundwater level data.

Long-term groundwater level data was collected at 26 wells from August 2014 to August 2015 (see Appendix A). Self-logging pressure transducers (CTD-Diver and Mini-Diver, Schlumberger Water Services; TROLL 9500, In-Situ Inc.) were used for continuous measurement of water pressure and specific conductivity, and were programmed to record 20 minutes. Conductivity data indicated freshwater in all monitoring wells meaning that groundwater heads did not require correction for saltwater density effects. Manual groundwater level measurements and transducer maintenance was performed during four field site visits over the monitoring period. Pressure transducers were also installed temporarily (~24 hours) in 13 select groundwater wells during these field visits to better quantify the tidal signal propagation through the aquifer (also labelled in Appendix A). A pressure transducer was used to record the barometric pressure fluctuations over the monitoring period. Groundwater pressure head data were converted to groundwater levels referenced to meters above sea level using digital global position satellite (DGPS) surveys, and projected to the North American Datum 1983 (NAD83). The accuracy of groundwater elevation measurement is estimated to be 0.005 m based on the accuracy of the DGPS receiver combined with environmental factors (e.g. cloud cover, wind, satellites orbital position) (ESG, 2015). Satellite imagery was used to estimate perpendicular distances between monitoring wells and the mean shoreline position on the north and south beaches.

Groundwater level time series were compared to environmental data including tide height, wave data, and precipitation data. Tide height data for Sable Island were available from Fisheries and Oceans Canada (www.tides.gc.ca), and data from an offshore wave buoy located approximately 16 km south of the island were provided by Ocean Ltd. (see Figure 3-2a). Wave data were available from 9 September to 16 November, 2014, and 20 June to 31 August, 2015. The tide height and wave data are considered to represent forcing conditions for both the north and south shorelines. Meteorological data (precipitation, wind speed) were available from Environment Canada weather stations located on Sable Island (Figure 3-2) (station 8204703 supplemented by data from station 8204700; Environment Canada's National Climate Archives, climate.weather.gc.ca).

3.2.3 Analysis of Tidal Signal Propagation

Spectral analysis was first used to decompose time series of barometric-pressure corrected groundwater levels and tidal data to identify the dominant frequencies, and thus dominant tidal modes, present in the groundwater level data. This was done using discrete Fast Fourier Transform (*FFT*) method and executed in MATLAB. Least-squares fitting of the identified dominant tidal mode (M2 harmonic with a period of 12.421 hours [$\omega = 12.14$ rad/d]; semi-diurnal) was then conducted using the groundwater level time series and tidal data to resolve the amplitude and phase of water level fluctuations (e.g. Merritt, 2004; Rotzoll and El-Kadi, 2008). Subsets of the long-term groundwater level time series, and corresponding tide height data, were analyzed for monitoring well locations with incomplete data records (due to instrument error or discontinuous monitoring). Data were selected for periods when groundwater table elevations did not exhibit strong trends (e.g. rising or falling of mean water level) that could be attributed to recharge, drainage flows, or evapotranspiration. Data subsets were first linearly detrended to remove any remaining trending effects (e.g. precipitation) and the amplitude and phase of the dominant tidal harmonic component was determined by least-squares fitting of data to the harmonic oscillation:

$$h(t) = h_0 + \alpha_i \cos(\omega t + \phi) \quad (3-1)$$

where h is groundwater level or tide level fluctuating about h_0 (average value of h), α_i is amplitude of the fluctuation (groundwater or tides), ω is frequency of the tidal component (12.14 rad/d for M2), t is time, and ϕ is the phase lag of fluctuation relative to a pure cosine wave (in radians). Attenuation of the tidal signal at each groundwater well location, also called tidal efficiency factor (TE) (e.g. Erskine, 1991; Merritt, 2004), was calculated by the ratio of fitted amplitude parameters:

$$\alpha_t = \frac{\alpha_{GWL}}{\alpha_{tide}} \quad (3-2)$$

where α_{GWL} and α_{tide} are the amplitudes of groundwater level and tide data, respectively. The phase lag of the groundwater level fluctuations relative to the phase of the tidal signal was calculated by:

$$\Delta\phi_t = \phi_{GWL} - \phi_{tide} \quad (3-3)$$

where ϕ_{GWL} and ϕ_{tide} are phase of the groundwater level and tide data, respectively. Where possible, α_t and $\Delta\phi_t$ at a monitoring location were calculated using multiple data subsets to test for stationarity, and mean α_t and $\Delta\phi_t$ were adopted for further analyses. Calculated α_t and $\Delta\phi_t$ for all groundwater well locations were spatially interpolated to illustrate the tidal signal propagation through the aquifer.

To improve characterization of the coastal aquifer system, calculated α_t and $\Delta\phi_t$ at monitoring well locations were used to estimate aquifer parameters with parameter values compared to those determined by in-situ field tests (Hennigar, 1976). The estimated aquifer parameters were also used to inform development of a numerical groundwater model (described in Section 3.2.5). Tidal harmonic analysis identified four distinct areas of high ocean-aquifer connectivity: (1) north beach area, (2) south beach area, (3) inland area around monitoring well MW12-9 (herein called Area 1), and (4) inland area around monitoring well LT-3 (herein called Area 2). Groundwater level fluctuations in these areas were subsequently analyzed individually. Data from monitoring wells installed adjacent to the north shoreline (Transect 1, A2-14-MW-2) were used to evaluate tidal signal propagation through the surficial nearshore aquifer; however, data collected near the south beach (Transect 6) was not analyzed further due to limited spatial data resolution in this area. In narrow or elongated islands, dual-tide interference can occur as tides propagate from opposite shorelines (e.g. Trefry and Bekele, 2004; Rotzoll et al., 2008), however, due to the rapid attenuation of the tidal signal in the surficial aquifer at the north and south shorelines, this is not likely to be the cause of complex groundwater table fluctuations observed on Sable Island (i.e. Area 1 and 2). Data from Areas 1 and 2 were used to test the hypothesis that the tidal signal propagates through a leaky confined aquifer connected to the ocean some finite distance offshore.

Aquifer parameters were estimated using a simplified analytical solution for one-dimensional (1D) groundwater flow in a homogeneous and isotropic unconfined aquifer:

$$h(x, t) = \alpha_{tide} \exp\left(-x\sqrt{S_y/2T\omega}\right) \sin\left(\frac{2\pi}{t_0} - x\sqrt{S_y/2T\omega}\right) \quad (3-4)$$

where x is perpendicular inland distance from the shoreline (Turner et al., 1997). The solution assumes a vertical beach face, uniform aquifer depth, and negligible vertical flows. Linear regression of $\ln(\alpha_t)$ -(x) and $\Delta\phi_t$ -(x) relationships define water table wave numbers k_r and k_i , respectively, and describe the rate of tidal signal amplitude attenuation and phase lag. Wave numbers k_r and k_i can be used to estimate aquifer depth (d) and transmissivity ($T = Kd$) if reliable estimates for K and S_y are available (Nielsen, 1990):

$$k_r = k_i = \sqrt{\frac{S_y\omega}{2Kd}} \quad (3-5)$$

From theory, wave numbers k_r and k_i should be equal for a 1D sandy and homogeneous aquifer model; however, field studies observe $k_r > k_i$ indicating that the tidal signal travels through the aquifer faster (is less lagged) than predicted by the observed tidal damping (Cartwright, 2004). Wave numbers k_r and k_i are used for estimates of aquifer diffusivity (D) (e.g. Rotzoll et al., 2008):

$$D_{amp} = \frac{\omega}{2k_r^2} \quad (3-6)$$

$$D_{pha} = \frac{x^2\omega}{2k_i^2} \quad (3-7)$$

Tidal mode propagation bias is quantified by slope factor (SF):

$$SF = \sqrt{\frac{D_{amp}}{D_{pha}}} \quad (3-8)$$

to measure the deviation from ideal, one-dimensional tidal propagation according to the Jacob-Ferris solution for which $SF = 1$ (Trefry and Bekele, 2004). Deviations from unity

are caused by subsurface heterogeneities (e.g. Trefry and Bekele, 2004), or non-linear effects such as capillarity and finite-depth effects (e.g. Cartwright, 2004).

3.2.4 Analysis of Storm Pulse Signal Propagation

Data collected during two offshore storm events (periods of intensified wave conditions) were used to quantify the response of groundwater levels to discrete storm pulse signals. Events which occurred on 15 – 21 September, 2014 and 1 – 8 October, 2014, were selected for the analysis because they were not accompanied by significant precipitation. For this analysis, a low-pass Hamming filter was first applied to groundwater level time series to remove high frequency fluctuations including those associated with tides (Crosbie et al., 2005). Water level fluctuations in the filtered dataset are attributed to wave processes, precipitation events, and evapotranspiration. Offshore significant wave height (H_s , in metres) and peak period (T_p , in seconds) data from the offshore wave buoy (Figure 3-2) were first used to calculate shoreline setup, η_s , by the empirical relationship of Hanslow and Nielsen (1993):

$$\eta_s = 0.048\sqrt{H_{0rms}L_0} \quad (3-9)$$

where H_{0rms} is the root-mean-square of the deep water wave height (calculated as $H_{0rms} = H_s/\sqrt{2}$) and L_0 is the deep water wavelength (calculated as $L_0 = gT_p^2/2\pi$). Although the beach was non-planar, beach slope ($\tan\beta$) was not considered in the calculation of η_s as Hanslow and Nielsen (1993) found considering slope did not improve estimates of shoreline setup for flat beaches. Time series of shoreline elevation, z_{SL} , was then calculated by:

$$z_{SL} = z_{tide} + \eta_s \quad (3-10)$$

where z_{tide} is the tide elevation (in metres above sea level [masl]). Shoreline elevation data was also filtered using a low-pass Hamming filter before comparing with the filtered groundwater level data.

The amplitude and phase of storm pulse fluctuations at individual wells was determined by analyzing filtered groundwater levels and estimated shoreline elevation (z_{SL}) during the two offshore storm events using least squares fitting to a Gaussian function of the form:

$$h(t) = h_0 + A \exp \left[-B(t - t_p)^2 \right] \quad (3-11)$$

where h is water level (groundwater or shoreline elevation) fluctuating about h_0 (mean groundwater level or shoreline elevation), A is the amplitude of the pulse, B is a time factor (B^{-2} represents duration of the storm event or groundwater level response), and t_p is the time when the peak h occurs (Li et al., 2004). Following Cartwright and Gibbes (2011), only the rising limb of groundwater and shoreline elevation data was considered in the fitting analysis because temporal asymmetry in groundwater level pulses (due to rapid aquifer filling compared with slow drainage) are not well described by the Gaussian function. Attenuation and phase lag of the storm pulse forcing through the aquifer was quantified by the comparison of fitted parameters:

$$\alpha_w = \frac{A_{GWL}}{A_{SL}} \quad (3-12)$$

$$\Delta\phi_w = t_{p,GWL} - t_{p,SL} \quad (3-13)$$

where A_{GWL} and A_{SL} are amplitude of groundwater level and shoreline elevation pulse fluctuation, respectively, and $t_{p,GWL}$ and $t_{p,SL}$ are time of peak groundwater level and shoreline elevation, respectively.

To evaluate the homogeneity of the coastal aquifer, field observations were compared to an analytical solution developed by Li et al. (2004) for a homogeneous unconfined aquifer exposed to a storm pulse signal at the shoreline:

$$h(x, t) = -2AB \int_{-\infty}^t (\tau - t_p) \exp[-B(\tau - t_p)^2] \operatorname{erfc} \left[\frac{x}{2\sqrt{D(t - \tau)}} \right] d\tau \quad (3-14)$$

where x is distance from mean shoreline position. Li et al. (2004) provides complete details on the analytical solution including boundary and initial conditions. A non-

dimensionalized form of Eq. (3-14) was used to compare propagation of storm pulse signals of different durations (e.g. different duration factor B), and to observed tidal signal propagation (Li et al., 2004). Non-dimensional phase lag $\Delta\phi_w^*$ is calculated as:

$$\Delta\phi_w^* = \Delta\phi_w \sqrt{B} \quad (3-15)$$

and non-dimensional distance from the shoreline, x^* is calculated as:

$$x^* = \frac{x}{2\sqrt{D/B^{1/2}}} \quad (3-16)$$

using storm pulse parameter B determined by fitting z_{SL} data to Eq. (3-11).

3.2.5 Numerical Groundwater Flow Modelling

Combined analysis of the tide- and storm-induced groundwater level fluctuations suggests that the coastal aquifer may be a leaky confined-unconfined system, where the confined aquifer is connected to the ocean at a finite distance offshore. A two-dimensional finite-difference saturated groundwater flow model implemented in MODFLOW-2000 (Harbaugh et al., 2000) was used to confirm that this hydrogeological conceptualization can explain the observed heterogeneous propagation of the tidal signal. The model domain represents a vertical cross-shore section through a coastal aquifer (Figure 3-3), analogous to a transect through the north beach at Sable Island (shown on Figure 3-2). Simulations were conducted using aquifer configurations with varying unconfined and confined aquifer depths, configuration of the confining layer (location, slope, width of discontinuity, conductivity $K_{confining\ layer}$), and specific yield (S_y) (see Appendix D). Varying these parameters changes aquifer D (ratio of T/S), and ultimately the ability of the tidal signal to propagate through the aquifer. Aquifer configurations were simulated until a reasonable match (i.e. minimum absolute error) was obtained between calculated and simulated α_t for locations labelled on Figure 3-3 (corresponding to locations of wells Transect 1, A2-14-MW-2, A3-14-MW-2, and MW12-9). The model has a total length of 600 m and a total depth (depth of unconfined and confined aquifer) of 300 m corresponding to the report by Hennigar (1976). The leaky confined-unconfined aquifer system was simulated using a 1 m thick, impermeable confining layer ($K = 10^{-4}$ m/d) with a 10 m wide discontinuity (leak)

located approximately 235 m landward of the shoreline. Layer and column size ranged from 0.5 – 2 m (Δz) and 1.5 – 20 m (Δx), respectively, with grid discretization tests performed to ensure the model solution was converged.

Tidal fluctuations at the ocean boundary were simulated using the ‘high- K ’ approach (e.g. Robinson et al., 2007) where an aquifer zone and high- K ocean zone are separated by the aquifer-ocean interface (i.e. beach face). The slope of the aquifer-ocean interface (β) varied from 0.1 at the shoreline ($x = 0$) to 15 m offshore, $\beta = 0.2$ from $x = 15 - 115$ m, and $\beta = 1$ (vertical) at the seaward boundary ($x = 115$ m). The location of mean

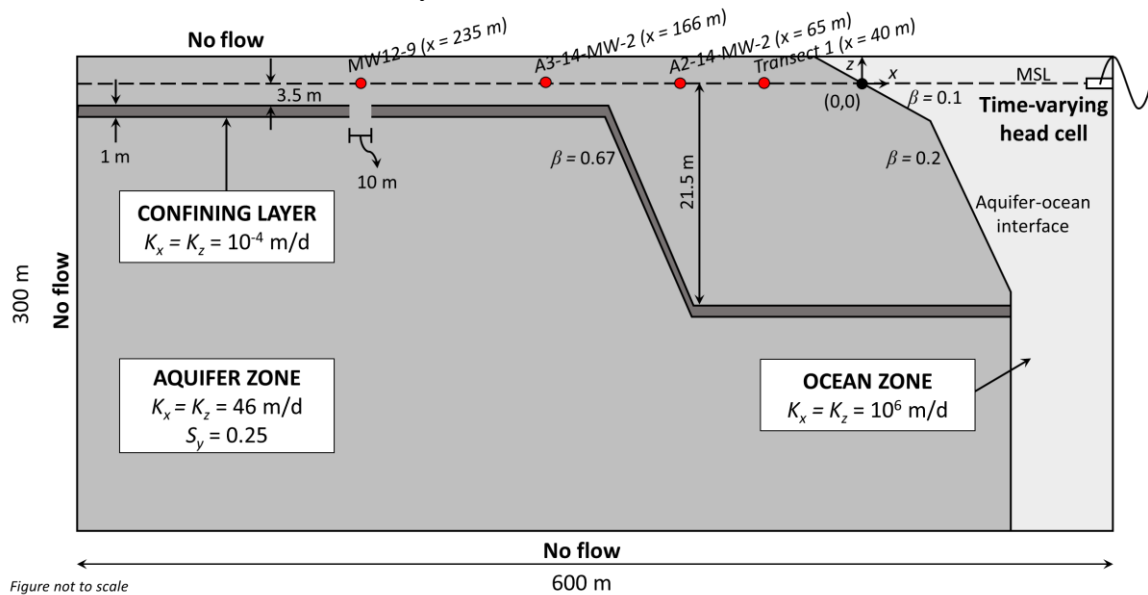


Figure 3-3 Geometry, boundary conditions, and parameters used to model an unconfined-leaky confined aquifer with a discontinuous impermeable confining layer that intersects the seabed 95 m offshore of the estimated mean shoreline position, i.e. the coordinate origin (0,0) (horizontally) which is at mean sea level (MSL) (vertically) as indicated by the dashed line. The model domain is divided into an aquifer zone (dark grey) and ocean zone (light grey) as indicated. Red dots indicate locations corresponding to monitoring well locations on Sable Island. The most seaward location (Transect 1) is situated 40 m from the estimated mean shoreline position. A tidal signal ($\alpha_{tide} = 0.55$ m, M2 tidal mode of $\omega = 12.14$ rad/d) is applied by a time-varying head cell, located approximately 155 m offshore. The landward boundary is located far inland of the shoreline (approximately 485 m) and assigned a now-flow boundary to neglect terrestrial groundwater flows.

shoreline position was 40 m from Transect 1 monitoring well, and the confining layer extended offshore with the confined aquifer intersecting the seabed 95 m seaward of the mean shoreline position. Model cells within the aquifer zone had $K = 46$ m/d which was determined by infiltration tests conducted by Hennigar (1976), and kept consistent for both unconfined and confined units. Recharge analysis using groundwater level and precipitation time series (Crosbie et al., 2005) found S_y varies between 0.20 – 0.40 across the island. A value of $S_y = 0.25$ was implemented in the model to fall within the range of estimated values, and also within the range commonly estimated for uniform sand (e.g. Johnson, 1967). A single harmonic tidal signal with $\alpha_{tide} = 0.55$ m (corresponding to the average tidal amplitude) and $\omega = 12.14$ rad/d (M2 tidal mode) was implemented by a time-varying head cell in the ocean zone. Model cells within the ocean zone had $K = 10^6$ m/d to ensure the tidal signal was transmitted to all saturated cells along the aquifer-ocean interface. No flow boundary conditions are implemented along the top, bottom, landward, and seaward edge of the domain. The model was first run to steady state with no tidal fluctuations. Tidal fluctuations were then simulated for 20 days – this simulation time was sufficient to reach the quasi-steady state with respect to groundwater table fluctuations. Density-dependent groundwater flow was not considered.

3.3 Results and Discussion

3.3.1 Time Series Analysis

A two-month subset of groundwater level data measured for selected wells (locations shown in Figure 3-2) are shown in Figure 3-4 together with time series of key environmental forcing (tide elevation, significant wave height data, and daily precipitation). As expected the groundwater table elevation near the shoreline (Transect 1, ~40 m from shoreline) experiences the largest fluctuations in response to the semi-diurnal tidal signal and offshore storm events (i.e. periods of high significant wave height) compared to inland groundwater levels. Groundwater level variations at inland wells (e.g. A3-14-MW-2 and Transect 4 located ~166 m and ~270 m from the shoreline, respectively) are mostly attributed to longer-term seasonal precipitation patterns and discrete precipitation events. The relative magnitude and frequency of precipitation events governs recharge to the unconfined aquifer with the relatively high sand permeability across the

island resulting in high aquifer recharge and negligible overland surface flows (Hennigar, 1976). However, strong semi-diurnal groundwater fluctuations are observed at some isolated inland locations (e.g. well MW12-9 and LT-3 located ~235 m and ~385 m from the shoreline, respectively).

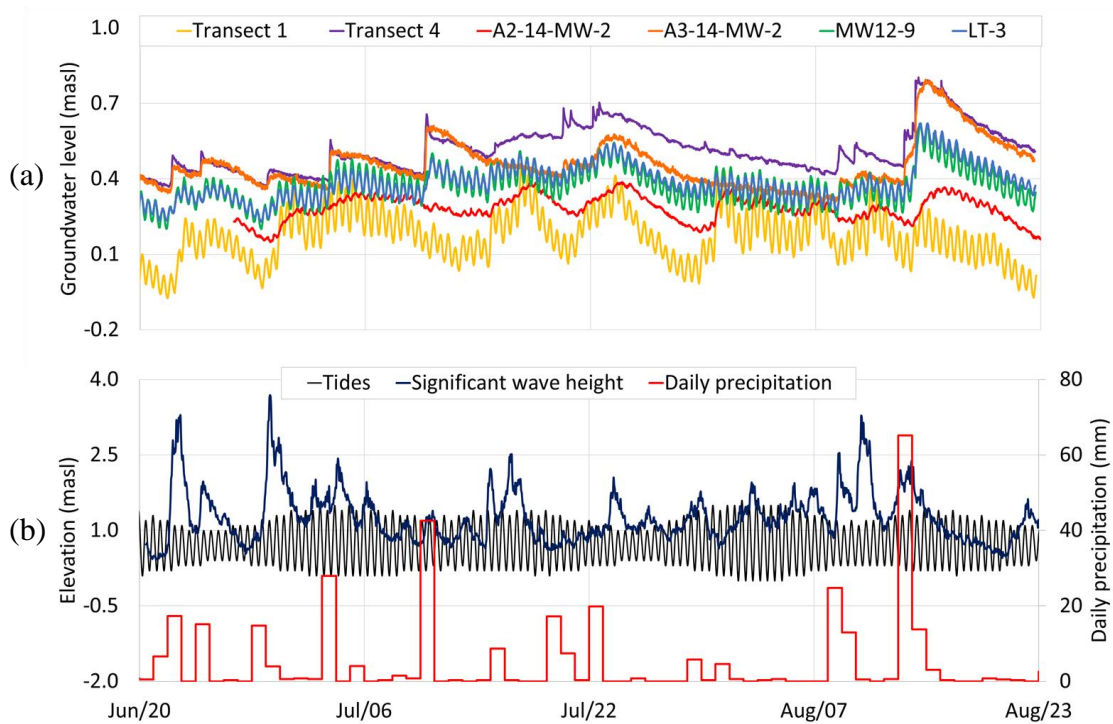


Figure 3-4 Continuous data of (a) groundwater table elevation, measured in metres above sea level (masl); (b) significant wave height (masl), tide height (masl), and daily precipitation measured in millimeters (mm) from 20 June – 21 August, 2015. This is a subset of the total data recording period which extended from 7 August, 2014 – 23 August, 2015. Locations of groundwater monitoring wells are shown in Figure 3-2.

3.3.2 Analysis of Tidal Signal Propagation

For tidal data, maximum spectra (shown in Figure 3-5a) is detected at the main lunar M2 frequency (1.932 cycles per day [cpd]) with smaller values detected at frequencies consistent with the main solar S2 component (2.00 cpd), and to a lesser degree, the lunar elliptic N2 component (1.896 cpd). This result corroborates what is described for the Northeast American continental shelf (Moody et al., 1984). Analysis of groundwater level

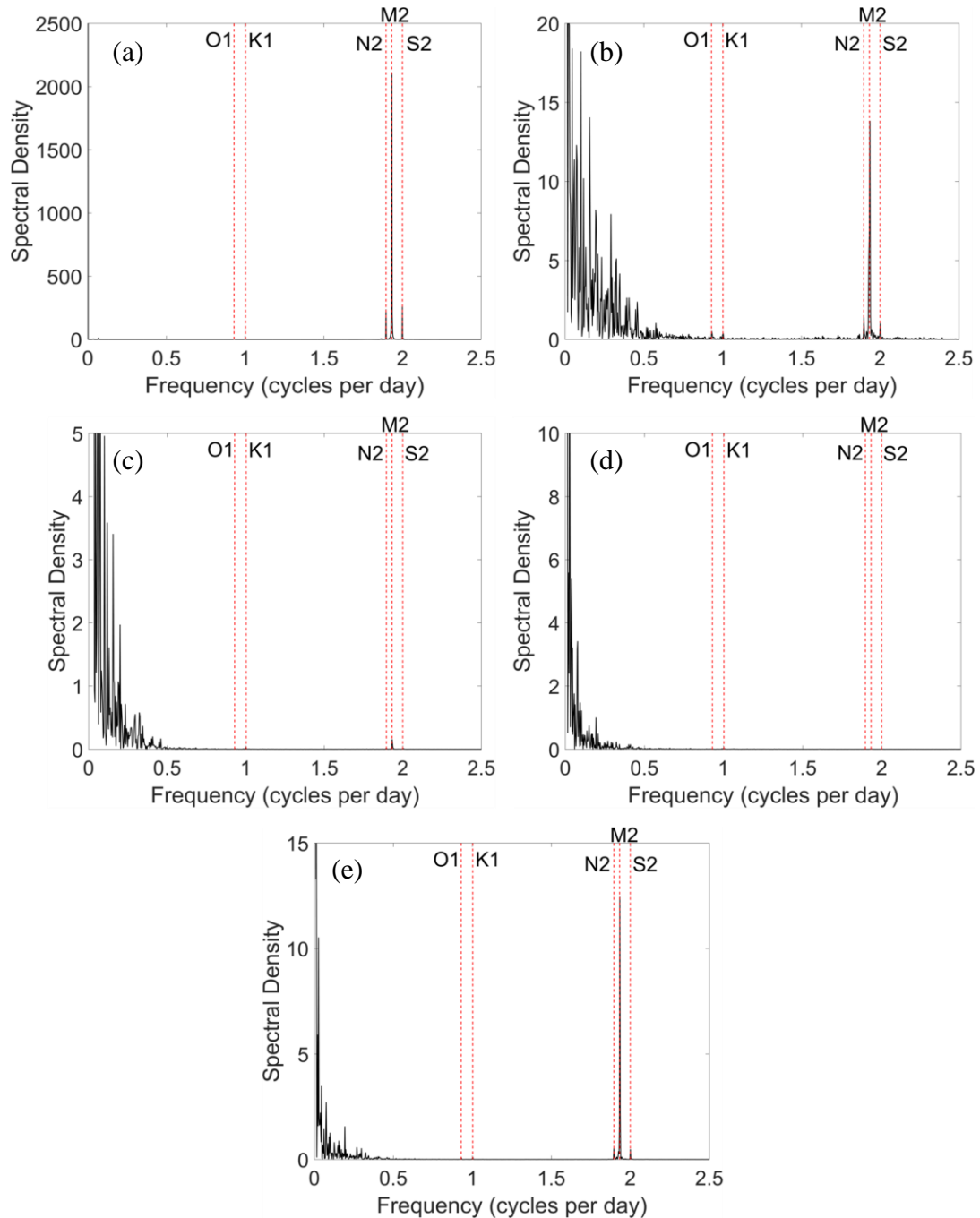


Figure 3-5 Fast Fourier Transform (*FFT*) analysis results for (a) tide height data over the period of Aug 2014 - Dec 2015, and groundwater monitoring wells (b) Transect 1; (c) A2-14-MW-2; (d) A3-14-MW-2; (e) MW12-9. *FFT* analysis conducted with groundwater level data available over the period of 15 Aug 2014 – 22 Aug 2015. Known frequencies of tidal constituents are labelled by red dashed lines.

data at Transect 1 (Figure 3-5b) also show a strong peak at the M2 frequency indicating, as expected, high aquifer-ocean connectivity. The tidal signal is increasingly attenuated through the aquifer, as indicated by a decrease in spectral density at the M2 frequency with increasing distance inland of the shoreline (see spectra for A2-14-MW-2 and A3-14-MW-3, Figure 3-5c and d); however, a strong spectral peak corresponding to the M2 frequency is detected for some inland wells located farther inland (see spectra for MW12-9, Figure 3-5e). Low-frequency (i.e. 0 – 0.5 cpd) spectra detected in all groundwater level time series are attributed to other environmental forcing (e.g. seasonal precipitation, discrete precipitation events, atmospheric pressure, evapotranspiration).

Spatial contour maps of α_t and $\Delta\phi_t$ values calculated by harmonic analysis are shown in Figure 3-6 to illustrate propagation of the semi-diurnal (M2) tidal signal through the Main Station (calculated values used in Figure 3-6 are provided in Appendix B). Groundwater wells near the north and south shorelines experience the largest tide-induced groundwater level fluctuations and shortest lags (e.g. $\alpha_t = 0.11$ and $\Delta\phi_t = 4.8$ hrs at Transect 1). Consistent with prior studies (e.g. Nielsen, 1990; Rotzoll and El-Kadi, 2008), tide-induced water table fluctuations are damped and delayed with increasing distance inland (e.g. $\alpha_t = 0.017$ and $\Delta\phi_t = 6.9$ hrs at A2-14-MW-2). However, Figure 3-6 also shows some relatively large tide-induced water table fluctuations at inland locations (e.g. $\alpha_t = 0.092$ and $\Delta\phi_t = 2.9$ hrs at MW12-9; $\alpha_t = 0.057$ and $\Delta\phi_t = 2.4$ hrs at LT-3). Highly heterogeneous propagation of the tidal signal across the study area suggests that the aquifer system may not be homogeneous as previously reported. Two distinct isolated inland areas have been identified that exhibit tide-induced water table fluctuations (as indicated by high α_t and low $\Delta\phi_t$ values). These areas, located around MW12-9 (Area 1) and around LT-3 (Area 2), are indicated in Figure 3-6. Data show that in these areas, groundwater levels fluctuate at amplitudes similar to those observed at the north beach (Transect 1), and more interestingly, are less lagged to the tidal signal.

While surface water features or complex land topography, resulting in varying depth of the water table below ground surface (e.g. Kong et al., 2015), are known to cause heterogeneous propagation of the tidal signal, these factors do not explain the isolated

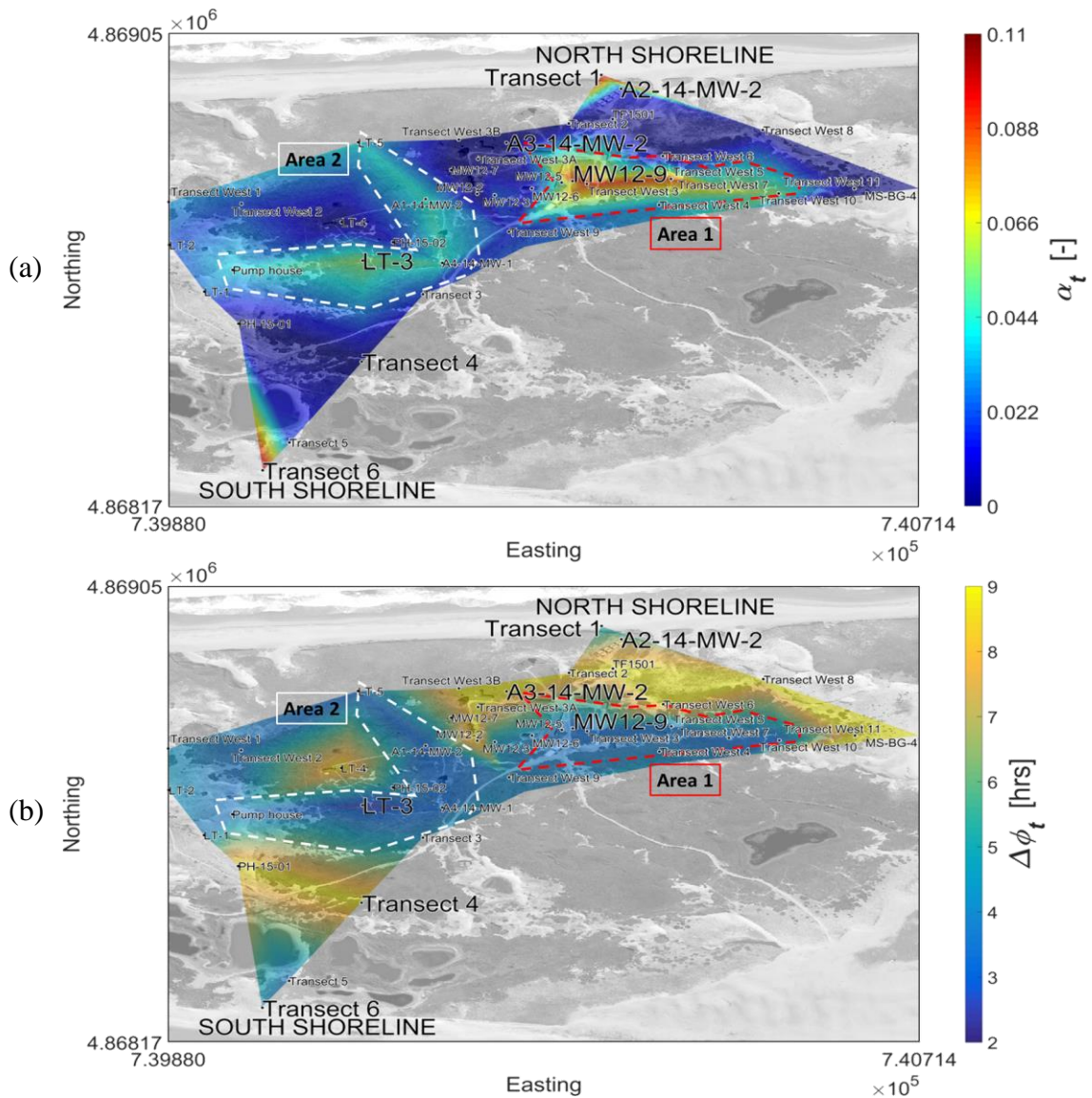


Figure 3-6 Tidal signal propagation across Sable Island’s Main Station. Coloured contours represent (a) amplitude attenuation ratio (α_t) [-] and (b) phase lag ($\Delta\phi_t$) [hrs] of groundwater level fluctuation relative to the dominant M2 tidal signal ($\omega = 12.14$ rad/d). Larger α_t and smaller $\Delta\phi_t$ indicate greater and more rapid groundwater level response to the tidal signal, respectively. Tidal source Area 1 is outlined in red dashed line, and Area 2 is outlined in white dashed line.

nature of the tide-induced groundwater fluctuations in Areas 1 and 2. Rather, fluctuations may be due to upward leakage of pressure fluctuations from a confined aquifer (Jeng et al., 2002). It is possible that buried organic layers associated with historic surface water ponds may have led to the formation of a leaky confined-unconfined aquifer system that results in the observed heterogeneous propagation of the tidal signal). Given the current spatial resolution of monitoring wells it is difficult to determine the spatial extent of the gap (discontinuity or thinning) in the hypothesized confining layer; however, data suggest that the leakage results in an inland tidal signal in the form of a line source – this is consistent with leakage at the edge of a buried surface water feature.

Independent data analysis for the inland tide-influenced areas (i.e. north beach, Area 1, Area 2), show that $\ln(\alpha_t)$ and $\Delta\phi_t$ are well correlated for all areas with the amplitude decay of the tidal signal increasing with the phase lag (Figure 3-7). Scatter from the linear relationship predicted by the 1D Jacob-Ferris solution in the north nearshore area (Figure 3-7a) may be attributed to non-linear effects such as aquifer heterogeneities and capillarity effects (Cartwright and Gibbes, 2011). For Areas 1 and 2 (Figure 3-7b and c), deviation from the 1D solution may be due to complexities of inland tidal source propagation. Data from only two wells are shown in Figure 3-7a for the north nearshore area as the tidal signal was rapidly damped inland of the shoreline, and wells further landward (i.e. ~120 m from shoreline) showed negligible fluctuation and therefore could not be included in the analysis.

Values for k_r , k_i , D , and SF are provided in Table 3-1 for the three tidal source areas (nearshore, Area 1 and Area 2). Plots of $\ln(\alpha_t)$ and $\Delta\phi_t$ versus distance to the inland tidal line source for Area 1 are shown in Figure 3-8a and b, respectively, to illustrate how the water table wave numbers k_r (rate of amplitude attenuation) and k_i (rate of phase lag) were calculated. Data show that, similar to previous studies (e.g. Trefry and Bekele, 2004; Rotzoll et al., 2008; Cartwright and Gibbes, 2011) k_r and k_i are not equal and therefore D_{amp} and D_{pha} are not equal. This results in SF values that deviate from unity. Previous studies conducted within various aquifer types have observed SF values within a range of 0.31 –

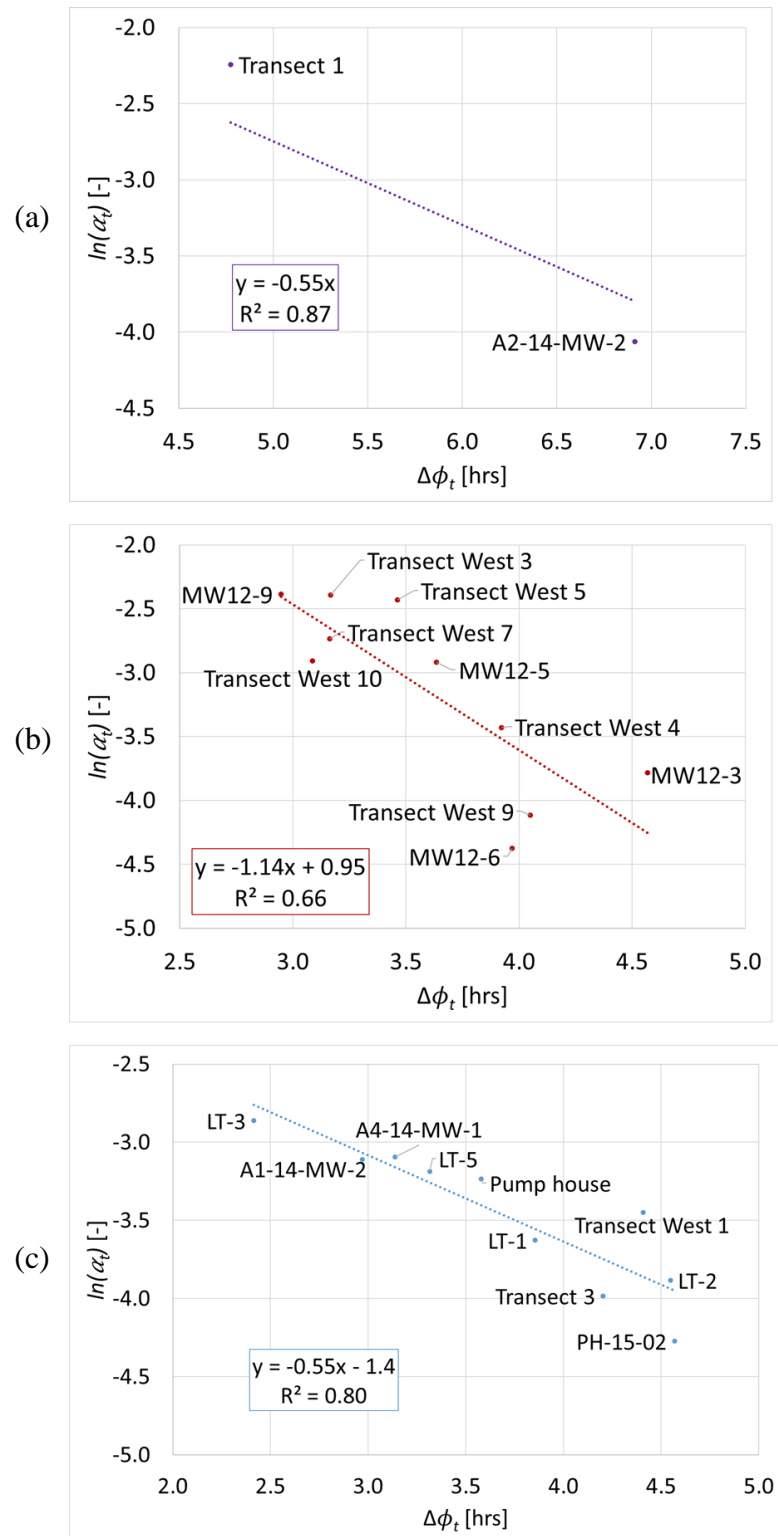


Figure 3-7 Calculated amplitude attenuation (α_t) [-] versus phase lag ($\Delta\phi_t$) [hrs] for groundwater monitoring wells clustered in areas with high aquifer-ocean connectivity (a) adjacent to the north beach shoreline, (b) Area 1, and (c) Area 2.

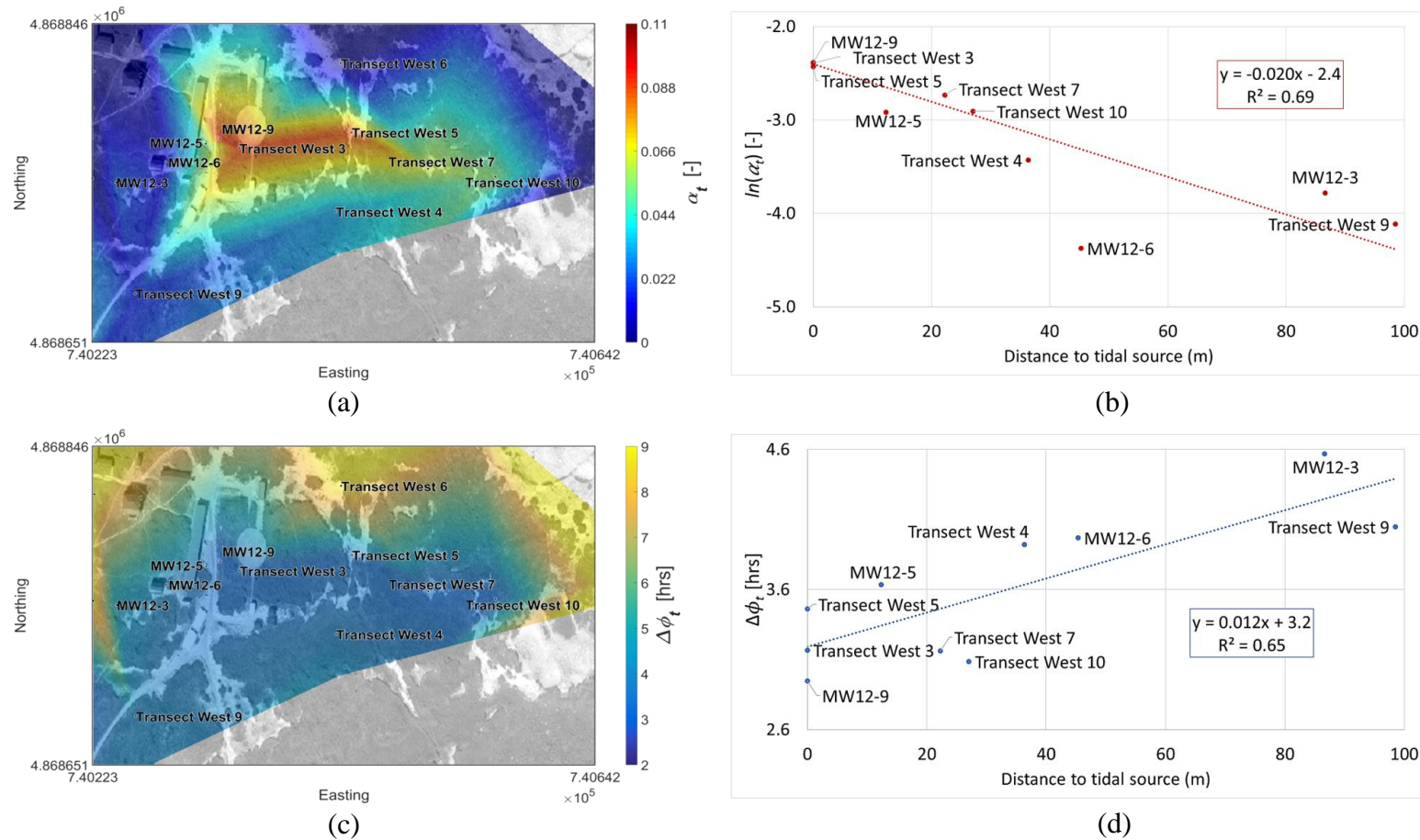


Figure 3-8 Coloured contours of calculated (a) amplitude attenuation (α_t) [-] and (c) phase lag ($\Delta\phi_t$) [hrs] for Area 1, as an example of an area of enhanced tidal influence. $\ln(\alpha_t)$ and $\Delta\phi_t$ versus distance (x) to hypothesized inland line source are shown in (b) and (d). Slope of linear regression lines in (b) and (d) estimate wave numbers k_r and k_i , respectively.

3.8 (e.g. Ferris, 1952; Carr and Van Der Kamp, 1969; Erskine, 1991; Trefry and Bekele, 2004), and numerical experiments performed by Trefry and Bekele (2004) concluded that macroscale horizontal layering in aquifer conductivity was the cause of propagation bias they observed ($SF = 0.43$, in a sand and limestone island aquifer in Western Australia).

Our results are consistent with previous studies and further indicate that the Sable Island aquifer is not homogeneous. Rapid attenuation of the tidal signal in the nearshore area, as well as the calculated propagation bias ($SF = 1.81$; Table 3-1), suggests that the surficial unconfined aquifer connected at the shoreline may be of non-uniform thickness perhaps due to a sloping confining layer (this theory is tested through numerical simulations described in Section 3.3.4).

Table 3-1 Aquifer parameters diffusivity (D) and slope factor (SF) estimated by amplitude-resolved (k_r) and phase-resolved (k_i) wave numbers calculated from tidal harmonics analysis.

Tidal Source Area	k_r	k_i	D_{amp} (m ² /d)	D_{pha} (m ² /d)	D_{avg} (m ² /d)	SF
Northshore	0.061	0.11	1660	500	2,160	1.81
Area 1	0.020	0.012	15,000	40,800	27,900	0.61
Area 2	0.019	0.037	17,500	4,530	11,000	1.97

3.3.3 Analysis of Storm Pulse Signal Propagation

Pulse-like fluctuations in groundwater levels are observed in response to discrete storm events and associated shoreline setup (Figure 3-9). Pulse attenuation (α_w) and time lag ($\Delta\phi_w$) values estimated by Gaussian least-squares fitting of groundwater level data and estimated shoreline elevation for two discrete storm events show increasing attenuation and lag of the pulse with increasing distance from the shoreline. This is illustrated in Figure

3-10 where the analytical solution (Eq. [3-14]) is compared to calculated values of α_w^* and $\Delta\phi_w^*$ that have been non-dimensionalized using Eq. (3-15) and (3-16) with $D = 1,280 \text{ m}^2/\text{d}$ (Hennigar, 1976). See Appendix C for calculated α_w and $\Delta\phi_w^*$ values. While the overall trends for the calculated values and analytical solution are consistent, the match is quite

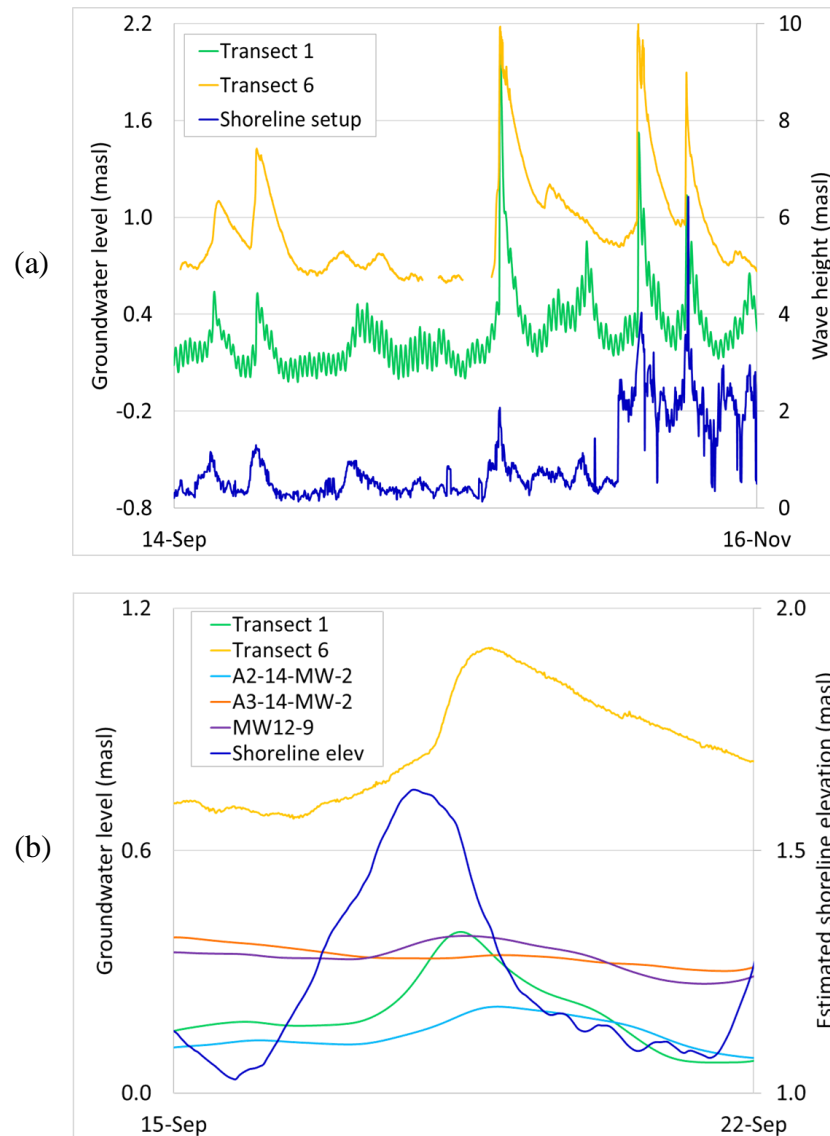


Figure 3-9 (a) Nearshore groundwater levels, in metres above sea level (masl), near the north (Transect 1) and south (Transect 6) shorelines, and shoreline setup (masl) calculated using data from an offshore wave buoy, from 14 Sept – 16 Nov, 2014. (b) Filtered groundwater levels (masl) and calculated shoreline elevation (masl) for a discrete storm event from 15 – 22 Sept, 2014.

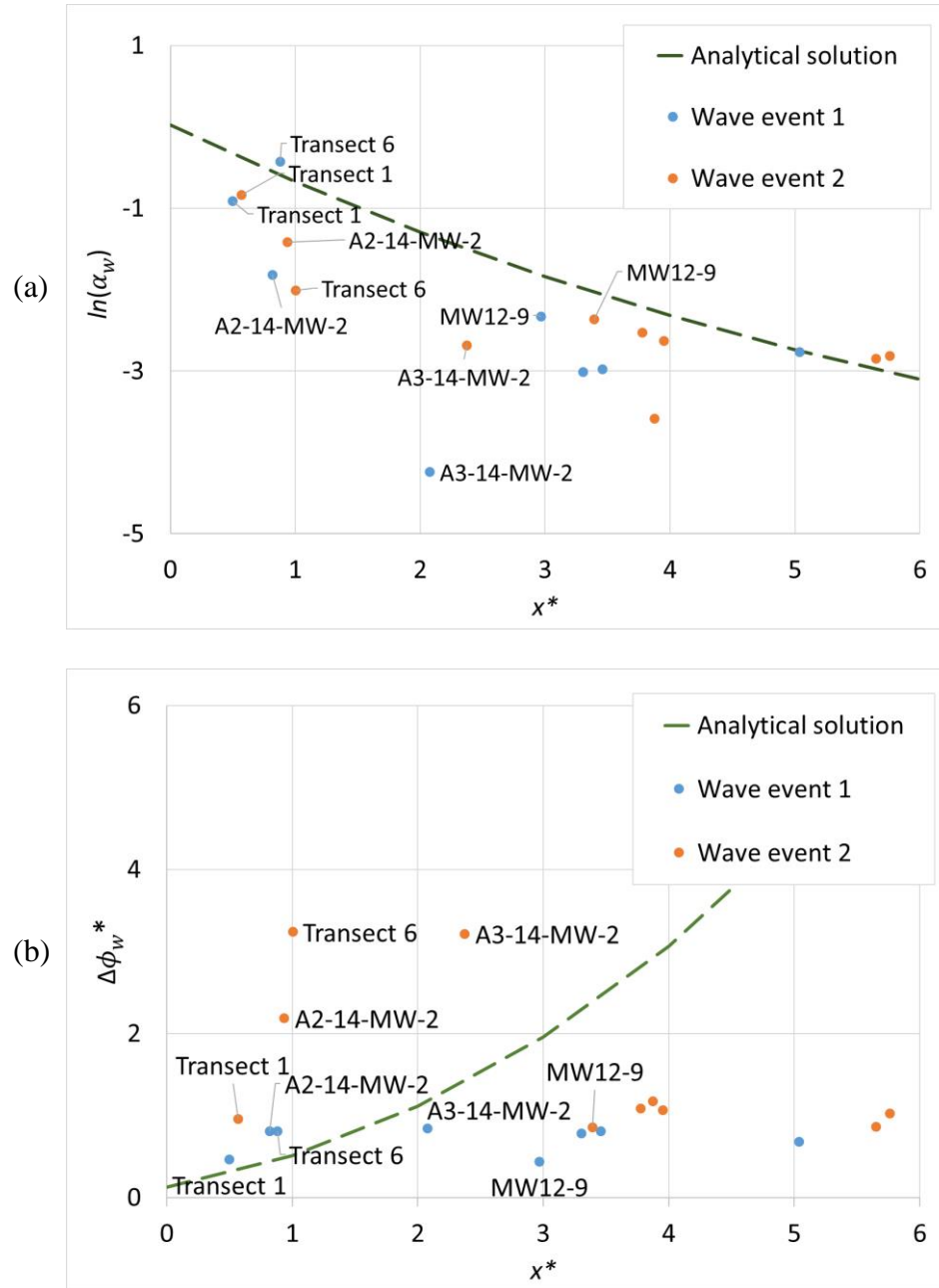


Figure 3-10 Analysis of storm pulse propagation for two isolated wave events (a) $\ln(\alpha_w)$ [-] versus non-dimensionalized distance (x^*) inland [-], and (b) $\Delta\phi_w^*$ [-] versus x^* . Field data for all monitoring wells are shown with labels provided only for select monitoring wells. Results are compared with storm pulse propagation predicted by an analytical solution describing storm-induced groundwater table fluctuations (green dashed line) according to Li et al. (2004).

poor. Calculated α_w values are better predicted by the analytical solution compared to calculated $\Delta\phi_w^*$; this contrasts with Cartwright and Gibbes (2011) who found the analytical solution better predicted $\Delta\phi_w^*$ than α_w . While some disagreement between calculated $\Delta\phi_w^*$, α_w , and analytical solution may be attributed to non-linear effects (i.e. sloping beach, finite aquifer depth) (Cartwright and Gibbes, 2011), the disagreement further suggests that the aquifer system may not be homogeneous and that aquifer values (S , T , K , d) previously reported by Hennigar (1976) may not adequately represent the system.

The storm pulse signal is observed to propagate farther through the unconfined aquifer from the shoreline compared to the tidal signal – this is consistent with the analytical solution of Li et al. (2004). For example, pulse-induced groundwater level fluctuations are observed at A3-14-MW-2 (located 166 m from the shoreline) (Figure 3-10) but data show negligible tide-induced fluctuations (Figure 3-6). Consistent with the propagation of the tidal signal, storm pulse signal propagation across the island is heterogeneous with storm pulse fluctuations at MW12-9 less attenuated and less lagged relative to, for example, A3-14-MW-2 which is located closer to the shore (Figure 3-10). More importantly, the pulse signal travels very rapidly to MW12-9 with the signal less lagged (average $\Delta\phi_w^* = 0.65$) compared to the pulse signal observed at Transect 1 (average $\Delta\phi_w^* = 0.71$), which is the closest monitoring well to the north shoreline. Fluctuations at MW12-9, however, are more damped (average $\alpha_w = 0.096$) relative to Transect 1 (average $\alpha_w = 0.42$); this contrasts with the tidal propagation analysis where both α_t and $\Delta\phi_t$ are similar for MW12-9 and Transect 1. Values calculated for other wells located within inland tidal source Areas 1 and 2 also show similar trends to MW12-9 (i.e. small α_w , small $\Delta\phi_w^*$) (Appendix C). This result suggests that the storm pulse signal may be rapidly propagating inland through a confined aquifer and is transmitted upwards into the unconfined aquifer by localized leakage within Areas 1 and 2. The greater attenuation of the storm pulse signal in Areas 1 and 2 compared to the tidal signal, yet similar phase lags for the tide and storm pulse signals, may be caused by the confined aquifer being connected to the ocean a finite distance offshore rather than at the shoreline. If this is the case, the magnitude of the wave setup pulse force acting on the confined aquifer would be less than the shoreline setup pulse force acting on the

unconfined aquifer, due to the positive slope in mean ocean surface level towards the beach caused by breaking waves (Figure 3-1) (Nielsen, 2009).

It is important to note that the poor match with the analytical solution and calculated α_w and $\Delta\phi_w^*$ (Figure 3-10) may also be associated with errors in estimated mean shoreline position, which was assumed constant for all storm events analyzed. In reality, the shoreline position will vary depending on wave run up, and thus, the magnitude of the storm event. The poor match could also be due to uncertainty in the timing and magnitude of the offshore wave heights (i.e. storm intensity) since the offshore wave buoy is located ~16 km from the island's south beach. Therefore, the time of deep sea waves reaching the north beach may be lagged relative to the buoy data due to ocean bed morphology, and wind energy (Rotzoll and El-Kadi, 2008). Measurements of the time-varying shoreline position, rather than assuming a constant mean shoreline position may also improve the non-dimensional storm pulse signal propagation analysis. Overall, however, our results suggest that more work is required to develop an analytical solution of storm pulse propagation that incorporates non-linear effects and complex aquifer conditions. Compared to the extensive understanding of tide-induced groundwater table fluctuations, there is limited understanding of storm pulse propagation through coastal aquifers, despite storm pulse forcing also being an important factor impacting groundwater levels in coastal environments (Turner et al., 1997).

3.3.4 Numerical Groundwater Flow Model

The combined analysis of tidal and storm pulse signal propagation indicates that Sable Island may have a leaky confined-unconfined aquifer system (Figure 3-1). Buried low-conductivity organic material from relic surface water ponds may have created a confining layer at depth, with heterogeneous distribution of organic material (i.e. heterogeneous in location, depth, thickness, or complete discontinuity) causing complex propagation of the tidal and storm pulse signals including isolated inland areas that respond rapidly to oceanic forcing. Relative to unconfined aquifers, confined aquifers more effectively transmit oceanic forcing signals due to decreased storage, and the signal may propagate upwards into an unconfined aquifer if leakage between the layers occurs. Relatively large tide-induced fluctuations observed in Areas 1 and 2 suggest that the confining layer in these areas is shallow, otherwise, the leaking tidal fluctuations would be completely damped as

the signal propagates vertically upwards resulting in negligible water table fluctuations. Further, since wells in Areas 1 and 2 show storm pulse response that is significantly damped, yet with lags similar to what is observed at nearshore wells (i.e. Transect 1, A2-14-MW-2), we propose that the confined aquifer is connected to the ocean slightly offshore. For this configuration, we expect the storm-induced wave setup pulse signal transmitted through the confined aquifer to be damped, but in phase, relative to the shoreline setup pulse signal. This configuration would result in the small α_w and small $\Delta\phi_w^*$ observed in Areas 1 and 2, relative to the nearshore wells. Numerical modelling simulations were used to evaluate whether this conceptual model can explain the observed heterogeneous propagation of the tidal signal through the aquifer, and in particular, the magnitude of the inland tide-induced water table fluctuations. Appendix D provides results from a suite of simulations were conducted with various aquifer configurations (e.g. varying unconfined and confined aquifer depths, configuration of the confining layer, and specific yield). A minimized absolute error between calculated and simulated α_t (Table 3-2) for monitoring wells was achieved using the model domain shown in Figure 3-3, especially for Transect 1 and MW12-9. Simulation results are shown in Figure 3-11 together with average α_t for monitoring wells Transect 1, A2-14-MW-2, and MW12-9 (negligible tide-induced water table fluctuations are observed at A3-14-MW-2 and are not shown). The range of calculated α_t values (using multiple subsets of time series data) for these wells is also indicated.

Table 3-2 Calculated and simulated amplitude attenuation factor (α_t) of an M2 semi-diurnal tide of 0.55 m amplitude.

Monitoring well	Calculated α_t	Simulated α_t
Transect 1	0.11	0.10
A2-14-MW-2	0.017	0.032
A3-14-MW-2	0.005	0.0
MW12-9	0.092	0.091

The model domain presented in Figure 3-11 slightly under-predicts the rate at which the tidal signal is attenuated in the nearshore unconfined aquifer (i.e. at A2-14-MW-2). Numerical experiments conducted with various configurations of the confining layer determined that a steep sloping confining layer ($\beta = 0.067$) was required to effectively

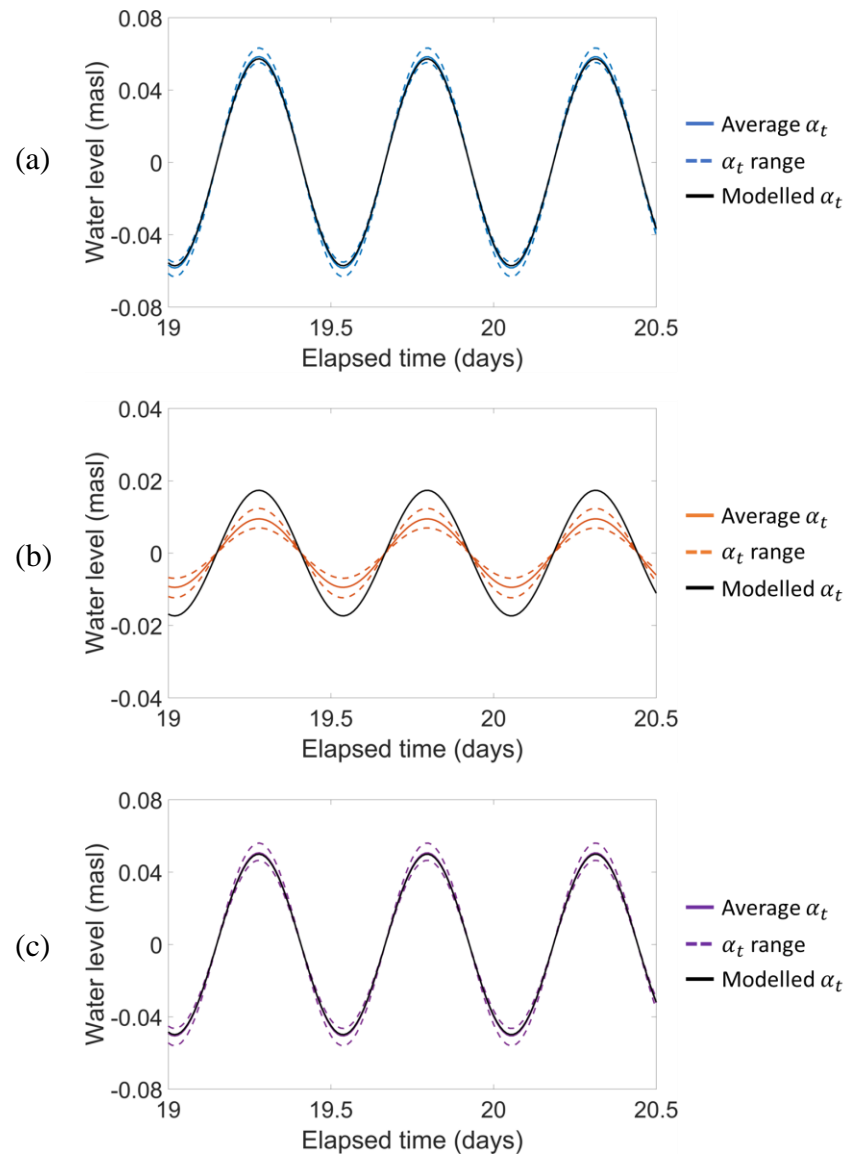


Figure 3-11 Comparison of average calculated tide-induced groundwater level fluctuations (solid coloured lines) and numerical simulation results (black lines) for monitoring wells (a) Transect 1, (b) A2-14-MW-2, and (c) MW12-9. Dashed coloured lines show the range of α_t values calculated using subsets of continuous groundwater level data. Note the different y-axis scale in (b).

dampen groundwater table fluctuations between the Transect 1 and A2-14-MW-2 locations as well as have negligible fluctuations at A3-14-MW-2 (Appendix D). The unconfined aquifer thickness is 3.5 m inland (i.e. at MW12-9) but 21.5 m near the shoreline (i.e. Transect 1). Best match between calculated and simulated groundwater level fluctuations inland (i.e. MW12-9) was achieved with a discontinuity in the confining layer. While it is difficult to estimate the width of the leak, a 10 m discontinuity provided sufficient leakage from the confined aquifer to result in phreatic groundwater level fluctuations at MW12-9 consistent with the observed data ($\alpha_t = 0.092$). This good match between calculated and simulated α_t at the MW12-9 location supports our theory that of propagation of the tidal signal to inland areas may be caused by a leaky confined-unconfined aquifer system, where a thin or discontinuous confining layer of organic material is buried at depth.

3.4 Conclusions

This study used combined analysis of tide- and storm pulse-induced groundwater table fluctuations to provide insight into the configuration of the coastal aquifer system on Sable Island, NS. Data analysis suggests that the aquifer is not a uniformly thick homogeneous and isotropic aquifer as suggested by prior field investigations. Nearshore groundwater levels were found to fluctuate in response to tidal and storm pulse signals with rapid attenuation of signals in the unconfined aquifer with increasing landward distance from the shoreline. Isolated areas up to approximately 400 m inland were also found to experience tide- and storm pulse-induced groundwater level fluctuations with only a small phase (time) lag in the water level fluctuations relative to the driving oceanic forcing signals. The storm pulse fluctuations observed at the isolated inland locations, however, were considerably attenuated relative the tidal fluctuations. The results suggest that the Sable Island aquifer system may be characterized by a two layer confined-unconfined aquifer system with localized upwards leakage at isolated inland locations where response to the oceanic forcing was observed. It is hypothesized that buried organic material (i.e. historical surface water ponds and swampy areas becoming dry, or overblown with dune sand) formed a confining layer at depth which allows the tidal and storm signals to propagate rapidly inland through a lower confined aquifer. Enhanced groundwater level fluctuations observed in isolated inland areas may be due to upward leakage of deeper, fluctuating

groundwater, in areas where the semi-impermeable confining layer is thin or discontinuous, and located at shallow depth. The large damping of the storm pulse signal at the inland wells relative to the damping of the tidal signal further suggests that the confined aquifer may be connected to the ocean some distance offshore; therefore, the confined aquifer is exposed to a smaller, yet in-phase, storm pulse signal, relative to the storm pulse signal observed at the shoreline. Conceptual numerical model simulations support this conceptualization of the aquifer system and results show a good match between simulated and observed tide-induced groundwater fluctuations. Measured groundwater level fluctuations did not compare well to tidal and storm pulse signal propagation predicted by 1D analytical solutions (e.g. Turner et al., 1997; Li et al., 2004). These discrepancies further indicate that the aquifer system on Sable Island is heterogeneous and highlight the need for an improved analytical solution for groundwater table fluctuations in response to storm pulse forcing for more complex aquifer scenarios.

Further data collection and analysis is recommended to confirm the study findings. For instance, field measurements such as laser-induced fluorescence, could be used to confirm the presence, depth and configuration of the confining layer. The numerical groundwater flow model presented is not fully calibrated to the field data but is used as a proof-of-concept to illustrate that a leaky confined-unconfined aquifer structure may explain the field observations. While the geologic process that would lead to a steep sloping confining layer inland of the north shoreline (i.e. between monitoring wells Transect 1 to A2-14-MW-2) is unclear, model results indicate that a homogeneous and isotropic unconfined aquifer of uniform depth is not able to explain the attenuation of the tidal signal observed. Additional higher resolution field data near the north shoreline would improve understanding of the tidal signal propagation and as such the configuration of the confining layer near the shoreline.

This study shows that a combined approach of analyzing signal propagation of both tides and storm-induced waves can provide insight into structural characterization of complex coastal aquifer settings, and reveal aquifer-ocean connectivity. This approach may be valuable for improved characterization of other aquifers worldwide that are exposed to tidal and storm pulse forcing from shorelines.

3.5 References

- Alcolea, A., E. Castro, M. Barbieri, J. Carrera and S. Bea (2007). "Inverse modeling of coastal aquifers using tidal response and hydraulic tests." Ground Water **45**(6): 711-722.
- Asadi-Aghbolaghi, M., M.-H. Chuang and H.-D. Yeh (2014). "Groundwater Response to Tidal Fluctuation in an Inhomogeneous Coastal Aquifer-Aquitard System." Water Resources Management **28**(11): 3591-3617.
- Carr, P. A. and G. S. Van Der Kamp (1969). "Determining aquifer characteristics by the tidal method." Water Resources Research **5**(5): 1023-1031.
- Cartwright, N. (2004). Groundwater dynamics and the salinity structure in sandy beaches. Division of Civil Engineering. Queensland, Australia, University of Queensland **PhD**: 210.
- Cartwright, N. and B. Gibbes (2011). Oceanic Pulse Forcing of a Beach Groundwater System. 20th Australasian Coastal and Ocean Engineering Conference 2011, COASTS 2011 and the 13th Australasian Port and Harbour Conference 2011, PORTS 2011. Perth, West Australia, Curan Associates Inc: 197 - 202.
- Cartwright, N., L. Li and P. Nielsen (2004). "Response of the salt-freshwater interface in a coastal aquifer to a wave-induced groundwater pulse: Field observations and modelling." Advances in Water Resources **27**(3): 297-303.
- Cartwright, N., P. Nielsen and L. Li (2004). "Experimental observations of watertable waves in an unconfined aquifer with a sloping boundary." Advances in Water Resources **27**(10): 991-1004.
- Chuang, M.-H. and H.-D. Yeh (2008). "Analytical Solution for Tidal Propagation in a Leaky Aquifer Extending Finite Distance under the Sea." Journal of Hydraulic Engineering **134**(4): 447-454.
- Chuang, M. H., C. S. Huang, G. H. Li and H. D. Yeh (2010). "Groundwater fluctuations in heterogeneous coastal leaky aquifer systems." Hydrology and Earth System Sciences **14**(10): 1819-1826.
- Crosbie, R. S., P. Binning and J. D. Kalma (2005). "A time series approach to inferring groundwater recharge using the water table fluctuation method." Water Resources Research **41**(1): 1-9.
- Danard, M., A. Munro and T. Murty (2003). "Storm Surge Hazard in Canada." Natural Hazards **28**(2): 407-434.
- Dong, L., D. Cheng, J. Liu, P. Zhang and W. Ding (2016). "Analytical analysis of groundwater responses to estuarine and oceanic water stage variations using superposition principle." Journal of Hydrologic Engineering **21**(1).

Duncan, J. R. (1964). "The effects of water table and tide cycle on swash-backwash sediment distribution and beach profile development." Marine Geology **2**(3): 186-197.

Environmental Sciences Group (ESG) (2015). 2015 Supplementary Phase III Environmental Site Assessment and Groundwater Dynamics Program Sable Island National Park Reserve Sable Island, Nova Scotia. Kingston, ON Canada, Royal Military College of Canada: 905.

Erskine, A. D. (1991). "Effect of tidal fluctuation on a coastal aquifer in the UK." Ground Water **29**(4): 556-562.

Ferris, J. G. (1952). Cyclic fluctuations of water level as a basis for determining aquifer transmissibility. Washington, D.C.

Freeze, R. A. and J. A. Cherry (1979). Groundwater. Englewood Cliffs, N.J, Prentice-Hall.

Geng, X., et al. (2014). "Numerical study of wave effects on groundwater flow and solute transport in a laboratory beach." Journal of Contaminant Hydrology **165**: 37-52.

Gonnea, M. E., A. E. Mulligan and M. A. Charette (2013). "Climate-driven sea level anomalies modulate coastal groundwater dynamics and discharge." Geophysical Research Letters **40**(11): 2701-2706.

Guo, H., J. J. Jiao and H. Li (2010). "Groundwater response to tidal fluctuation in a two-zone aquifer." Journal of Hydrology **381**(3-4): 364-371.

Guo, Q., H. Li, M. C. Boufadel, Y. Xia and G. Li (2007). "Tide-induced groundwater head fluctuation in coastal multi-layered aquifer systems with a submarine outlet-capping." Advances in Water Resources **30**(8): 1746-1755.

Hanslow, D. and P. Nielsen (1993). "Shoreline Set-Up on Natural Beaches." Journal of Coastal Research(15): 1-10.

Harbaugh, A. W., E. R. Banta, M. C. Hill and M. G. McDonald (2000). MODFLOW-2000, The U.S. Geological Survey Modular Ground-Water Model - User Guide to Modularization Concepts and the Ground-Water Flow Process. Open-File Report.

Hazen, A. (1982). Some physical properties of sands and gravels: with special reference to their use in filtration. Boston, Massachusetts, The State Board of Health of Massachusetts.

Hegge, B. J. and G. Masselink (1991). "Groundwater-Table Responses to Wave Run-up: An Experimental Study from Western Australia." Journal of Coastal Research **7**(3): 623-634.

Heiss, J. W. and H. A. Michael (2014). "Saltwater-freshwater mixing dynamics in a sandy beach aquifer over tidal, spring-neap, and seasonal cycles." Water Resources Research **50**(8): 6747-6766.

Hennigar, T. W. (1976). Water Resources and Environmental Geology of Sable Island, Nova Scotia, Nova Scotia Department of Environment: 56.

Hsieh, P. C., H. T. Hsu, C. B. Liao and P. T. Chiueh (2015). "Groundwater response to tidal fluctuation and rainfall in a coastal aquifer." Journal of Hydrology **521**: 132-140.

Jacob, C. E. (1950). Flow of groundwater. Engineering Hydraulics. H. Rouse. New York, John Wiley & Sons: 321 - 386.

Jacob, C. E. (1950). Flow of groundwater. New York.

Jeng, D. S., L. Li and D. A. Barry (2002). "Analytical solution for tidal propagation in a coupled semi-confined/phreatic coastal aquifer." Advances in Water Resources **25**(5): 577-584.

Jeng, D. S., B. R. Seymour, D. A. Barry, L. Li and J. Y. Parlange (2005). "New approximation for free surface flow of groundwater: Capillarity correction." Advances in Water Resources **28**(10 SPEC. ISS.): 1032-1039.

Jha, M. K., D. Namgial, Y. Kamii and S. Peiffer (2008). "Hydraulic Parameters of Coastal Aquifer Systems by Direct Methods and an Extended Tide–Aquifer Interaction Technique." Water Resources Management **22**(12): 1899-1923.

Jiao, J. J. and Z. Tang (1999). "An analytical solution of groundwater response to tidal fluctuation in a leaky confined aquifer." Water Resources Research **35**(3): 747-751.

Johnson, A. I. (1967). Specific yield: compilation of specific yields for various materials. Water Supply Paper. Washington, D.C.

Kim, J. H., et al. (2005). "Use of time series analysis for the identification of tidal effect on groundwater in the coastal area of Kimje, Korea." Journal of Hydrology **300**(1-4): 188-198.

Kong, J., et al. (2015). "Effects of vadose zone on groundwater table fluctuations in unconfined aquifers." Journal of Hydrology **528**: 397-407.

Li, G. and C. Chen (1991). "Determining the length of confined aquifer roof extending under the sea by the tidal method." Journal of Hydrology **123**(1): 97-104.

Li, H. and J. J. Jiao (2001). "Tide-induced groundwater fluctuation in a coastal leaky confined aquifer system extending under the sea." Water Resources Research **37**(5): 1165-1171.

Li, L. and D. A. Barry (2000). "Wave-induced beach groundwater flow." Advances in Water Resources **23**(4): 325-337.

- Li, L., D. A. Barry, F. Stagnitti and J. Y. Parlange (1999). "Submarine groundwater discharge and associated chemical input to a coastal sea." Water Resources Research **35**(11): 3253-3259.
- Li, L., D. A. Barry, F. Stagnitti and J. Y. Parlange (2000). "Groundwater waves in a coastal aquifer: A new governing equation including vertical effects and capillarity." Water Resources Research **36**(2): 411-420.
- Li, L., D. A. Barry, F. Stagnitti, J. Y. Parlange and D. S. Jeng (2000). "Beach water table fluctuations due to spring-neap tides: Moving boundary effects." Advances in Water Resources **23**(8): 817-824.
- Li, L., N. Cartwright, P. Nielsen and D. Lockington (2004). "Response of coastal groundwater table to offshore storms." China Ocean Engineering **18**(3): 423-431.
- Masselink, G., P. Russell, I. Turner and C. Blenkinsopp (2009). "Net sediment transport and morphological change in the swash zone of a high-energy sandy beach from swash event to tidal cycle time scales." Marine Geology **267**(1-2): 18-35.
- Merritt, M. L. (2004). Estimating Hydraulic Properties of the Floridan Aquifer System by Analysis of Earth-Tide, Ocean-Tide, and Barometric Effects, Collier and Hendry Counties, Florida. Tallahassee, Florida, United States Geological Survey: 76.
- Moody, J. A., et al. (1984). Atlas of tidal elevation and current observations on the Northeast American continental shelf and slope. U.S. Geological Survey bulletin. Reston, V.A. **1611**.
- Moore, W. S. (2010). "The Effect of Submarine Groundwater Discharge on the Ocean." Annual Review of Marine Science **2**(1): 59-88.
- Nielsen, P. (1990). "Tidal dynamics of the water table in beaches." Water Resources Research **26**(9): 2127-2134.
- Raubenheimer, B., R. T. Guza and S. Elgar (1999). "Tidal water table fluctuations in a sandy ocean beach." Water Resources Research **35**(8): 2313-2320.
- Robinson, C., B. Gibbes, H. Carey and L. Li (2007). "Salt-freshwater dynamics in a subterranean estuary over a spring-neap tidal cycle." Journal of Geophysical Research: Oceans **112**(C9): C09007.
- Robinson, C., P. Xin, L. Li and D. A. Barry (2014). "Groundwater flow and salt transport in a subterranean estuary driven by intensified wave conditions." Water Resources Research **50**(1): 165-181.
- Rotzoll, K. and A. I. El-Kadi (2008). "Estimating hydraulic properties of coastal aquifers using wave setup." Journal of Hydrology **353**(1-2): 201-213.

- Rotzoll, K., A. I. El-Kadi and S. B. Gingerich (2008). "Analysis of an unconfined aquifer subject to asynchronous dual-tide propagation." Ground Water **46**(2): 239-250.
- Shepherd, R. G. (1989). "Correlations of Permeability and Grain Size." Groundwater **27**(5): 633-638.
- Shih, D. C. F., G. F. Lin, Y. P. Jia, Y. G. Chen and Y. M. Wu (2008). "Spectral decomposition of periodic ground water fluctuation in a coastal aquifer." Hydrological Processes **22**(12): 1755-1765.
- Slooten, L. J., J. Carrera, E. Castro and D. Fernandez-Garcia (2010). "A sensitivity analysis of tide-induced head fluctuations in coastal aquifers." Journal of Hydrology **393**(3-4): 370-380.
- Song, Z., L. Li, J. Kong and H. Zhang (2007). "A new analytical solution of tidal water table fluctuations in a coastal unconfined aquifer." Journal of Hydrology **340**(3): 256-260.
- Teo, H. T., D. S. Jeng, B. R. Seymour, D. A. Barry and L. Li (2003). "A new analytical solution for water table fluctuations in coastal aquifers with sloping beaches." Advances in Water Resources **26**(12): 1239-1247.
- Trefry, M. G. and E. Bekele (2004). "Structural characterization of an island aquifer via tidal methods." Water Resources Research **40**(1): W015051-W0150521.
- Turner, I. L. (1995). "Simulating the influence of groundwater seepage on sediment transported by the sweep of the swash zone across macro-tidal beaches." Marine Geology **125**(1): 153-174.
- Turner, I. L., B. P. Coates and R. I. Acworth (1997). "Tides, waves and the super-elevation of groundwater at the coast." Journal of Coastal Research **13**(1): 46-60.
- Van Der Kamp, G. and J. E. Gale (1983). "Theory of earth tide and barometric effects in porous formations with compressible grains." Water Resources Research **19**(2): 538-544.
- Wang, Q., H. Zhan and Z. Tang (2013). "Groundwater response to dual tidal fluctuations in a peninsula or an elongated island." International Journal for Numerical and Analytical Methods in Geomechanics **37**(15): 2456-2470.
- Xia, Y., H. Li, M. C. Boufadel, Q. Guo and G. Li (2007). "Tidal wave propagation in a coastal aquifer: Effects of leakages through its submarine outlet-capping and offshore roof." Journal of Hydrology **337**(3-4): 249-257.
- Xin, P., C. Robinson, L. Li, D. A. Barry and R. Bakhtyar (2010). "Effects of wave forcing on a subterranean estuary." Water Resources Research **46**(12).

Chapter 4

4 Summary and Conclusions

4.1 Summary

In coastal settings, groundwater dynamics (i.e. levels and flows) are highly complex due to the influence of various environmental forcing such as tides and waves. This thesis made use of an extensive field dataset collected on Sable Island, NS, Canada to evaluate oceanic forcing and implement a novel approach of combined signal analysis and numerical modelling to improve understanding of the structure of the coastal aquifer system on Sable Island. Tides and offshore storms may be important controls for fate and transport processes of anthropogenic contaminants that are often found in coastal environments. For example, highly dynamic coastal groundwater dynamics, like what is observed on Sable Island, may enhance spreading of groundwater contaminants or dissolution of soil contamination (i.e. metals, various hydrocarbons) to the groundwater. Understanding aquifer-ocean connectivity and potential impacts to contaminant transport will become increasingly important given future climate changes projections of sea level rise and more intense and frequency storms. This study is the first to investigate coastal aquifer structure by comparison of tidal and storm-induced wave signal attenuation through the use of a robust and long-term groundwater monitoring network within a complex aquifer system (i.e. data indicates it is a leaky confined-unconfined system).

Long-term time series data of groundwater levels collected across the Main Station area on Sable Island indicated high spatial and temporal variability attributed to seasonal precipitation patterns and isolated rain events, as well as to oceanic forcing of tides and isolated storm events. Spectral analysis indicated that nearshore groundwater levels fluctuate in direct response to the dominant sinusoidal tidal mode (identified as the M2 semi-diurnal mode with frequency $\omega = 12.14$ rad/d). Propagation of the M2 tide was quantified by least-squares curve fitting of groundwater level and tide height data to calculate tidal signal propagation factors (i.e. amplitude attenuation α_t , and phase lag $\Delta\phi_t$). Results indicated that, as predicted by theory, the tidal signal is rapidly attenuated with

increased landward distance from the shoreline, such that the tidal signal is completely damped within ~120 m inland of the north shoreline. However, analysis also revealed that two distinct and isolated inland areas (up to ~400 m inland of the north beach) exhibit groundwater level fluctuations in response to tides. This indicates high aquifer-ocean connectivity that cannot be explained by a simple (homogeneous, isotropic) unconfined aquifer that terminates at the shoreline. A leaky confined-unconfined aquifer system may exist which results in the tidal signal propagating to these isolated inland locations. Groundwater level fluctuations in response to two isolated storm events were also evaluated. Least-squares fitting of a Gaussian pulse function to groundwater levels and estimated shoreline elevation data were used to estimate storm pulse signal propagation factors (i.e. amplitude attenuation α_w , and phase lag $\Delta\phi_w$). Results showed rapid attenuation of the storm pulse signal through the nearshore aquifer. Inland areas (that were seen to exhibit tide-induced fluctuations) also showed response to the storm pulse signal; however, while the pulse attenuation (α_w) in these areas was a fraction of that observed at nearshore wells, the phase lag values ($\Delta\phi_w$) were similar. This is an important finding that supports the leaky confined-unconfined aquifer hypothesis. Data suggested that fluctuations in the inland groundwater levels may be due to a connection between the inland areas and the ocean, via a confined aquifer with upwards leakage of groundwater causing pressure fluctuations into the overlying unconfined aquifer. The data further suggested that the confined aquifer may be connected to the ocean within the surf zone where the storm-induced setup pulse is reduced in magnitude compared to shoreline setup forcing the unconfined aquifer.

From the combined signal analysis, it was proposed that Sable Island may have a leaky confined-unconfined aquifer system, where confined aquifer storage allows rapid propagation of both tidal and storm pulse signals to reach isolated inland locations. Enhanced water table fluctuations observed in isolated areas may be due to upwards leakage of groundwater as a result of thinning, or complete discontinuity, of a buried low- K confining layer. This new conceptualization contrasts previous site investigations that reported Sable Island as having a homogeneous and isotropic unconfined aquifer of uniform thickness (Hennigar, 1976). Propagation of the tidal and storm pulse signals were also compared to analytical solutions (e.g. Turner et al., 1997; Li et al., 2004) and a poor

match between observed and predicted pulse attenuation also suggests the presence of aquifer heterogeneities, as well as the potential importance of non-linear processes (e.g. sloped aquifer bottom due to a sloped low- K confining layer at depth, sloping beach face, infiltration by wave run-up, etc.). A numerical model was developed in MODFLOW-2000 (Harbaugh et al., 2000) to test the hypothesized conceptualization, and in particular, whether a leaky confined-unconfined aquifer could explain the observed heterogeneous propagation of the tidal signal. Simulations revealed that significant tide-induced inland groundwater levels could result when there was upwards leakage of groundwater from a confined aquifer connected to the ocean a finite distance offshore. Due to decreased aquifer storage in confined aquifers the tidal signal is able to propagate inland and leakage transmits the signal upwards to induce water table fluctuations in the unconfined aquifer. Numerical groundwater flow simulations indicated that leakage-induced water table fluctuations are influenced by aquifer storage (S_y), aquifer depth, leak width, and length of the offshore roof. Reasonable match between simulated and observed groundwater level fluctuations was obtained, however, the model was conceptual and was not fully calibrated to field data. Due to the high level of uncertainties in estimating aquifer parameters, the model presented in this thesis is not assumed to be completely representative of the aquifer structure on Sable Island.

4.2 Recommendations

This thesis has shown that a combined approach of tidal and storm pulse signal analyses can be used to enhance understanding of coastal hydrogeology in a complex aquifer setting, and it is likely that this approach can be used in similar environments worldwide. Recommendations for future work are identified, with some arising from limitations on data collection and methods of analysis:

- Observed tidal signal propagation should be evaluated against more complex analytical solutions, for example, for leaky confined-unconfined aquifers (e.g. Li et al., 2002) or confined aquifers with an offshore roof (e.g. Li and Chen, 1991). These complex solutions have never before been applied to estimate aquifer values (e.g. aquifer diffusivity, D). Further, analytical solutions are required to better

understand propagation of tidal signals from inland leakage sources and derive new wave number (k) relationships for estimating aquifer parameters in complex aquifer settings.

- There is a need to better quantify the attenuation of the tide and storm pulse forcing near the shorelines on Sable Island, with only two data points currently available for calculating attenuation rates near the north shoreline and no data available for the south shoreline area
- The analytical solution by Li et al. (2004) is the only known solution for propagation of storm-induced wave pulses through a coastal aquifer; however, it is derived for a simple system (e.g. 1D, homogeneous and unconfined aquifer with a vertical boundary) and should be expanded for use in more complex coastal aquifers (e.g. layered, heterogeneous aquifers, sloping beach face). Findings by Cartwright and Gibbes (2011) also suggest that seawater infiltration by wave run-up is an important process, however, no work has been done to investigate the effects of run-up on storm pulse propagation. Seawater infiltration may be especially important for low-lying coastal environments that are prone to flooding during storms (i.e. Sable Island south beach).
- The numerical model presented in this thesis needs to be fully calibrated and validated to field data. Calibration metrics should include both amplitude attenuation and phase lag of groundwater levels (the current model is only assessed for amplitude attenuation of the tidal signal). The model should next be used to evaluate storm pulse propagation by implementing storm-induced setup as the ocean boundary condition. Long-term times series data available would allow for model validation using subsets of the full data record, and doing so would transform the numerical model into a useful predictive tool for risk management planning on the island and to evaluate the response to climate change projections (i.e. sea level, storm intensity and frequency).
- The numerical model is currently used to assess groundwater flow dynamics only; however, once validated, transport simulations could be conducted to evaluate the influence of tide and storm driven groundwater dynamics on contaminants. This would enhance understanding of the impacts of oceanic forcing on pollutant

transport in this dynamic coastal groundwater setting. This would be valuable for management of Sable Island and also other contaminated coastal environments. Other processes that could be incorporated into the current model include precipitation (seasonal, and event based; for which data is available) and evaporation, unsaturated flow effects (by using additional MODFLOW packages, or other modelling software such as FEFLOW or SEAWAT), or the multiphase flow and partitioning processes associated with non-aqueous phase contaminants.

- Estimates of storm pulse amplitude attenuation and lag could be improved by real-time measurement of shoreline position elevation during a storm event (by time-lapse photography), rather than estimating shoreline setup by an empirical relationship with wave height (Hanslow and Nielsen, 1993) and implementing a constant, mean shoreline position assumed from satellite imagery. Alternatively, the current shoreline elevation time series could be improved by estimating the time lag between wave buoy recordings and when wave energy reaches the beach, since wave data used in this study is collected by a buoy located ~16 km southwest of the island. Tidal analysis may also benefit from nearshore measurements, since data in this study are obtained from a tidal gauge located ~17 km northeast of the island.
- Advanced field investigation could be conducted to confirm the presence of the hypothesized buried organic lenses. The use of geophysical (e.g. electrical resistance survey) or spectroscopic methods (e.g. laser-induced fluorescence) may reveal the location and configuration (i.e. thickness, width) of low- K lenses. If found, this would verify the leaky confined-unconfined aquifer conceptualization proposed in this thesis.

4.3 References

Cartwright, N. and B. Gibbes (2011). Oceanic Pulse Forcing of a Beach Groundwater System. 20th Australasian Coastal and Ocean Engineering Conference 2011, COASTS 2011 and the 13th Australasian Port and Harbour Conference 2011, PORTS 2011. Perth, West Australia, Curan Associates Inc: 197 - 202.

Erskine, A. D. (1991). "Effect of tidal fluctuation on a coastal aquifer in the UK." Ground Water **29**(4): 556-562.

- Hanslow, D. and P. Nielsen (1993). "Shoreline Set-Up on Natural Beaches." Journal of Coastal Research(15): 1-10.
- Harbaugh, A. W., E. R. Banta, M. C. Hill and M. G. McDonald (2000). MODFLOW-2000, The U.S. Geological Survey Modular Ground-Water Model - User Guide to Modularization Concepts and the Ground-Water Flow Process. Open-File Report.
- Hennigar, T. W. (1976). Water Resources and Environmental Geology of Sable Island, Nova Scotia, Nova Scotia Department of Environment: 56.
- Li, G. and C. Chen (1991). "Determining the length of confined aquifer roof extending under the sea by the tidal method." Journal of Hydrology **123**(1): 97-104.
- Li, L., N. Cartwright, P. Nielsen and D. Lockington (2004). "Response of coastal groundwater table to offshore storms." China Ocean Engineering **18**(3): 423-431.
- Li, L., D. S. Jeng and D. A. Barry (2002). "Tidal fluctuations in a leaky confined aquifer: localised effects of an overlying phreatic aquifer." Journal of Hydrology **265**(1-4): 283-287.
- Merritt, M. L. (2004). Estimating Hydraulic Properties of the Floridan Aquifer System by Analysis of Earth-Tide, Ocean-Tide, and Barometric Effects, Collier and Hendry Counties, Florida. Tallahassee, Florida, United States Geological Survey: 76.
- Turner, I. L., B. P. Coates and R. I. Acworth (1997). "Tides, waves and the super-elevation of groundwater at the coast." Journal of Coastal Research **13**(1): 46-60.

Appendices

Appendix A: Groundwater Monitoring Network

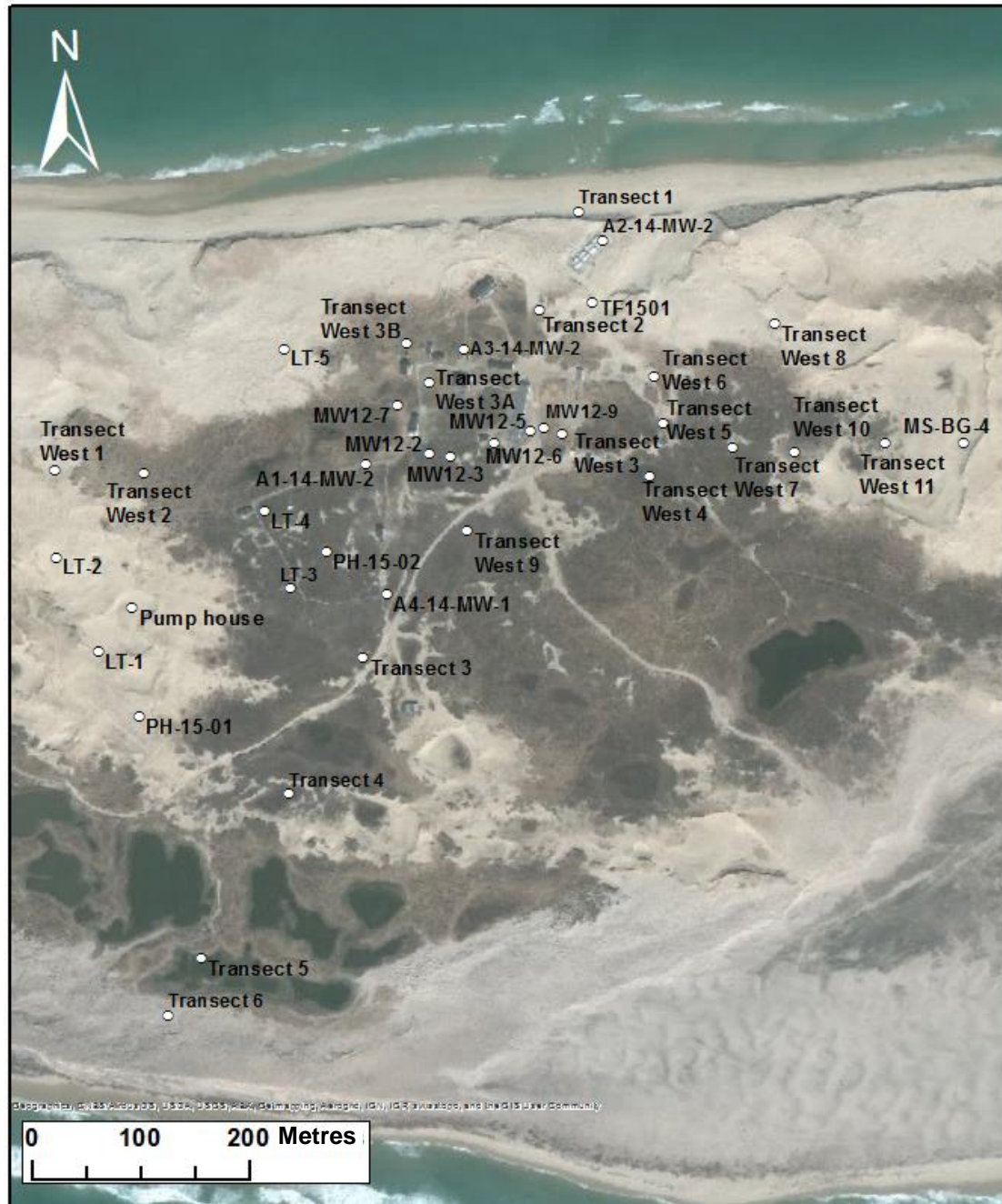


Figure A-1 Sable Island Main Station labelled with monitoring wells used for continuous data collection for analysis of tidal and storm pulse signal propagation, and their respective I.D.s. Imagery provided by Esri Basemaps.

Table A-1 Continuous groundwater level monitoring well schedule.

WELL I.D.	WELL CASING (IN)	WELL DEPTH (M)¹	PRESSURE TRANSDUCER MONITORING PERIOD (DD/MM/YYYY)
MW12-2	0.5	1.97	7/8/2014 – 9/8/2014
MW12-3	0.5	2.10	16/8/2014 – present
MW12-5	0.5	1.56	9/8/2015 17/8/2015 – 19/8/2015
MW12-6	0.5	2.76	7/8/2014 – 9/8/2014 15/8/2014 – 20/11/2014
MW12-7	0.5	1.52	7/8/2014 – 10/8/2014
MW12-9	0.5	2.34	7/8/2014 – present
A1-14-MW-2	2	1.56	9/8/2014 – 10/8/2014 16/8/2014 – present
A2-14-MW-2	2	5.41	20/8/2014 – present
A3-14-MW-2	2	1.94	16/8/2014 – present
A4-14-MW-1	2	2.56	9/8/2014 – 10/8/2014 15/8/2014 – 26/6/2015 12/8/2015 – present
MS-BG-04	2	1.19	20/8/2015 – 21/8/2015
Transect 1	2	3.14	8/8/2014 – present
Transect 2	2	3.14	8/8/2014 – 9/8/2014 12/6/2015 – present
Transect 3	2	1.72	8/8/2014 – 9/8/2014

Transect 4	2	1.61	9/8/2015 – 10/8/2015 18/11/2015 – present
Transect 5	2	-	8/8/2014 – 9/8/2014 11/8/2014 – 12/8/2014
Transect 6	2	2.15	8/8/2014 – 12/6/2015 ² 12/6/2015 – present
Transect 7	2	-	11/8/2014 – 12/8/2014
TF-15-01	2	3.15	30/5/2015 – 20/8/2015 ² 20/8/2015 – present
Transect West 1	2	4.57	11/8/2014 – present
Transect West 2	2	3.12	8/8/2014 – 11/8/2015 20/11/2014 – present
Transect West 3	2		
Transect West 3A	2	1.61	11/8/2015 – present
Transect West 3B ³	2	1.62	18/11/2014 – 12/6/2015 ³ 11/8/2015 – present
Transect West 4	2	1.54	10/8/2014 – 11/8/2014
Transect West 5	2	1.61	10/8/2015 – 12/6/2015 ³ 12/6/2015 – present
Transect West 6	2		13/8/2014
Transect West 7	2	2.58	12/8/2015 – 20/8/2015
Transect West 8	2	1.57	12/8/2015 – 15/8/2015
Transect West 9	2	1.59	14/8/2015 – 15/8/2015 22/8/2015 – present

Transect West 10	2	2.41	17/8/2015 – present
Transect West 11	2	1.60	20/8/2015 – 21/8/2015
MW Pump house	2	1.50	20/8/2014 – 12/6/2015 ³ 12/6/2015 – present
LT-1	2	1.49	18/11/2014 – present
LT-2	2	5.48	20/11/2014 – 25/5/2015 ² 31/5/2015 – present
LT-3	2	1.60	18/11/2014 – present
LT-4	2	1.95	18/11/2014 – present
LT-5	2	4.10	18/11/2014 – present
PH-15-01	2	1.60	14/8/2015 – present
PH-15-02	2	1.58	17/8/2015 – present

¹ Well depths measured August, 2015.

² Wildlife/environmental interference detected, re-installation required.

³ Well decommissioned and reinstalled to ensure bottom of well was also below water table elevation during dry periods.

Appendix B: Calculation of Tidal Signal Attenuation Factors

Analysis of groundwater level and tide height time series data was conducted to calculate tidal signal attenuation factors, using a method of least-squares fitting of continuous data (i.e. groundwater levels and tide height) to the harmonic oscillation:

$$h(t) = h_0 + \alpha_i \cos(\omega t + \phi) \quad (\text{B-1})$$

where h is groundwater level or tide level fluctuating about h_0 (average value of h), α_i is amplitude of the fluctuation (groundwater or tides), ω is frequency of the dominant tidal component (12.14 rad/d for M2 semi-diurnal harmonic), t is time, and ϕ is the phase lag of fluctuation relative to a pure cosine wave (in radians). Amplitude attenuation factor (α_t) and phase lag ($\Delta\phi_t$) were calculated as (e.g. Erskine, 1991; Merritt, 2004):

$$\alpha_t = \frac{\alpha_{GWL}}{\alpha_{tide}} \quad (\text{B-2})$$

$$\Delta\phi_t = \phi_{GWL} - \phi_{tide} \quad (\text{B-3})$$

where α_{GWL} and ϕ_{GWL} are amplitude and phase of groundwater level data, respectively, and α_{tide} and ϕ_{tide} are amplitude and phase of tide data, respectively. Attenuation factors α_t and $\Delta\phi_t$ are used to quantify propagation of the tidal signal through Sable Island aquifers. Calculated values for all groundwater monitoring locations are shown in Table B-1.

Table B-1 Tidal signal attenuation factors of amplitude attenuation (α_t) and phase lag ($\Delta\phi_t$) calculated at monitoring wells on Sable Island, by least-squares fitting of groundwater level and tide height time series data to the M2 semi-diurnal tidal harmonic oscillation ($\omega = 12.14$ rad/d).

Monitoring well I.D.	Estimated distance to tidal source ¹ [m]	Calculated α_t [-]	Calculated $\Delta\phi_t$ [hrs]
A1-14-MW-2 ²	7	0.045	3.0
A2-14-MW-2 ²	65	0.017	6.9
A3-14-MW-2 ²	166	0.005	7.3
A4-14-MW-1 ²	12	0.045	3.1
LT-1 ²	58	0.027	3.9
LT-2 ²	46	0.021	4.5
LT-3 ²	0	0.057	2.4
LT-4 ²	314	0	8.9
LT-5 ²	43	0.041	3.3
MS-BG-4 ³	251	0	8.9
MW12-2 ³	262	0	8.9
MW12-3 ²	87	0.023	4.6
MW12-5	12	0.054	3.6
MW12-6	45	0.013	4.0

MW12-7	217	0.002	6.7
MW12-9 ²	0	0.092	2.9
PH-15-01 ²	344	0	8.9
PH-15-02	352	0.014	4.6
Pump house ²	18	0.039	3.6
TF1501 ³	122	0	8.9
Transect 1 ²	40	0.11	4.8
Transect 2	130	0.003	8.7
Transect 3	44	0.019	4.2
Transect 4 ³	273	0	8.9
Transect 5	122	0.020	3.6
Transect 6	70	0.11	4.4
Transect West 1 ²	36	0.032	4.4
Transect West 2 ²	208	0.020	3.5
Transect West 3	0	0.091	3.2
Transect West 3A ³	196	0	8.9
Transect West 3B ³	161	0	8.9
Transect West 4	36	0.032	3.9
Transect West 5	0	0.088	3.5

Transect West 6 ³	191	0	8.9
Transect West 7	22	0.065	3.2
Transect West 8 ³	143	0	8.9
Transect West 9	98	0.016	4.0
Transect West 10	27	0.055	3.1
Transect West 11 ³	251	0	8.9

¹ Tidal source areas identified as the north and south shorelines and isolated inland tidal line source areas Area 1 and 2.

² Reported values are average α_t and $\Delta\phi_t$ calculated by analysis of multiple subsets of data time series.

³ Attenuation factors assumed to be $\alpha_t = 0$ and $\Delta\phi_t = 8.9$ (i.e. maximum lag calculated at a monitoring well) to represent no tidal influence observed in groundwater level time series data.

The following figures show least-squares fitting results from select monitoring locations in order to illustrate the least-squares fitting procedure (Eq. [B-1]) used to calculate α_t and $\Delta\phi_t$.

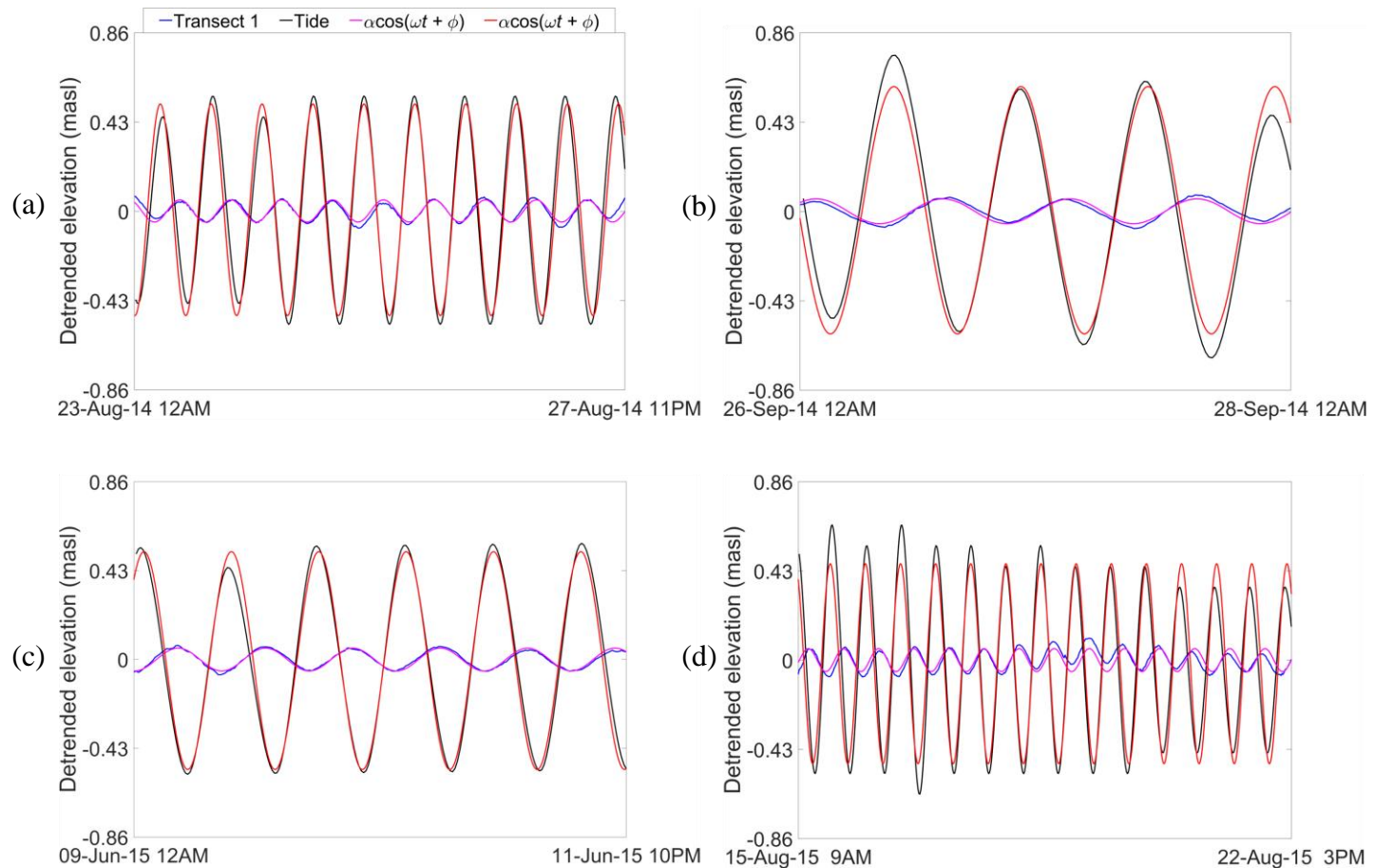


Figure B-2 Transect 1 harmonic least-squares fitting results for four subsets of time series data (a) 26 – 28 September, 2014, (b) 23 - 27 August, 2014 (c) 9 – 11 June, 2015 and (d) 15 – 22 August, 2015. In all figures, detrended groundwater level data is in blue and harmonic fit [$h(t) = h_0 + \alpha_i \cos(\omega t + \phi)$] is in pink; tide height data is in black and harmonic fit is in red.

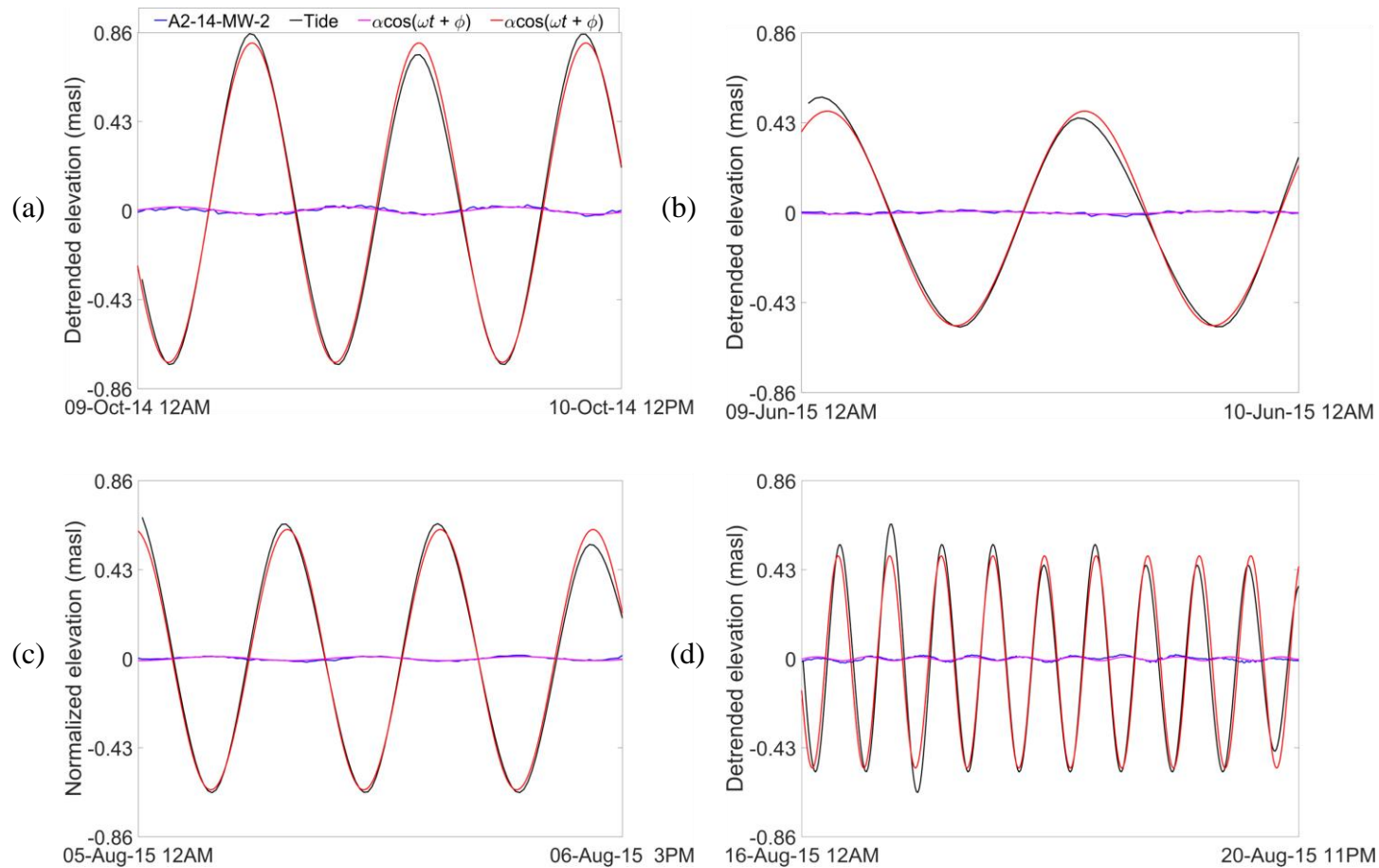


Figure B-3 A2-14-MW-2 harmonic least-squares fitting results for four subsets of time series data (a) 9 – 14 October, 2014, (b) 9 – 10 June, 2014 (c) 5 – 6 August, 2015 and (d) 16 - 20 August, 2015. In all figures, detrended groundwater level data is in blue and harmonic fit $[h(t) = h_0 + \alpha_i \cos(\omega t + \phi)]$ is in pink; detrended tide height data is in black and harmonic fit is in red.

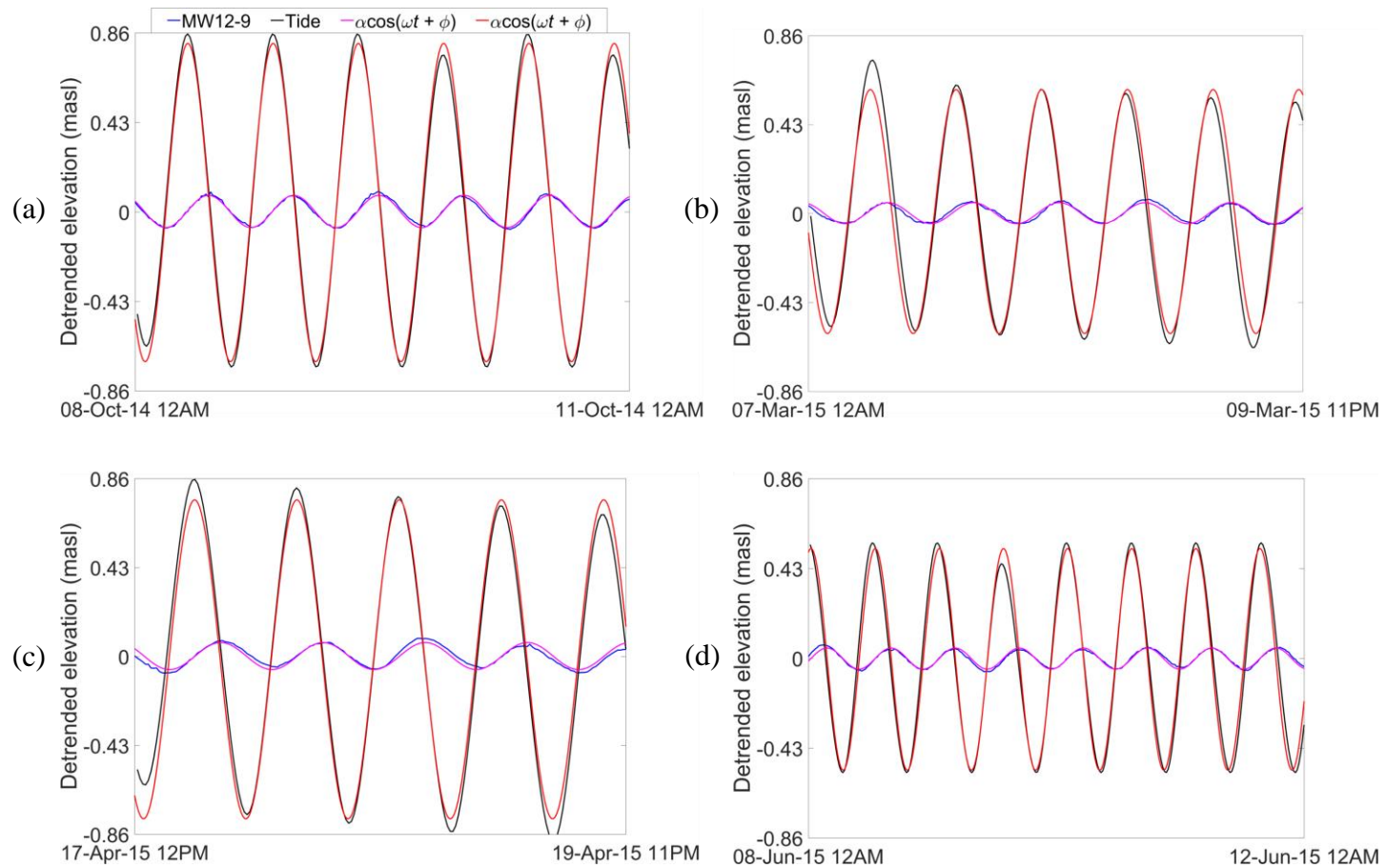


Figure B-4 MW12-9 harmonic least-squares fitting results for four subsets of time series data (a) 8 - 11 October, 2014, (b) 7 – 9 March, 2014 (c) 17 - 19 April, 2015 and (d) 8 – 12 June, 2015. In all figures, detrended groundwater level data is in blue and harmonic fit $[h(t) = h_0 + \alpha_i \cos(\omega t + \phi)]$ is in pink; detrended tide height data is in black and harmonic fit is in red.

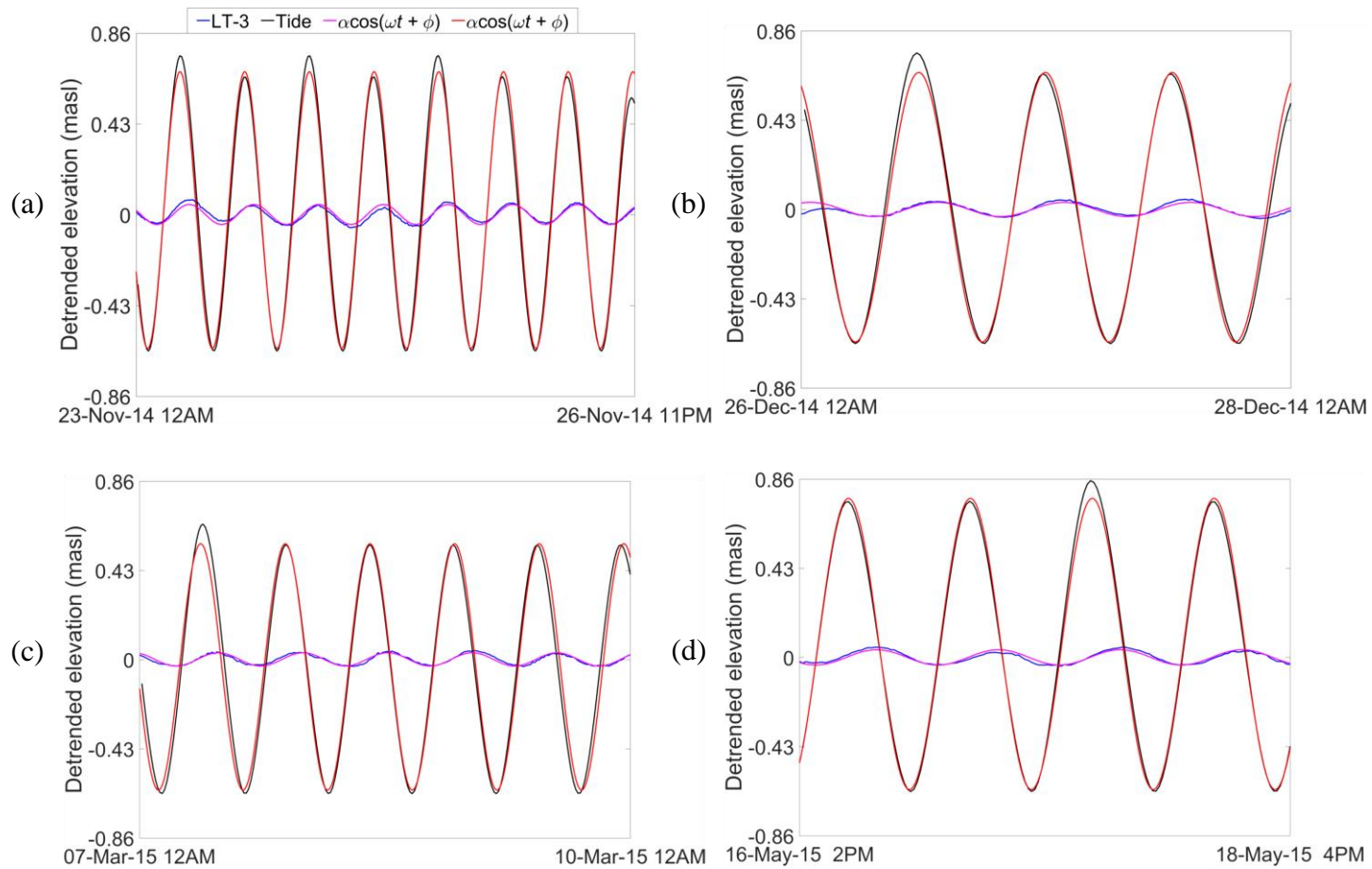


Figure B-5 LT-3 harmonic least-squares fitting results for four subsets of time series data (a) 23 – 26 November, 2014, (b) 26 – 28 December, 2014 (c) 7 – 10 March, 2015 and (d) 16 – 18 May, 2015. In all figures, detrended groundwater level data is in blue and harmonic fit $[h(t) = h_0 + \alpha_i \cos(\omega t + \phi)]$ is in pink; detrended tide height data is in black and harmonic fit is in red.

References

Erskine, A. D. (1991). "Effect of tidal fluctuation on a coastal aquifer in the UK." Ground Water **29**(4): 556-562.

Merritt, M. L. (2004). Estimating Hydraulic Properties of the Floridan Aquifer System by Analysis of Earth-Tide, Ocean-Tide, and Barometric Effects, Collier and Hendry Counties, Florida. Tallahassee, Florida, United States Geological Survey: 76.

Appendix C: Calculation of Storm Pulse Signal Attenuation Factors

Analysis of groundwater level data and storm-induced shoreline setup was conducted to evaluate storm pulse signal propagation through the Sable Island aquifer. Shoreline setup (η_s) was estimated by the empirical relationship of Hanslow and Nielsen (1993):

$$\eta_s = 0.048\sqrt{H_{0rms}L_0} \quad \text{C-1}$$

where H_{0rms} is the root-mean-square of the deep water wave height (calculated as $H_{0rms} = H_s/\sqrt{2}$, where H_s is significant wave height in metres) and L_0 is the deep water wavelength (calculated as $L_0 = gT_p^2/2\pi$, where T_p is peak wave period in second). Shoreline elevation (z_{SL}) was calculated by:

$$z_{SL} = z_{tide} + \eta_s \quad \text{C-2}$$

where z_{tide} is the tide elevation (in metres above sea level [masl]). Groundwater level data and calculated shoreline elevation was filtered through a low-pass Hamming filter to isolate wave-induced water fluctuations. Amplitude attenuation and phase lag of groundwater level response to storm-pulse signal was evaluated by least-squares fitting of continuous, and filtered, water level data to a Gaussian function of the form:

$$h(t) = h_0 + A \exp\left[-B(t - t_p)^2\right] \quad \text{C-3}$$

where h is water level (groundwater or shoreline elevation) fluctuating about h_0 (mean groundwater level or shoreline elevation), A is the amplitude of the pulse, B is a time factor (B^{-2} represents duration of the wave event or groundwater level response), and t_p is the time when the peak h occurs (Li et al., 2004). Following Li et al. (2004), only the rising limb of groundwater and shoreline elevation data was considered in the fitting analysis. Analysis was conducted using data observed over two offshore storm events (periods of intensified wave conditions), that occurred on 15 – 21 September, 2014, and 1 – 8 October, 2014.

Attenuation and phase lag of the storm pulse forcing through the aquifer was quantified by the comparison of fitted parameters:

$$\alpha_w = \frac{A_{GWL}}{A_{SL}} \quad \text{C-4}$$

$$\Delta\phi_w = t_{p,GWL} - t_{p,SL} \quad \text{C-5}$$

where A_{GWL} and A_{SL} are amplitude of groundwater level and shoreline elevation pulse fluctuation, respectively, and $t_{p,GWL}$ and $t_{p,SL}$ are time of peak groundwater level and shoreline elevation, respectively. Storms of various size and duration (i.e. A_{SL} and B) can be compared by calculating non-dimensional distance from the shoreline x^* (Li et al., 2004):

$$x^* = \frac{x}{2\sqrt{D/B^{1/2}}} \quad \text{C-4}$$

where D is aquifer diffusivity (of units L^2/T), and a non-dimensional form of Eq. B-5:

$$\Delta\phi_w^* = \Delta\phi_w\sqrt{B} \quad \text{C-5}$$

Calculated values of α_w and $\Delta\phi_w$ for groundwater monitoring wells are shown in Table C-1 for the storm events analyzed. Least-squares fitting results from select monitoring locations are shown in Figures C-1 and C-2 for wave event 1 (15 – 21 September, 2014) and wave event 2 (1 – 8 October, 2014), respectively, to illustrate the method used to calculate α_w and $\Delta\phi_w^*$.

Table C-1 Non-dimensional storm pulse signal attenuation factors of amplitude attenuation (α_w) and phase lag ($\Delta\phi_w^*$), and distance to the shoreline (x^*), calculated at monitoring wells on Sable Island. Factors calculated by Gaussian pulse least-squares fitting of groundwater level and estimated shoreline position time series data for two isolated storm events.

Monitoring well I.D.	Estimated x^* [-]	Calculated α_w [-]	Calculated $\Delta\phi_w^*$ [-]
Wave Event 1: 15 -21 September, 2014			
Transect 1	0.50	0.40	0.46
A2-14-MW-2	0.82	0.16	0.81
A3-14-MW-2	2.1	0.014	0.84
MW12-9	2.0	0.097	0.44
MW12-3	3.3	0.049	0.78
Transect West 1	3.5	0.051	0.81
Pump house	5.0	0.063	0.68
Wave Event 2: 1 – 8 October, 2014			
Transect 1	0.57	0.43	0.96
A2-14-MW-2	0.94	0.24	2.2
A3-14-MW-2	2.4	0.068	3.2
MW12-9	3.4	0.094	0.85
MW12-3	3.8	0.080	1.1

A1-14-MW-2	3.9	0.028	1.2
Transect West 1	4.0	0.072	1.1
A4-14-MW-2	5.7	0.058	0.86
Pump house	5.8	0.060	1.0

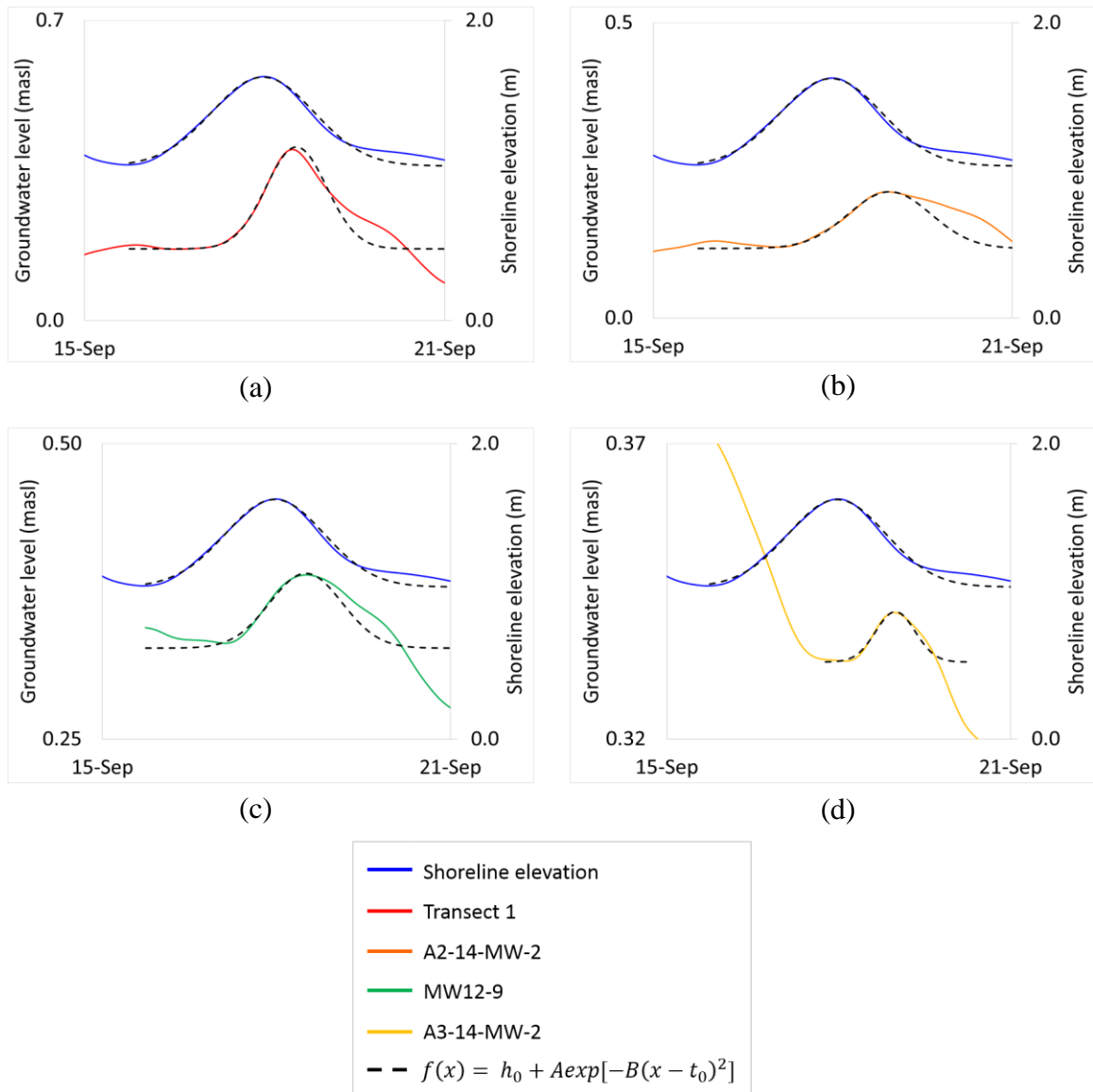


Figure C-6 Gaussian least-squares fitting results for wave event 1 (15 – 21 September, 2014). All plots show Hamming filtered shoreline elevation in blue, and Hamming filtered groundwater levels for (a) Transect 1 (red), (b) A2-14-MW-2 (orange), (c) MW12-9 (green), and (d) A3-14-MW-2 (yellow). Gaussian fits ($h(t) = h_0 + A \exp[-B(t - t_p)^2]$) are in black dashed lines (Li et al., 2004).

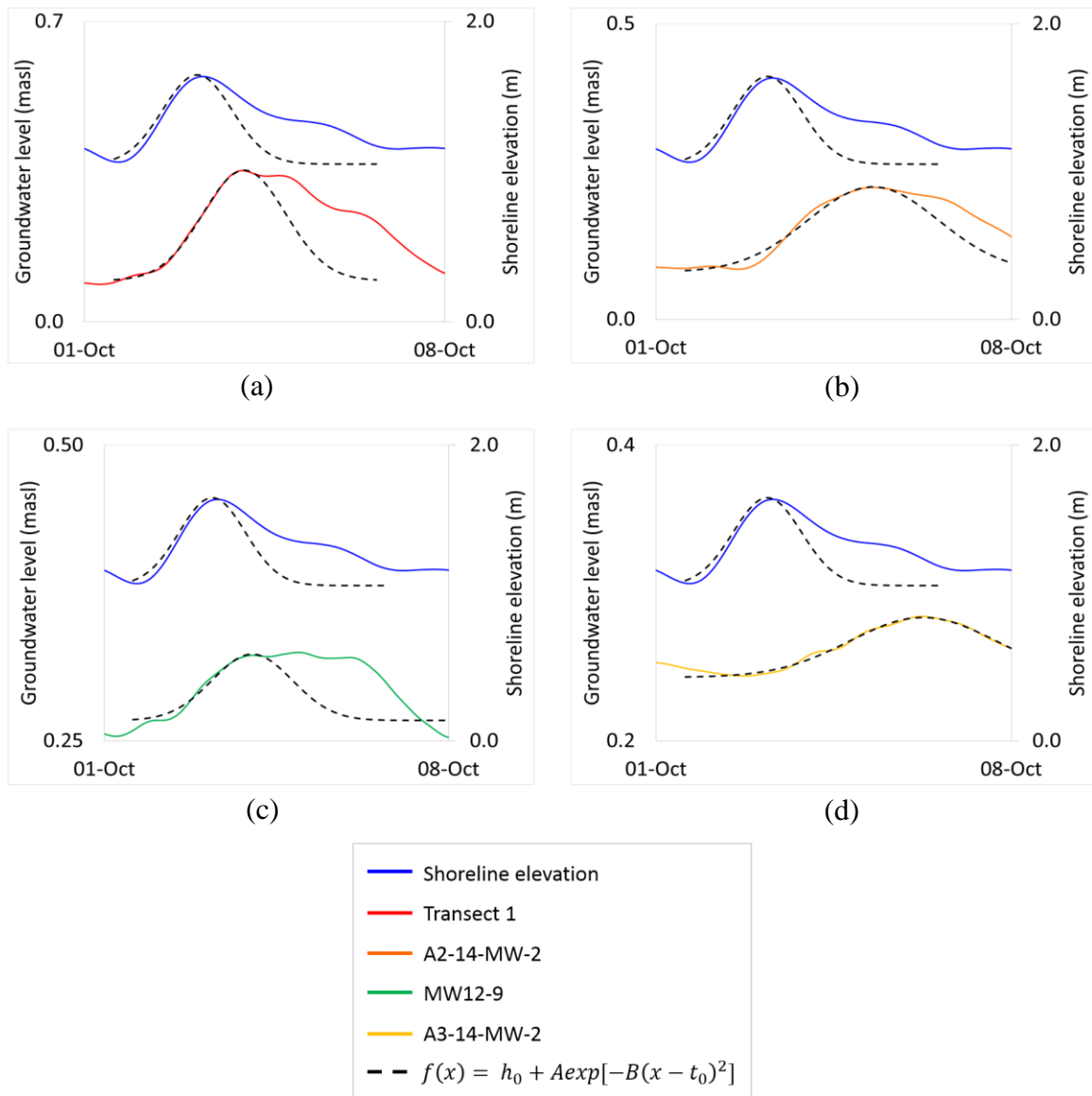


Figure C-7 Gaussian least-squares fitting results for wave event 2 (1 – 8 October, 2014). All plots show Hamming filtered shoreline elevation in blue, and Hamming filtered groundwater levels for (a) Transect 1 (red), (b) A2-14-MW-2 (orange), (c) MW12-9 (green), and (d) A3-14-MW-2 (yellow). Gaussian fits $(h(t) = h_0 + A\exp[-B(t - t_p)^2])$ are in black dashed lines (Li et al., 2004).

References

Hanslow, D. and P. Nielsen (1993). "Shoreline Set-Up on Natural Beaches." Journal of Coastal Research(15): 1-10.

Li, L., N. Cartwright, P. Nielsen and D. Lockington (2004). "Response of coastal groundwater table to offshore storms." China Ocean Engineering **18**(3): 423-431.

Appendix D: Numerical Simulations

A suite of numerical simulations were performed using MODFLOW-2000 to evaluate the effect of various coastal aquifer configurations on the aquifer tidal propagation. Simulation tidal signal attenuation factors (α_t) at monitoring well locations were compared with α_t values calculated from the Sable Island field data. Model performance was quantified by calculating absolute error between calculated and simulated α_t values. The simulation that provided the lowest absolute errors is presented in Chapter 3. Simulations were conducted to evaluate the effect of varying unconfined and confined aquifer depths, configuration of confining layer (location, slope, width of discontinuity, conductivity $K_{confining\ layer}$), and aquifer specific yield (S_y). Results from select simulation cases are summarized in Table D-1 with comparison of calculated and simulated α_t values (and absolute error) for monitoring wells Transect 1, A2-14-MW-2, A3-14-MW-2, and MW12-9. Supporting figures are provided in Figures D-1 to D-4 to show model domains and head results, and illustrate the impacts of the aquifer structure and parameter values on the tide-induced groundwater level fluctuations.

Table D-1 Comparison of tidal signal attenuation factor (α_t) calculated from field data and from suite of groundwater flow models. For all models the set-up and parameter values were the same as for the model described in Chapter 3 except for the configuration/parameter value which was varied as described below.

Case	Parameter Varied	Transect 1 (abs. error)	A2-14-MW-2 (abs. error)	A3-14-MW-2 (abs. error)	MW12-9 (abs. error)
	Calculated α_t (harmonics analysis)	0.11	0.017	0.005	0.092
1	Leaky confined-unconfined aquifer (case presented in Chapter 3)	0.10 (0.01)	0.032 (0.015)	0 (-)	0.091 (0.001)
2	No discontinuity (i.e. layered confined-unconfined aquifer with no leakage)	0.10 (0.01)	0.032 (0.015)	0 (-)	0 (0.092)
3	Fully unconfined aquifer (depth = 300 m)	0.17 (0.06)	0.098 (0.081)	0.031 (0.031)	0.018 (0.074)
4	Confining layer slope $\beta = 0.10$ (depth at MW12-9 = 3.5 m, depth at Transect 1 = 6 m)	0.058 (0.052)	0.01 (0.007)	0 (-)	0.095 (0.003)
5	$S_y = 0.36$	0.066 (0.044)	0.015 (0.002)	0 (-)	0.072 (0.02)
6	$S_y = 0.20$	0.15 (0.04)	0.052 (0.035)	0 (-)	0.094 (0.002)

7	Leaky confined-unconfined aquifer with uniform confining layer depth = 3.5 m	0.014 (-0.096)	0 (-0.017)	0 (-)	0.12 (0.028)
8	Leaky confined-unconfined aquifer with uniform confining layer depth = 21.5 m	0.10 (-0.01)	0.033 (0.016)	0 (-)	0.029 (-0.063)
9	5 m wide discontinuity	0.11 (-)	0.034 (0.017)	0 (-)	0.077 (-0.015)
10	$K_{confining\ layer} = 10^{-3}$ m/d	0.11 (-)	0.035 (0.017)	0 (-)	0.084 (-.008)

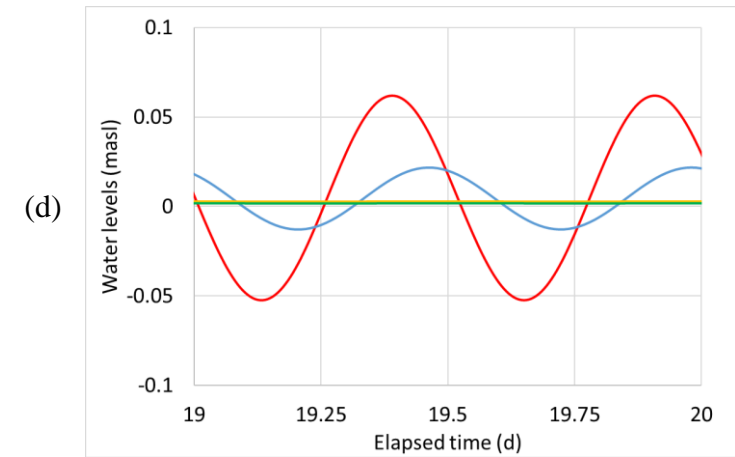
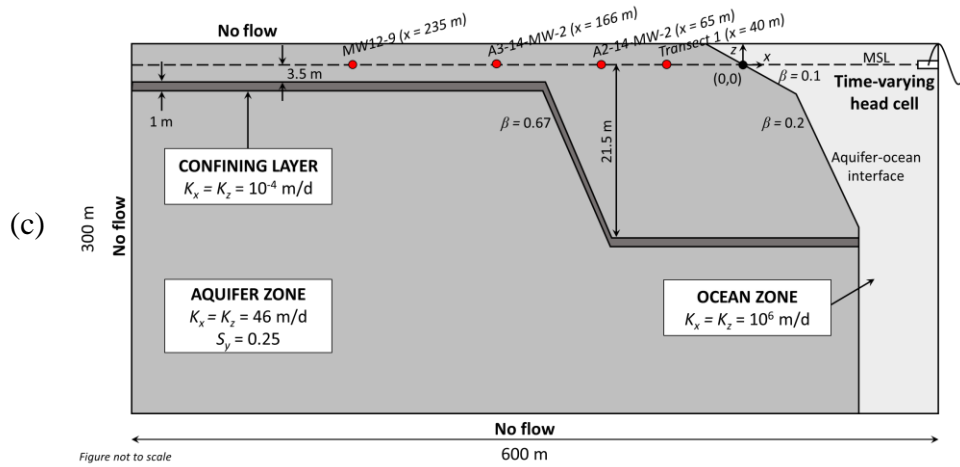
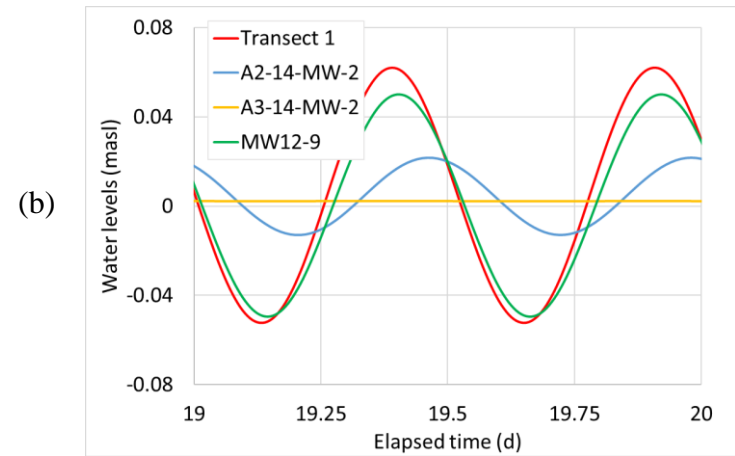
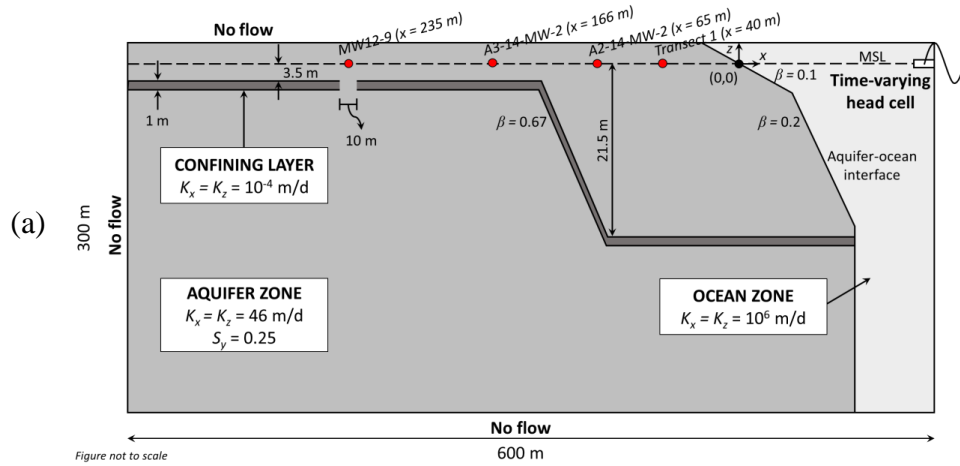


Figure D-1 Simulation results for a heterogeneous leaky confined-unconfined aquifer with 10 m wide discontinuity (a – b, case 1 Table D-1), and with no discontinuity (c – d; case 2 in Table D-1). Results in (b) and (d) represent Sable Island monitoring locations Transect 1 (red), A2-14-MW-2 (blue), A3-14-MW-2 (yellow) and MW12-9 (green) indicated in (a) and (c).

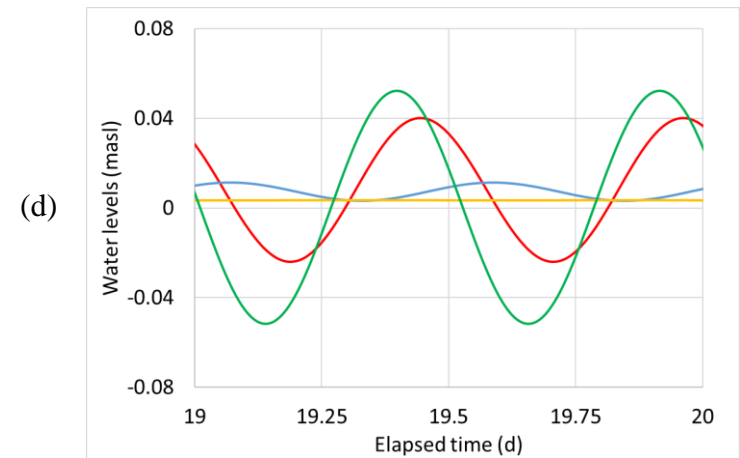
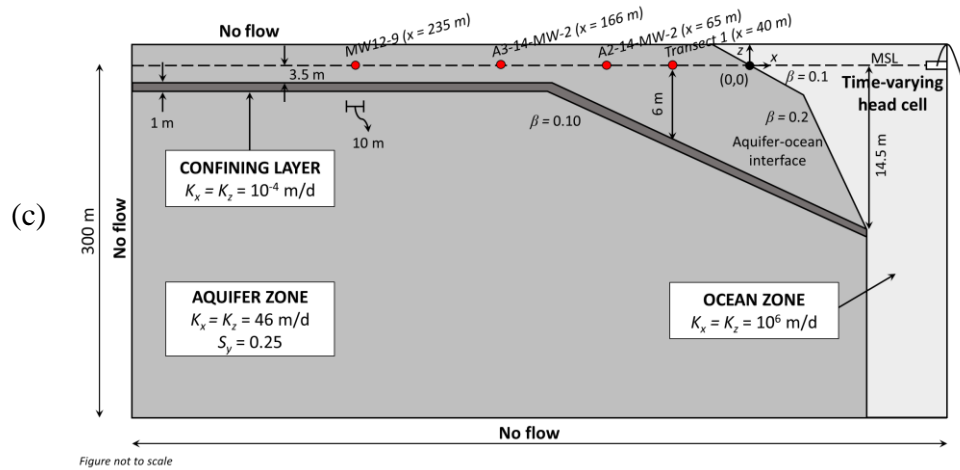
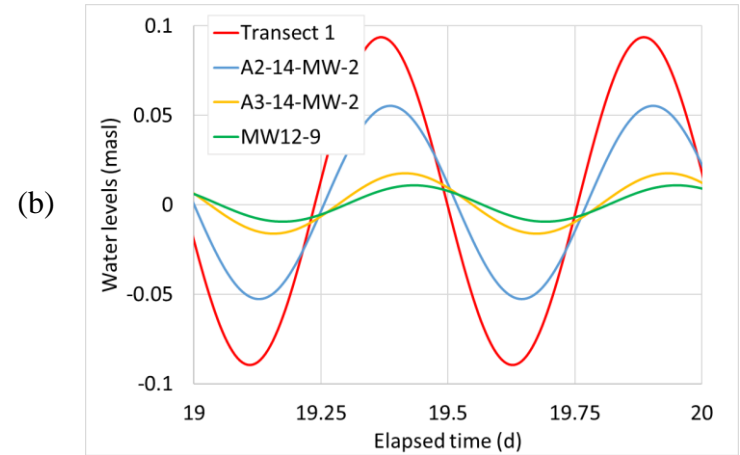
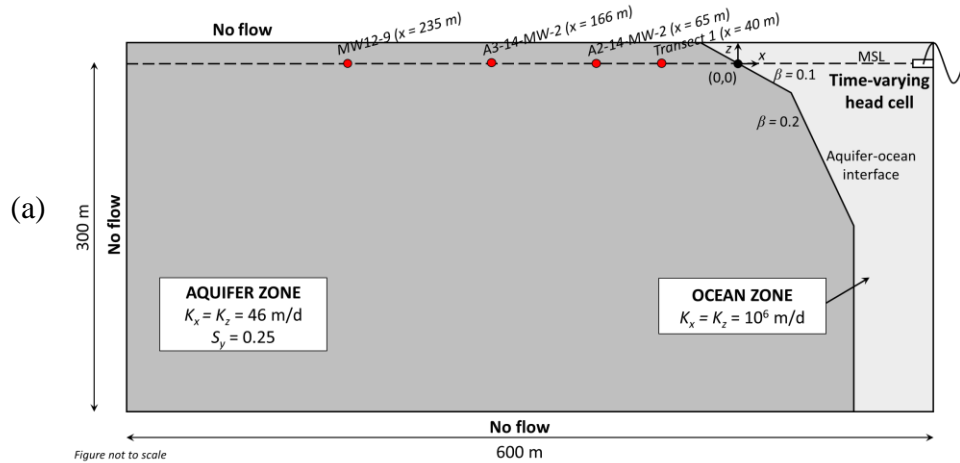


Figure D-2 Simulation results for a homogeneous unconfined aquifer (a – b, case 3 Table D-1), and leaky confined-unconfined aquifer with shallow sloping confining layer (c – d; case 4 in Table D-1). Results in (b) and (d) represent Sable Island monitoring locations Transect 1 (red), A2-14-MW-2 (blue), A3-14-MW-2 (yellow) and MW12-9 (green) indicated in (a) and (c).

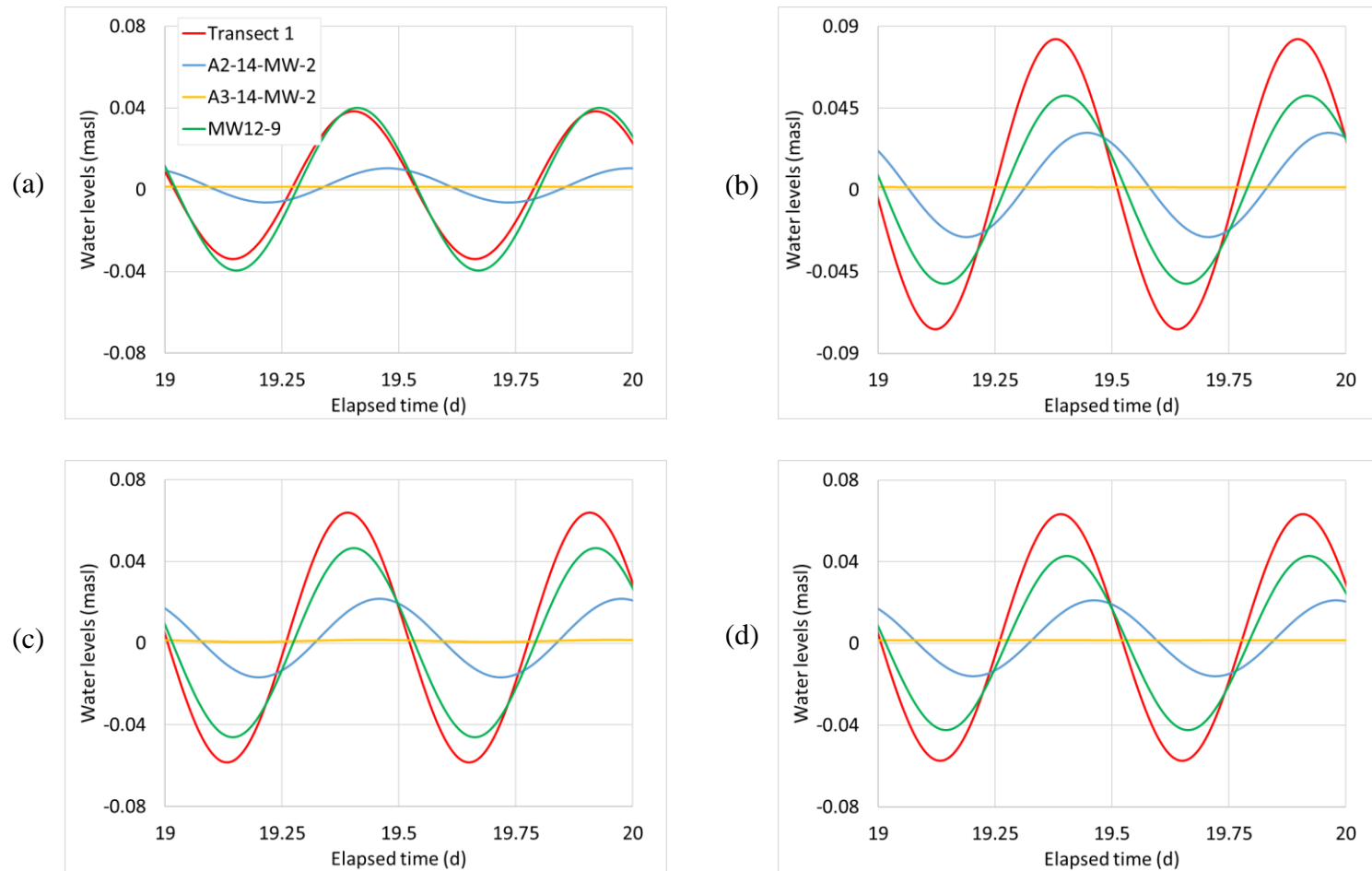


Figure D-4 Simulated heads for varied leaky confined-unconfined aquifer domains (case 1 in Table D-1) varied with (a) $S_y = 0.36$ (case 5), (b) $S_y = 0.20$ (case 6), (c) $K_{confining\ layer} = 10^{-3}$ m/d (case 9), and (d) 5 m wide inland discontinuity (case 10). Results represent Sable Island monitoring locations Transect 1 (red), A2-14-MW-2 (blue), A3-14-MW-2 (yellow) and MW12-9 (green).

Appendix E: Governing Equations for MODFLOW-2000

MODFLOW-2000 is a finite-difference code developed by the U.S. Geological Survey (USGS) to solve the three-dimensional (3D) equation for constant density groundwater flow through porous media (Harbaugh et al., 2000):

$$S_s \frac{\partial h}{\partial t} = \frac{\partial}{\partial x} \left(K_x \frac{\partial h}{\partial x} \right) + \frac{\partial}{\partial y} \left(K_y \frac{\partial h}{\partial y} \right) + \frac{\partial}{\partial z} \left(K_z \frac{\partial h}{\partial z} \right) + R^* \quad (\text{D-1})$$

where S_s is the specific storage of the porous media [L^{-1}], $\partial h / \partial t$ is the change in hydraulic head, h [L] with time t [T], K_i is the hydraulic conductivity in the i -plane where i is the x , y , or z -direction [LT^{-1}], $\partial h / \partial i$ is the change in hydraulic head with space in the i -plane, and R^* is the volumetric source or sink term [T^{-1}]. The coordinate directions are assumed to be aligned with the major axes of K_i (Harbaugh et al., 2000). The finite difference approach defines the continuous aquifer system by a grid of cells (i.e. x -plane discretized into columns, y -plane into rows, and z -plane into layers) where discrete points in space and time (i.e. nodes) are located at the centre of each cell. Time is also discretized into time steps to calculate h at each node. An approximate solution to Eq. (D-1) is calculated using simultaneous linear algebraic equations which are generated by replacing the partial differentials in Eq. (D-1) with change in head (Δh) at each node calculated over each discretized time step of length Δt (Harbaugh et al., 2000).

Flow of groundwater into and out of each cell is calculated by the sum of flow across each cell face (from adjacent cells) according to Darcy's law. For example, flow into cell (x,y,z) across the left-hand face, $Q_{x-1 \rightarrow x}$:

$$Q_{x-1 \rightarrow x} = -K_x A_{yz} \left(\frac{h_{x,y,z} - h_{x-1,y,z}}{d_{x-1 \rightarrow x}} \right) \quad (\text{D-2})$$

where A_{yz} is cross-sectional area of the cell face (equal to $d_y d_z$, for this example). Eq. (D-2) is applied across all six faces of cell (x,y,z) .

This study used MODFLOW-2000 to simulate two-dimensional (2D) fully saturated groundwater flow in a leaky confined-unconfined coastal aquifer with no recharge or evapotranspiration (i.e. $R^* = 0$). Thus, Eq. (D-1) is simplified for a 2D cross-section perpendicular to the shoreline (i.e. $\partial h / \partial y = 0$), quasi-steady state (i.e. $\partial h_{avg} / \partial t = 0$, where oscillating tides cause groundwater fluctuations about mean head h_{avg}) and homogeneous and isotropic aquifer properties (i.e. $K_x = K_z$). For 2D groundwater flow through homogenous and isotropic confined aquifers, Eq. (D-1) is transformed to:

$$S \frac{\partial h}{\partial t} = T \left[\frac{\partial}{\partial x} \left(\frac{\partial h}{\partial x} \right) + \frac{\partial}{\partial z} \left(\frac{\partial h}{\partial z} \right) \right] \quad (\text{D-3})$$

where S is storage coefficient [-] and T is the transmissivity [L^2T^{-1}] (constant in all directions). Both S and T are related to aquifer thickness b and S_s by:

$$S = \int_0^b S_s(b) db \quad (\text{D-4})$$

$$T_i = \int_0^b K_i(b) db \quad (\text{D-5})$$

indicating that changes in flow conditions in confined aquifers are driven by changes in storage due to compression of the soil matrix. In contrast, groundwater flow through unconfined aquifers are driven by changes in h and Eq. (D-1) becomes:

$$S_y \frac{\partial h}{\partial t} = K \left[\frac{\partial}{\partial x} \left(h \frac{\partial h}{\partial x} \right) + \frac{\partial}{\partial z} \left(h \frac{\partial h}{\partial z} \right) \right] \quad (\text{D-6})$$

where S_y is specific yield [-] which varies with h :

$$S_y = S_s h \quad (\text{C-7})$$

The Wetting Capability function in MODFLOW-2000 was used in this study to allow simulation of the rising water table across model layers according to user-defined settings of wetting threshold (THRESH) and factor (WETFCT). Factor THRESH dictates how model cells become saturated (i.e. whether cells accept flow from other cells located directly below it, or by the four horizontally adjacent cells), and factor WETFCT determines when the cell becomes saturated (according to the elevation of h relative to the elevation of the cell's bottom face) (Harbaugh et al., 2000).

References

Harbaugh, A. W., E. R. Banta, M. C. Hill and M. G. McDonald (2000). MODFLOW-2000, The U.S. Geological Survey Modular Ground-Water Model - User Guide to Modularization Concepts and the Ground-Water Flow Process. Open-File Report.

Curriculum Vitae

Name: Victoria Angela Trglavcnik

Post-secondary Education and Degrees: University of Western Ontario
London, Ontario, Canada
2009 – 2014 BESc.

Honours and Awards: Association of Universities and Colleges of Canada Graduate Award
2014

Geotechnical Research Council Graduate John Booker Award
2015

Geotechnical Research Council Graduate L.G. Soderman Award
2016

Related Work Experience Teaching Assistant
The University of Western Ontario
2014 - 2016